Diagnostic Methods and Parameters to Characterize Droplets and Particles in Suspension Plasma Spray

Ali Akbarnozari

A Thesis
In the Department
of
Mechanical, Industrial, and Aerospace Engineering

Presented in Partial Fulfillment of the Requirements
For the Degree of
Doctor of Philosophy (Mechanical Engineering) at
Concordia University
Montreal, Quebec, Canada

July 2019

CONCORDIA UNIVERSITY

SCHOOL OF GRADUATE STUDIES

This is to certify that the thesis prepared

By: Ali Akbarnozari

Entitled: Diagnostic Method and Parameters to Characterize Droplets and Particles in Suspension Plasma Spray

and submitted in partial fulfillment of the requirements for the degree of

Doctor Of Philosophy (Mechanical Engineering)

complies with the regulations of the University and meets the accepted standards with respect to originality and quality.

Signed by the final examining committee:

_____ Chair
Dr. Catherine Mulligan

_____ External examiner
Dr. Sylvain Coulombe

_____ External to Program
Dr. Mojtaba Kahrizi

_____ Examiner
Dr. Sivakumar Narayanswamy

_____ Examiner
Dr. Lyes Kadem

_____ Thesis Co-Supervisor
Dr. Christian Moreau

_____ Thesis Co-Supervisor
Dr. Ali Dolatabadi

Approved by: _____
Dr. Ivan Contreras, Graduate Program Director

August 26, 2019

Dr. Amir Asif, Dean
Gina Cody Faculty of Engineering and Computer Science

ABSTRACT

Diagnostic Methods and Parameters to Characterize Droplets and Particles in Suspension Plasma Spray

Ali Akbarnozari, Ph.D.

Concordia University, 2019

Suspension plasma spray (SPS) is an emerging coating process for making surfaces with superior properties. In the SPS process, ceramic particles are mixed with water or ethanol to form a suspension. A plasma torch provides the heat and momentum to evaporate liquid phase of the injected suspension, melt the coating particles, propel the in-flight particles toward a substrate, and eventually form a coating layer. However, the SPS process relies strongly on the coupon test and trials to find optimum spray conditions for plasma, suspension injection, and substrate location. At the end, an optimum spray condition set in a spray booth may not reproduce the same coating result in other booths. An effective control over the spray process improves the reproducibility of the spray conditions and consequently coating structures. Therefore, monitoring systems are employed to better understand and control the required spray condition. The monitoring included accessing state of droplets after the atomization of suspension and state of in-flight particles near the substrate. For further development of the SPS process, the suspension can be injected by an effervescent atomizer. This research aims to contribute in further improving the process and developing the diagnostic tools in SPS.

For a further improvement of the SPS process, an effervescent atomizer was investigated as an alternative way instead of the current methods of injection of the suspension in the plasma jet. Performance of the effervescent atomizer was investigated at room temperature by phase Doppler particle anemometry (PDPA). Size of droplets and shape of the atomized spray in a crossflow configuration was almost independent of the suspension concentration. Size of droplets depends on the atomization at the exit of the orifice and the breakup in the crossflow. Velocity of

droplets at downstream is the velocity of the crossflow. It was found that the shape of spray was conserved in the crossflow and relatively smaller droplets were enveloped by the larger droplets.

As a contribution to adapt a diagnostic system for SPS, a two-color pyrometer was modified and investigated to measure temperature of in-flight particles. The in-flight particles are released after evaporation of the liquid phase of suspension droplets. A high cooling rate of the in-flight particles in terms of distance from the torch and radiation of plasma are main challenges for temperature measurement. To remove these limitations, the temperature was measured by a single-point measurement system based on thermal emission which equipped by readjusted bandpass filtering. The result of online temperature and velocity measurement was in a good agreement with the offline validation by collecting the splats and analyzing the samples. Moreover, the measurement condition has an impact on temperature, and the impact can be minimized by elimination of the stray radiation.

As a fundamental research work to develop a diagnostic system for SPS, a light diffraction (LD) system was adapted and investigated to measure size of in-flight particles. Refraction of the laser in the measurement volume and radiation from plasma were two main challenges of the size measurement. A shield of an optimized aperture was employed to control the condition of measurement volume. By applying a narrow bandpass filter at a right wavelength and selecting a right angle to collect the scattered signal from the in-flight particles, the size of particles was measured. A good agreement between the result of online measurements under the plasma condition and studying the feedstock particles in the wet cell unit in the room condition validated the size measurement.

DEDICATION

Dedicated to my loving parents.

تقدیم به پدر و مادر عزیزم

ACKNOWLEDGEMENTS

I would like to express my greatest gratitude to my advisors Dr. Christian Moreau and Dr. Ali Dolatabadi. Thank you for giving me the chance to accompany you and your team for this research. Your advice, support, and patience have inspired me all the time in my research and in my life. It has been an honored working with you.

I wish to thank Dr. Fadhel Ben Ettouil and Dr. Shahin Amiri, members of Thermal Spray and Multiphase Flow Laboratory. Fadhel and Shahin, you have always supported me in this journey and the hardest times of the research were the nicest moments with you.

I am thankful to Mr. Gilles Huard and Mr. Robert Oliver for their help to prepare the experimental setups. Thank you, Ehsan, Hamed, Kourosh, Bishoy, Elham, Amr, Milad, Mehdi, Fariba, Alexandre, Siavash, Firoozeh, Saeid, and Morvarid, my friends in our group and Amir Hosein in the department of physics for constructive discussions and priceless help. I would like to thank to Mr. Luc Pouliot, Mr. Olivier Bomber, and their colleagues from Tecnar Automation to provide a measurement system and to help in doing experiments.

This work was financially supported by the Natural Science and Engineering Research Council of Canada (NSERC), Canada Research Chairs program, and Tecnar automation.

I should extend my appreciation to my sisters Maryam, Laleh, Parvin and their families specially Shahin. Your endless love and support made it possible to start and reach to the end. Thank you Kasia for your kindness and accompaniment motivated me for writing the thesis. Thank you Reza for making cheerful moments during my stay in Montreal. My friends Karine, Sulé, Omid Kahbasi, and Diane, thank you for always being there for me to enjoy the moment and to finish strong.

Finally, I like to say the sincerest thanks to my parents, Massi and Ahmed, for their continuous support and unconditional love. You are extraordinary parents who have flourished my life and have encouraged me to get my goal.

TABLE OF CONTENTS

LIST OF FIGURES

LIST OF TABLES

List of Abbreviations

APS	Atmospheric plasma spray
SPS	Suspension plasma spray
FT	Fourier transforms
HVOF	High velocity oxy-fuel
LD	Light diffraction
PDPA	Phase Doppler particle analyzer
PIV	Particle image velocimetry
SEM	Scanning electron microscope
SNR	Signal-to-noise ratio
TBC	Thermal barrier coating
YSZ	Yttria stabilized zirconia

CHAPTER 1. INTRODUCTION

Thermal spray coatings have opened new horizons in industry to produce materials more resistant to extreme working conditions. All started by Maximilian Ulrich Schoop who introduced thermal spray in 1909 [1]. Technically, thermal spray is the process for coating common materials such as metals or alloys by spraying molten or semi-molten metallic or ceramics powders to form a protective layer against erosive, corrosive, and/or hot working conditions [2]. The thermal spray processes are categorized based on the type of heat sources. As an example, in atmospheric plasma spray (APS), a high powder electric arc is established between an anode and cathode in a mixture of argon, helium, or other gases forming a high-temperature plasma jet, which provides momentum and heat to the coating particles. APS is widely used to make thermal barrier coating (TBC), corrosion-resistance surfaces [3] , biomedical prosthesis [4], and many more applications [5-7]. In this process, coating particles of 10 – 100 μm are injected by a carrier gas into the plasma jet. Recently, spraying of finer particles was used to produce coatings with unique microstructures. In fact, this process was called suspension plasma spray (SPS) in which the particles of 0.5 – 5.0 μm are released into the hot plasma by a liquid carrier. However, the complexity of SPS and number of effective parameters [8] necessitate a continuous monitoring of the process. Online monitoring is a technique to make repeatable, reproducible, and reliable coatings. There are significant challenges and technical limitations for any measurement of particle properties such as size, velocity, or temperature in the thermal spray processes [9]. Some examples of these challenges are plasma radiation, turbulent flow, a high level of noise light, and micro-size of particles. Therefore, a diagnostic system should be adapted to the measurement condition. For example, robust systems were developed to measurement the particle parameters in the APS process [10]. A similar system hasn't been developed for SPS at the time of writing this thesis. This chapter introduces the SPS process, characterization methods, importance and challenges of online measurement, objective of the thesis, and organization of the thesis.

1.1.Suspension Plasma Spray

SPS is a coating process in which a suspension carrier releases the fine particles into a plasma jet to produce a coating layer on a substrate [11,12]. A typical suspension is composed of around 20 weight percent particles such as metal oxides or alloys and around 80 weight percent liquid such as water or ethanol. The suspension can be introduced into the plasma radially or axially where it releases the particles. Figure 1.1 shows a schematic of a typical SPS process. The plasma gas is made typically of a mixture of argon with helium or hydrogen. The plasma gas is heated by a high-current electrical arc between the anode and cathode inside the torch. The plasma leaves the torch at high temperature and high velocity. The heat of plasma melts the in-flight particles. The high-velocity plasma flow accelerates the in-flight particles toward the substrate. The molten particles impinge to the substrate and spread over it to form splats. Accumulation of splats on the substrate form the coating layer. Fauchais et al. [13] revisited opportunities in SPS included coatings with lower thermal diffusivity, higher hardness, and higher toughness. One of the main advantages of SPS is to produce a unique microstructure with a wide range of porosity and thickness. A nanostructure with fine pores can be produced because of fine size of coating particles [14]. Also, a very thin dense coating can be produced by the same powder under different conditions. However, Fauchais et al [15] summarized some limitations in the SPS process such as the transfer of micro- or nanometer-sized particles in plasma jets, influence of suspension characteristics, and interaction between the plasma and liquid. Limitations of SPS related to the injection of coating particles into the plasma was highlighted also on in another study [13]. In addition to that, clogging of the injector is a common issue during SPS. In the next part, the injection of suspension is explained in more detail.

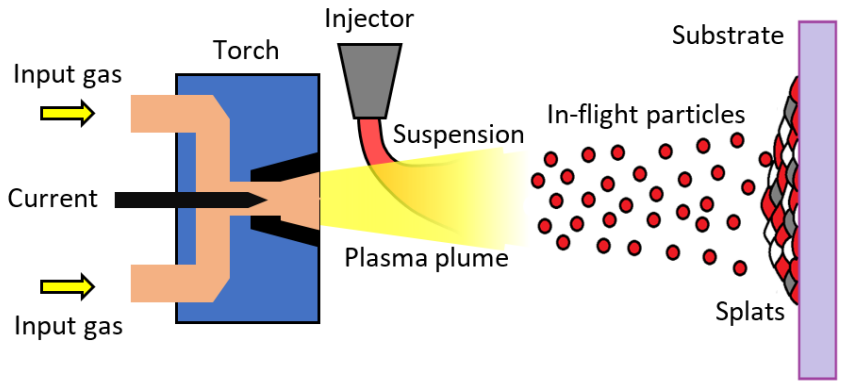

Figure 1.1. Schematics of SPS process showing the plasma plume, injector, and substrate

1.1.1. Spray Atomization

The suspension is introduced to the plasma plume in the form of a liquid jet or atomized spray. In SPS, when a suspension jet is used, it is atomized by the plasma plume into droplets. In both configurations, the droplets are evaporated by the high-temperature plasma plume releasing the coating particles [16].

Figure 1.2 shows a jet injector which is the common method of injection used SPS (left image) and the effervescent atomizer suggested as an alternation injection method to further development of SPS (right image). In the first method, the gas flow perpendicular to the column of liquid causes propagation of instabilities on the surface of liquid. As a result, the liquid column turns into finger-shape ligaments. Further propagation of instability breaks up the ligaments into large droplets. Continuing toward downstream, the large droplets break up into smaller droplets. Instead of injecting a liquid jet, the suspension can be injected into the plasma plume by using an atomizer. Esfarajani and Dolatabadi [17] modeled the flow of suspension in effervescent atomizer and they showed a reduced dependency of internal flow to the solid concentration. In effervescent atomizers, the atomizing gas is injected in the liquid before exiting the atomizer [18,19]. Therefore, a gas bubble is formed and bursts at the exit and causes instabilities in the liquid. As observed in the liquid jet configuration, ligaments and large droplets form before the formation of smaller droplets. The next step in SPS is to separate the coating particles from the liquid and prepare the particles to make a coating. Forces such as inertial force, aerodynamic force, viscous force, and surface tension are dominant forces that control the atomization of liquid. The Weber number (We)

is the ratio of aerodynamic and surface tension forces ($We = \rho_l\, u_l^2\, d_d/\sigma$) which indicates the tendency of liquid for breakup. Ohnesorge number (Oh), the ratio of viscous and surface tension forces ($Oh = \mu_l/\sqrt{\rho_l\, d_d\, \sigma}$), shows the resistance of liquid to breakup. Momentum Flux ratio is the ratio of liquid momentum over the momentum of transverse gas ($q = \rho_l\, u_l^2/\rho_g\, u_g^2$). The momentum flux ratio of effervescent atomizer is defined either in terms of a liquid jet at specific GLR [20] or in terms of surface area of an aerated atomizer [21] which the first definition was used in this study to reduce the complexity of calculations.

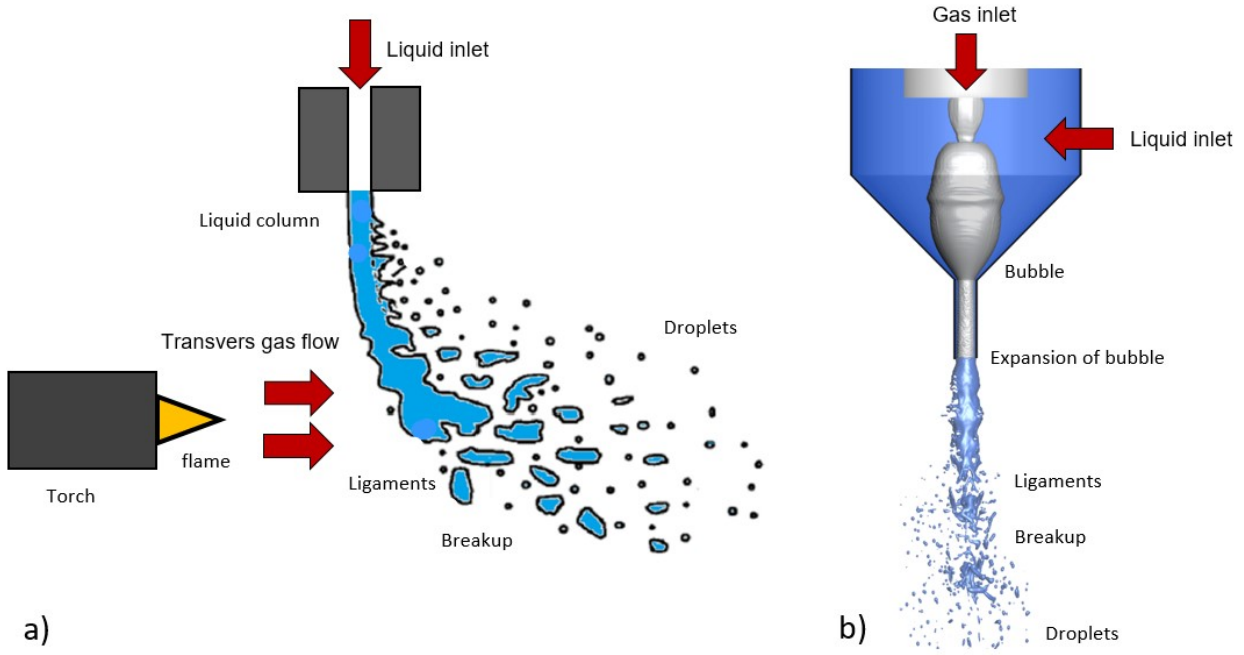

Figure 1.2. Injection of liquid to generate droplets by introducing (left) a liquid column in transverse flow and (right) by an effervescent atomizer

1.1.2. Evolution of Droplet

Suspension droplets have enough momentum to penetrate the plasma flow which it is not the case for submicron particles due to their low mass [22]. After penetration into the plasma flow, the suspension droplets are heated and accelerated by the high-temperature high-velocity gas flow. Figure 1.3 shows the evolution of droplets in SPS where the plasma flow can break up the droplets in smaller ones. Within a few microseconds, the plasma provides enough heat to evaporate the liquid phase of the suspension [22]. During the evaporation, the particles get closer and finally agglomerate together after complete evaporation of the liquid. Then the heat of plasma melts the

particles thoroughly. Then, the momentum of flow drags particles toward the substrate. The size of agglomerated molten particles is generally different from the original size of feedstock material which is used to make the suspension. Further toward the substrate, the size of in-flight particles is prone to change because of evaporation. Finally, each particle impinges on the substrate, spreads over the surface, cools down, and produces a disc-shaped splat [23]. Accumulation of splats on the substrate builds a coating layer. Characteristics of in-flight particles such as size, velocity, and temperature right before impingement have a strong influence on the microstructure and properties of the deposited coating.

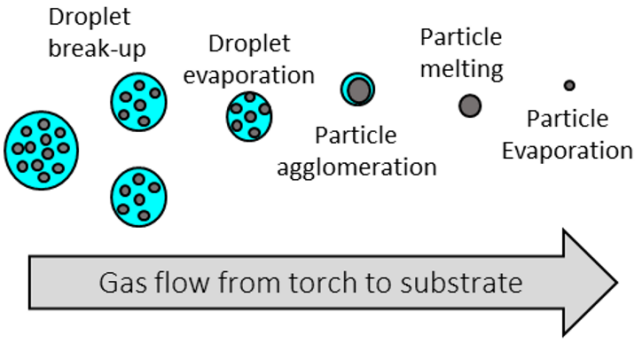

Figure 1.3. Schematic showing the phenomena involved in the suspension plasma spray process

In-flight particles impinge on the substrate and make the coating. Figure 1.4 shows a typical SPS microstructure called the columnar or cauliflower structure which resulted from the shadow effect. To explain more, the particle trajectory near the substrate depends on the particle size and velocity. Since the velocity and size of the particles are interrelated, any change in the size of particle defines a new trajectory for the particles. At the impact, asperities on substrates is a base for relatively larger particles to deposit and make the columnar structure. Empty spaces between the columns can be filled with the relatively smaller particles that followed the gas flow parallel to the substrate. The resulting coating microstructure is formed generally of columns and pores.

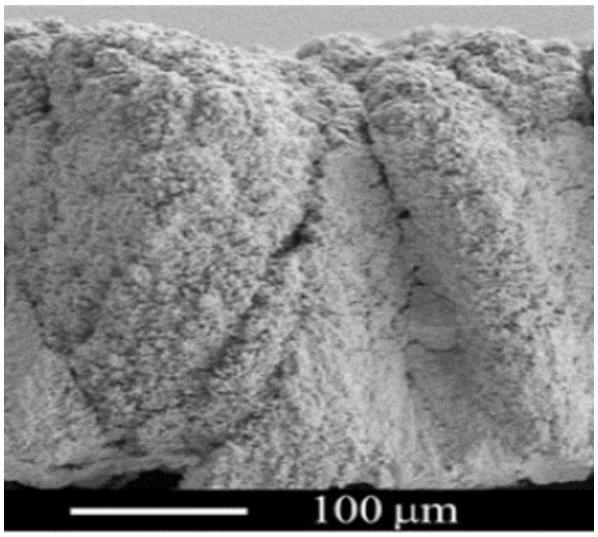

Figure 1.4. Shadow effect to form a typical columnar or cauliflower microstructure by SPS [24]

1.2. Online Process Monitoring

Online monitoring of in-flight particles supplies information that helps to produce coatings with the same desired properties in a consistent manner [25]. Monitoring of the process seems crucial for either well-established production lines like APS or processes in development like SPS. In SPS, for example, minor changes in flow rate of inlet plasma gas or changes in current applied to the torch result in different microstructures [26]. To elaborate more, it should be mentioned that microstructures of coating ultimately depends on characteristics of in-flight particles before the deposition on the substrate. The main characteristics of in-flight particles are their size, velocity, and temperature. However, they are difficult to predict from the actual spray conditions and, consequently should be measured online.

1.2.1. Importance of Online Measurement

Online measurement in SPS is necessary because the size, velocity, temperature, and trajectory of suspension droplets and in-flight particles continuously change [27]. The size of suspension droplets depends on the injection and spray conditions. For example, using a jet injector or an effervescent atomizer generates two different droplet size distributions. Furthermore, the size of suspension droplets has an impact on size of in-flight particles. In the previous section, for example, it was explained that the size of in-flight particles is different from the size of the feedstock material due to its agglomeration and evaporation. This change in size of particles is one

of the main reasons to monitor the particles during the process. As another example, the in-flight particles are cooled down rapidly as they travel away from the torch. It is worth mentioning that the cooling rate of particles in SPS is higher than that in APS due to their smaller size. Thus, a change in particle size can lead to change in temperature. As a final example, Figure 1.5 shows that the normal velocity of in-flight particles near the substrate changes significantly as a function of their size [28]. The normal velocity of a particle near a substrate was calculated for particles between 1 and 40 µm with an initial velocity of 400 m/s. As shown in Figure 1.5, the normal velocity for a particle of 40 µm does not change significantly with the distance to the substrate and is still around 400 m/s close to the substrate. However, the velocity of a 1-µm particle reduces to around zero for the same initial velocity. Normal velocity and trajectory of particles near the substrate influence directly the coating microstructure. These examples confirm the importance of online particle monitoring of size and velocity in SPS. However, there are some challenges for online measurement throughout the process.

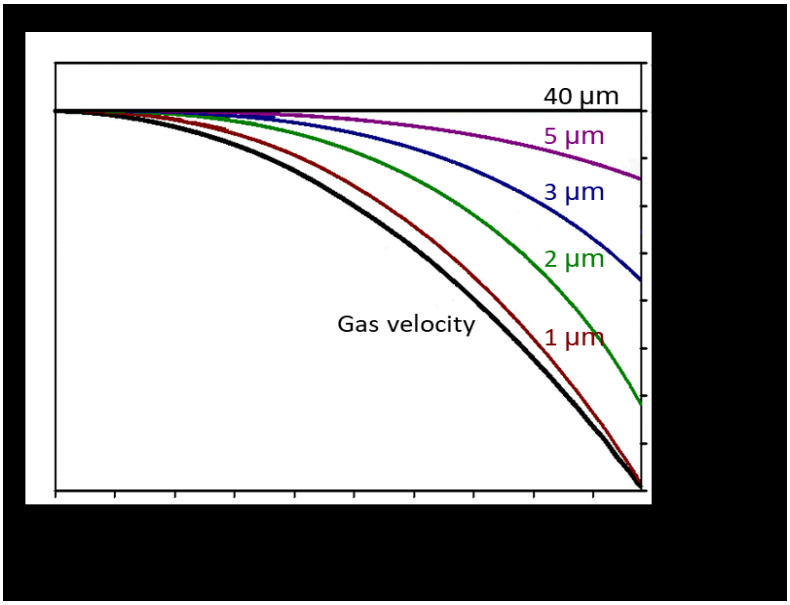

Figure 1.5. Normal velocity of an in-flight particle near the substrate as a function of the particle size [28]

1.2.2. Challenges and Limitations of Measurement

A successful measurement depends on dealing adequately with challenges to capture a distinctive signal from target droplets or particles in the measurement volume disturbed by noises.

Some limitations of the SPS process and monitoring were discussed in past studies [9,15]. These limitations include mostly the measurement of size and temperature of in-flight particles. More specifically, low intensity of a signal from the particles compared to high intensity of noise, refraction of light, radiation from plasma, turbulent flow, and limitation of characterization systems are the major challenges for the size measurement of in-flight particles. Now each of the listed challenges is explained in more detail. First, the plasma spray is a harsh environment where temperature is high, plasma radiation [29] and reflection are propagated in all directions around the torch. There is a turbulent flow of gas loaded with powders. In this respect, non-intrusive measurement systems such as imaging and optical systems are more practical for particle characterization. For a successful measurement of size by an optical system, the plasma radiation at the measurement volume should be minimized. This can also be the case for the measurement of temperature by a thermal emission method. Knowing that the optical signal from a particle reduces as the particles are smaller, signal from micron and submicron size particles should have minimum intensity to be recognized by a measurement system. As suspension droplets in the plasma are concerned, contained particles and the medium conditions make challenges find optical properties of the droplets and consequently a challenge for using diagnostic systems [30]. Moreover, a hot gas flow and temperature gradient can disturb an ideal condition for measurement.

1.3.Literature Review

1.3.1. Spray Characterization

Characterization of droplets and in-flight particles in SPS needs to be ameliorated. Research in this area has already started. Pawlowski [31] performed an intensive study on the injection of a suspension by a jet injector and a twin-flow atomizer. Generally, the suspension is transported from the feedstock reservoirs to the injector by either a peristaltic pump or by a pneumatic pump as shown in Figure 1.6. Fauchais et al. [32,33] studied the behavior of the suspension and plasma-suspension interactions by a shadowgraph technique (Figure 1.7) and particle imaging velocimetry (PIV) in SPS. Marchand et al. [34,35] studied the spray and droplets generated from axial injection from a twin-fluid atomizer during the SPS process.

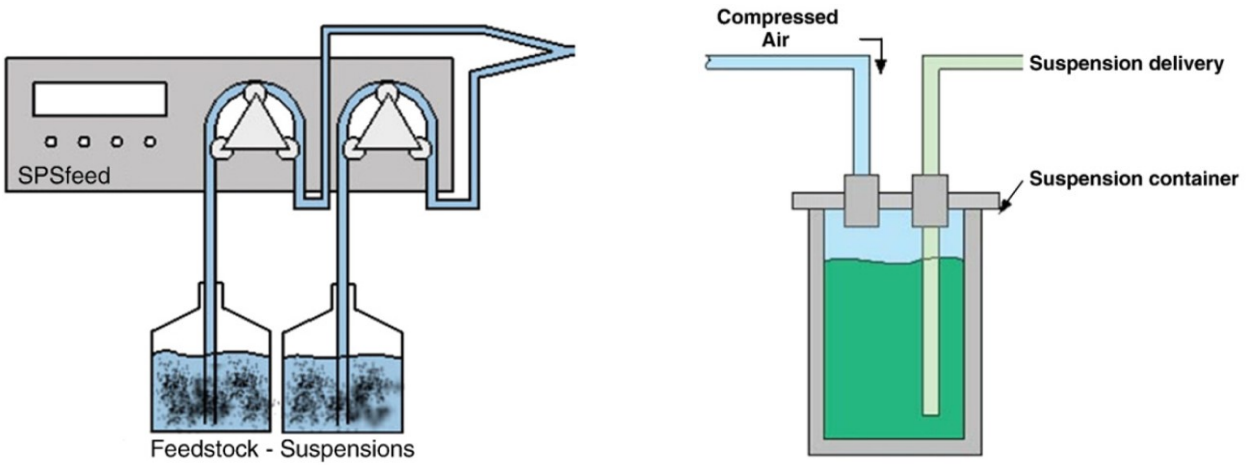

Figure 1.6. Suspension injection system in SPS (left) peristaltic pumps and (right) pneumatic pump [31]

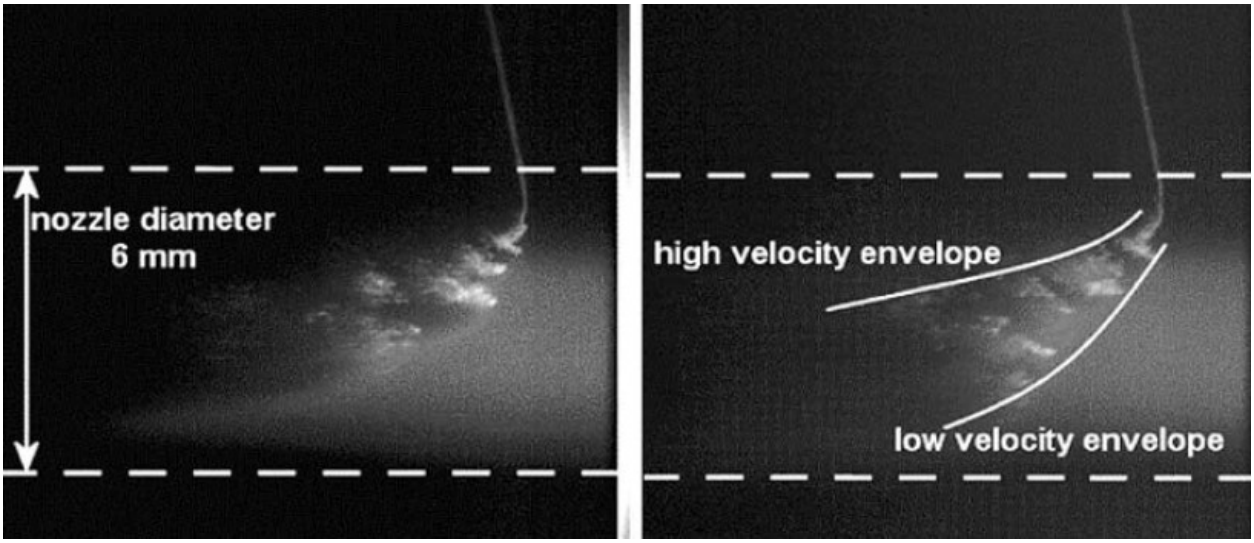

Figure 1.7. Shadowgraph of typical plasma-suspension interaction and boundaries of suspension in crossflow from the torch (high and low velocity envelope)[33]

Although the effervescent atomizer has not been used in thermal spray, it was characterized in different studies. Santangelo and Sojka [36] investigated the near-nozzle flow from an effervescent atomizer. According to their studies, the annular liquid breaks up to ligaments and eventually to droplets at the periphery when the gas at the core of flow was rapidly expanded as shown in Figure 1.8. This phenomenon situates small droplets at the center of spray and large droplets at the periphery.

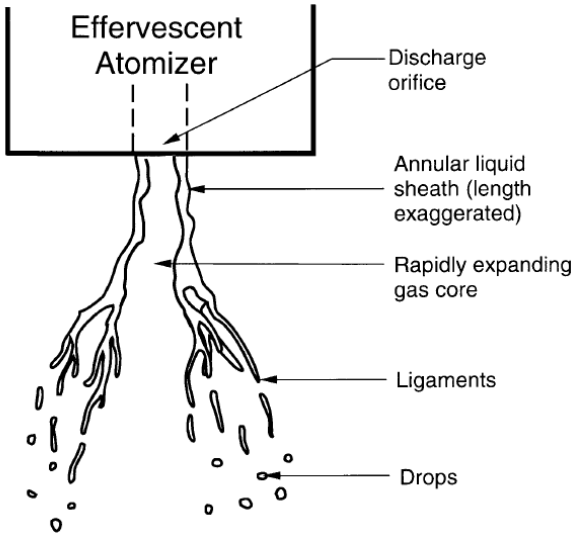

Figure 1.8. Near-nozzle flow from an effervescent atomizer, the annular flow at the periphery and rapidly expanding gas core resulted ligaments and droplets [36]

Sovani et al. [37] reviewed the effect of the liquid rheological properties on the characteristics of droplets, mainly on the Sauter mean diameter (SMD) of droplets. Figure 1.9 shows the change of the droplet SMD as a function of the GLR and injection pressure [38]. Lund et al. [39] investigated the effect of viscosity and surface tension of the liquid on the SMD in terms of GLR as shown in Figure 1.10. They reported that the SMD reduces slightly as a function of viscosity and GLR. However, the surface tension had a more significant effect on the droplet size. At a similar viscosity, the SMD reduces by increasing the surface tension. Mahesh et al. [40] showed that the effervescent atomizer has a great potential for injection with high mass flow rates. Fang Zhao et al. [41] reviewed applications of effervescent atomizers in gas turbine combustors, boilers, and mist-fire suppression. Design and characterization of new effervescent atomizers were carried out by different investigators such as Zeremba et al. [42] and Liu et al. [43]. The main issue of using an effervescent atomizer is to generate a steady spray. Sun et al. [44] investigated the internal and external flow pattern of an effervescent atomizer and they concluded that the internal flow had a great effect on the fluctuation of spray. Wittner et al. [45] reported steadiness of spray generated from the effervescent atomizer was better for liquids with higher viscosities.

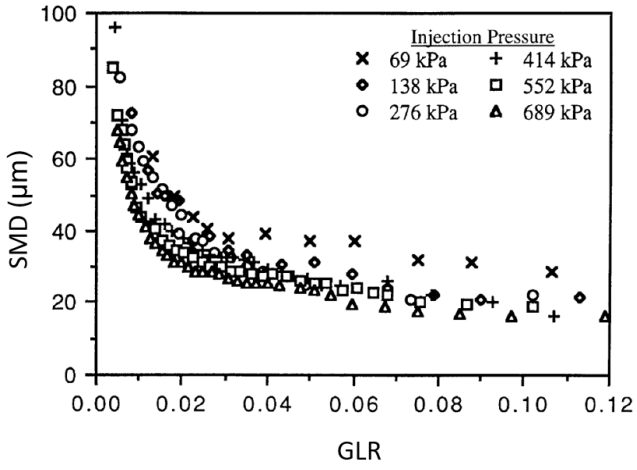

Figure 1.9. Variation of Sauter mean diameter (SMD) with injection pressure and GLR studied by Whitlow et al. [38]

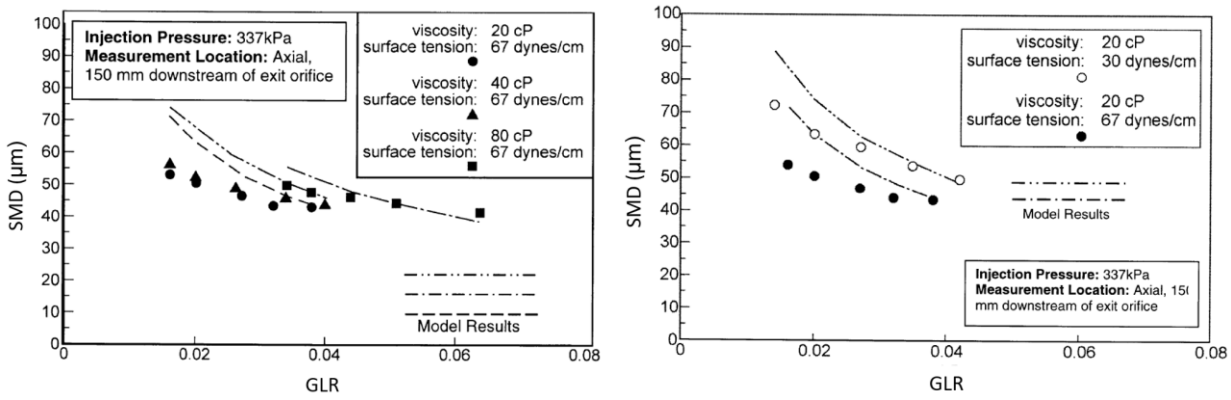

Figure 1.10. Influence of viscosity (left) and surface tension (right) on SMD as a function of GLR studied by Lund et al. [39]

Hrishikesh et al. [46] studied the mass distribution of a spray from an effervescent atomizer and showed that the mass distribution was maximum at the centerline. In fact, the maximum mass distribution at the centerline should be favorable for SPS applications. In addition, dependency of the spray characteristics generated by the effervescent atomizer to the rheological properties of suspensions was investigated [47]. The result showed that the performance of the effervescent atomizer is almost independent of viscosity of the suspension. Moreover, Ochowiak et al. [48] used an effervescent atomizer to spray the solutions of a polymer having non-Newtonian characteristics. Their result indicated that the risk of clogging at the exit of the atomizer during the injection of suspension is considerably reduced because of its large orifice size. Moreover, penetration length of spray from the effervescent atomizer was investigated by Fan et al. [49].

They showed that suspension atomized with an effervescent nozzle can penetrate a crossflow. The majority of the studies on characterization of the effervescent atomizer were carried out with water, or with a mixture of two or more liquids [50]. There were limited studies on the spray of suspension created by an effervescent atomizer in crossflow. In this area, Saleh et al. [51] investigated trajectory and penetration of suspension in terms of gas to liquid ratio and momentum flux ratio at room temperature near the exit of the atomizer as shown in Figure 1.11. Studying droplets to characterize the spray of an effervescent atomizer in the SPS process was not found in previous studies.

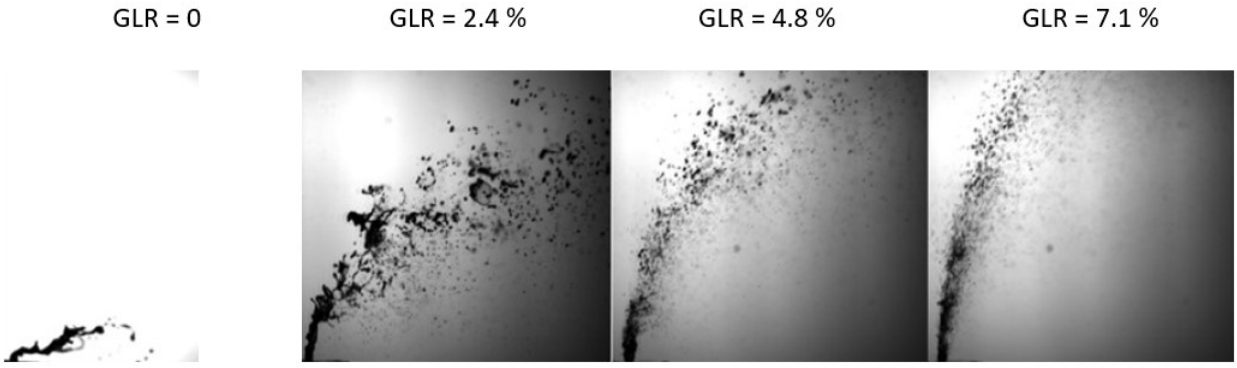

Figure 1.11. Trajectory and penetration of 5wt% glass suspension sprayed by the effervescent atomizer in crossflow at GLR from 0 to 7% [52]

1.3.2. Temperature Measurement

Online characterization of in-flight particles has been carried out with different methods in plasma spray processes. Temperature measurement of in-flight particles was first investigated in the works of Vardelle et al. [53], Mishin et al. [54], Fincke et al. [55,56] , Coulombe and Boulos [57] , Solonenko [58], and Moreau et al. [59-62]. However, most of these methods were designed for APS process or they were not adapted to the SPS conditions. Fauchais et al. [63] and Mauer et al. [64,65] reviewed research and development of diagnostic systems of in-flight particles and they tabulated the methods in terms of measurement of temperature, velocity, size, number density, and shape. DPV 2000 (Tecnar Automation Ltd., St. Bruno, Canada) is a leading commercialized diagnostic system that measures velocity, size, and temperature of in-flight particles in different thermal spray processes. It is based on a single-counting measurement with a two-slit mask at the tip of an optical fiber in the sensor head to characterize particles between 10 and 100 μm. It has a two-color pyrometer to measure temperature. Each particle in the measurement volume sends an

optical signal with two peaks that is used to determine the velocity of the particle (time-of-flight measurement) as shown in Figure 1.12.

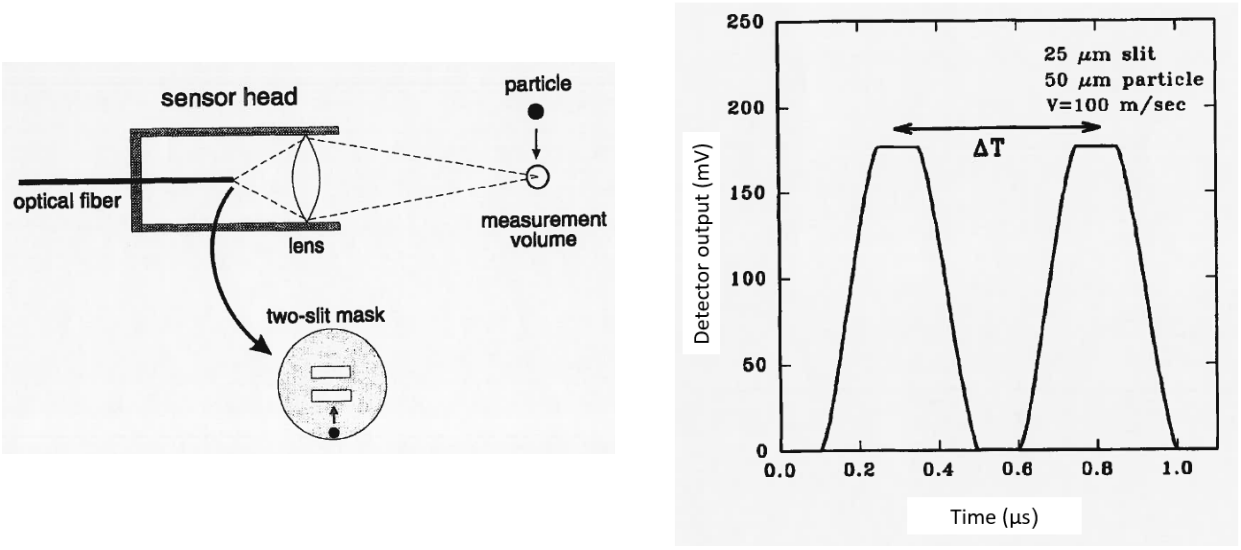

Figure 1.12. (Left) DPV 2000 sensor head and (right) theoretical optical signal for a 50 μm particle passing at 100 m/s in the measurement volume [60]

AccuraSpray (Tecnar Automation Ltd., St. Bruno, Canada) is a characterization system, based on works by Moreau et al. [66], which is designed to measure the temperature and velocity of in-flight particles in spray processes. An imaging diagnostic system was developed based on works of Vattulainen et al. [67] and commercialized as SprayWatch (Oseir Ltd., Tampere, Finland). This system measures the particle temperature from long-exposure-time images for two-color pyrometry and the particle velocity by the length of the particle streaks as shown in Figure 1.13. ThermaViz [68,69] (Stratonics Inc., CA, USA) is a two-wavelength imaging pyrometer to measure temperature. Based on the two-color pyrometry, the In-flight Particle Pyrometer (IPP) was developed based on the work of Swank et al. at Idaho National Engineering Laboratory. Wroblewski et al. [70] discussed correlating temperature of particles to the molten volume flux across the plume. Mauer et al. compared AccuraSpray with the DPV-2000 for APS powders and they found good agreement between the measured temperatures of in-flight particles by both systems [71]. All of these diagnostic systems are designed for particle diagnosis in thermal spray processes in general but not for SPS that relies on much smaller in-flight particles (0.5- 5 μm). Among them, AccuraSpray was used to study temperature and velocity of in-flight particles

in SPS [72]. However, the possibilities and limitations of these measurements need to be better studied in SPS conditions.

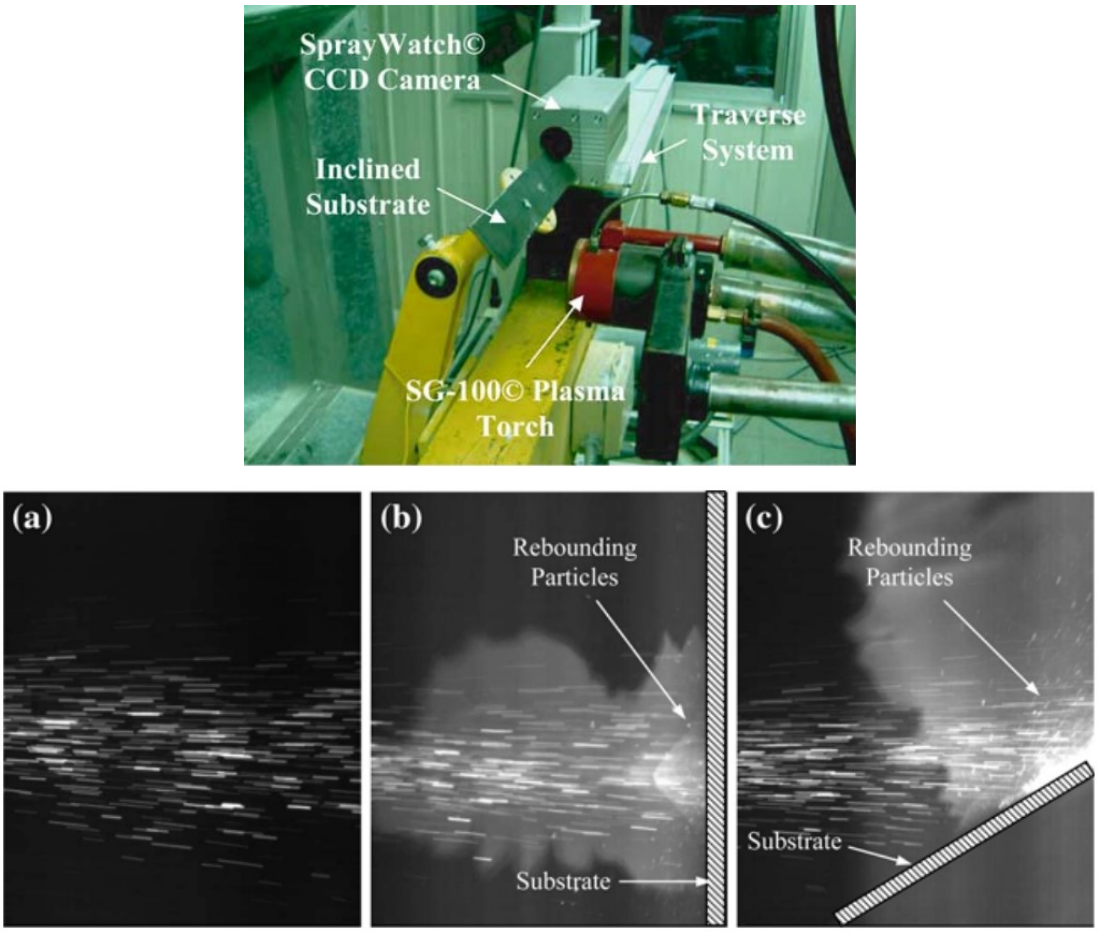

Figure 1.13. SprayWatch (Oseir Ltd., Tampere, Finland) (top) the test setup for measurement (bottom) imaging results for (a) freestream, (b) perpendicular substrate, and (c) inclined substrate [73]

1.3.3. Size Measurement

The pioneers in development of diagnostic systems mentioned for temperature measurement like Vardelle et al. [53], Mishin et al. [54], Fincke et al. [55,56] , Coulombe and Boulos [57] , Solonenko [58], and Moreau et al. [59-62] studied particle size measurement as well. Moreau et al. [74] explained how the monitoring the spray process provided a tool to control coating properties in research centers and on the production floors. Mauer et al. [64,65] reviewed DPV 2000, SprayWatch, Laser Doppler Anemometry (LDA), Phase Doppler Anemometry (PDA), and particle shape imaging (PSI) as the devices to measure size of in-light particle in the APS

process. Zimmermann et al. [75] compared Accuraspray and LDA for velocity measurement of in-flight particles. Regarding the size, Cetegen et al. [76] measured the diameter of the particles by Phase Doppler Particle analyzer (PDPA) in the APS process. In addition to optical methods, there were some research to measure the size of in-flight particles through imaging techniques such as: Particle Shape Imaging (PSI) based on works by Zimmermann et al. [77] and Landes [78]. Figure 1.14 shows the PSI and a typical measurement result. They used a double-laser technique and superposition of images of particles at the measurement volume to improve characterization of particles from the acquired images.

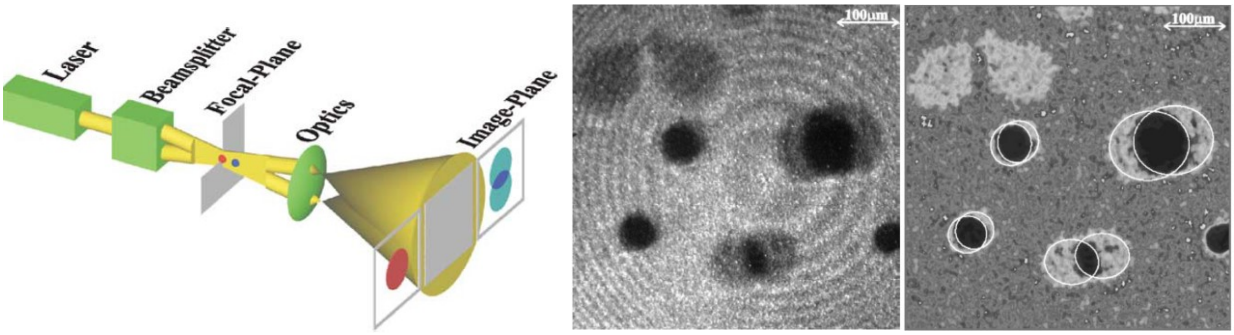

Figure 1.14. Particle Shape Imaging (PSI) (left) double-laser beam illumination technique with an image of particles in the focal plane in red and an image of particles out of the focal plane in blue (middle) raw image on the camera, and (right) the corrected image [77]

In another example, Wroblewski et al. [70] estimated the size of particles by using CCD arrays and applying topological criteria. In all available diagnostic systems except for PDPA, size of particles with a diameter smaller than 5 µm was not achieved [64] and fine particles of SPS were not able to be recognized. For a particular case, Rampon et al. [79] reported the use of a Laser Diffraction (LD) method to measure the droplet size of the YSZ suspension and in-flight particles. Their results of size distribution required to be validated. In addition to online characterization, offline characterization of in-flight particles was carried out by collecting the particles on a substrate or in water. McDonald et al. [80] carried out splat studies and temperature measurement for the APS process. As an offline characterization method, Delbos et al. [23] sampled in-flight particles on a glass lamella at the tip of a moving pendulum and they measured the diameter of collected splats by Atomic Force Microscopy (AFM). Zeng et al. [81] collected in-flight particles in liquid nitrogen for further analysis during the APS process. Tarasi et al. [82] took samples of in-flight particles of alumina-zirconia collected in water and determined the average size in

scanning electron microscope (SEM) micrographs as shown in Figure 1.15. Aubignat et al. [83,84] studied online droplets of alumina suspension generated by a twin-fluid atomizer and they collected the in-flight particles on the substrate for SEM analysis and size measurement. Keeping the limitations and previous research in mind, the next section introduces several methods for particle characterization with their limitations and the current state of research.

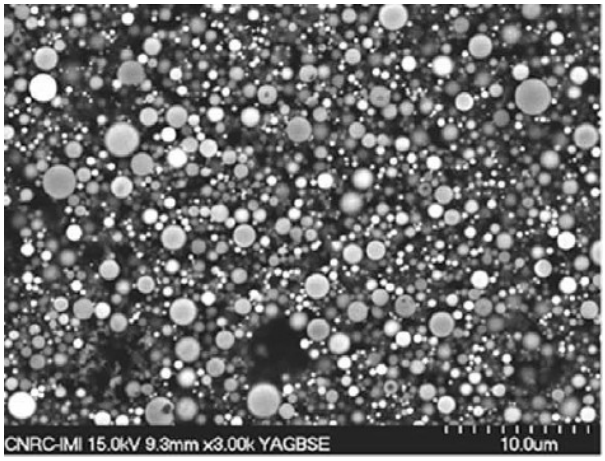

Figure 1.15. SEM micrograph of the in-flight particles collected in water during the SPS process [82]

1.4.Characterization Methods

Diverse measurement techniques for characterization of particles were developed and improved in the last decades [85-87]. However, each of them can provide reliable result for specific applications and measurement conditions. Therefore, some measurement techniques were selected for this research as they were compatible with the SPS conditions and they could provide reliable results. Imaging and light scattering methods [88] are used to measure size and velocity of fine droplets and particles whereas thermal radiation is employed to measure temperature [89] as shown in Figure 1.16. Generally, these techniques can be categorized in two classes: single-particle measurement and ensemble measurement. In single-particle measurement, each particle is detected and characterized separately from the others. In ensemble measurement, signals from a group of particles are used for characterization. Also, the single particle counting provides local information of a spray and the ensemble measurement reveals an average information in a more global scale. As an example, phase Doppler particle analyzer (PDPA) is a single particle counting and light diffraction method is an ensemble measurement. PDPA measures the size and velocity of moving

droplets or particles and light diffraction is used to measure size. Finally, thermal radiation emitted by an ensemble of particles can be collected and analyzed to measure the temperature of this particle ensemble. The basic knowledge of working principle of these systems is essential to conduct a reasonable and reliable measurement.

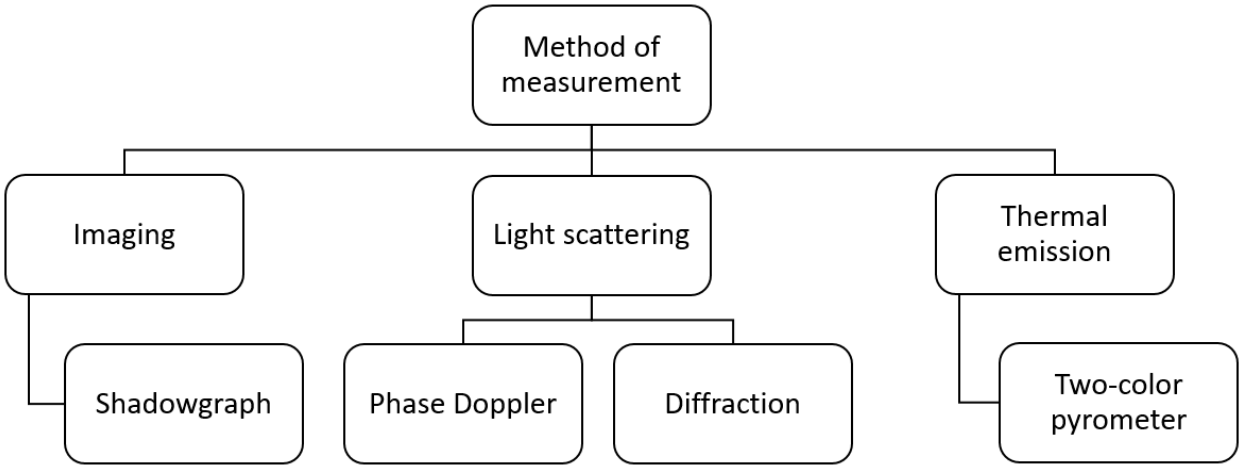

Figure 1.16. Methods applied for characterization of suspension droplets and in-flight particles

1.4.1. Phase Doppler Particles Analyzer

A detailed description of the PDPA technique was given by Bachalo et al. [90,91] . Figure 1.17 shows a schematic of PDPA which includes a laser source to illuminate the particles and a detector to receive the scattered signal from the particles. Two laser beams issued from the same laser are recombined at the focal distance of the lens and they make a measurement volume of bright-dark fringes. This method is based on the laser signal scattered from the particles moving in the measurement volume through the series of bright and dark lines. The amplitude modulation of the scattered light can be interpreted as the beating between the two beams scattered at slightly different wavelengths (Doppler shift). The droplet velocity is computed directly from the Doppler shift frequency of the captured signal. The droplet size is calculated from the same signal captured from three detectors. Using the three detectors eliminates the problem of ambiguity in the measurement. The droplet size was measured from the small phase difference between the signals of two different detectors where d_p is the particle diameter, m is relative refractive index, ψ is the angle between detector A, B, and C, θ is the angle between the laser beams.

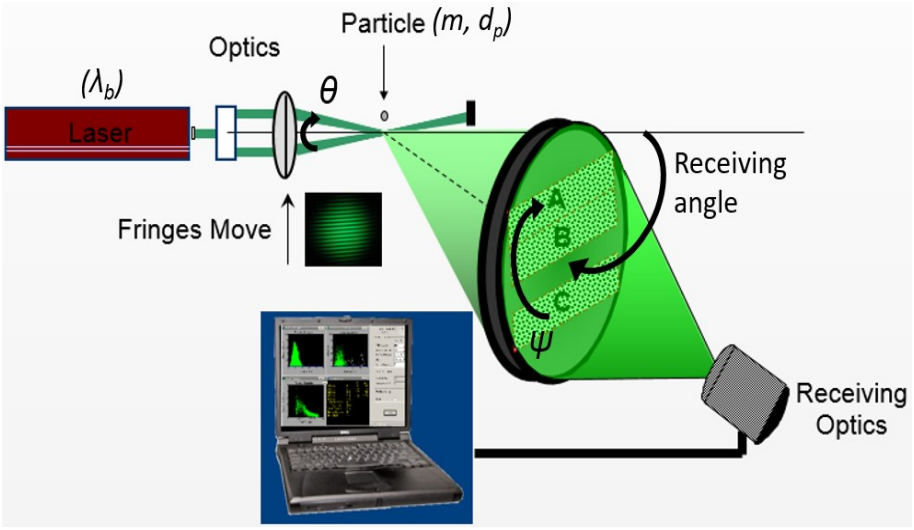

Figure 1.17. Schematics of PDPA for characterization of a moving particle [92]

Albrecht et al. [93] explained in detail how size of droplets is calculated from a phase shift of signals between two detectors (receivers) of the PDPA. Figure 1.18 shows the spatial arrangement of laser beams and receivers in PDPA. The phase shift of the signal, as a result of passing of a droplet into the measurement volume, is a function of the angle between the laser beam *(θ)*, the off-axis angle of the receivers to direction of the laser beam *(ϕ)*, and the elevation angle of the receivers *(ψ)*. A phase Doppler system measures the phase shift of the signal and the droplet size is calculated from the phase change between the receiver 1 and receiver 2 ($\Delta\Phi_{12}$) by Eq 1.1. However, it is required to have two phase changes to remove ambiguity to calculate the droplet size. Therefore, the same equation is used for the receiver 1 and the other receiver (receiver 3) which is only in a different elevation angle ($\Delta\Phi_{13}$).

$$\Delta\Phi_{12} = \frac{4\pi}{\lambda_b} d_P \left(\sqrt{1 + m^2 - m\sqrt{2}\sqrt{1 + \sin\Psi_r \sin{}^{\theta}/_{2} + \cos\Psi_r \cos\phi_r \cos{}^{\theta}/_{2}}} \right. \quad \text{Eq. 1.1}$$

$$\left. - \sqrt{1 + m^2 - m\sqrt{2}\sqrt{1 - \sin\Psi_r \sin{}^{\theta}/_{2} + \cos\Psi_r \cos\phi_r \cos{}^{\theta}/_{2}}} \right)$$

Where d_p and m are particle size and relative index of refraction respectively.

$$m = \frac{n_P}{n_m} \qquad \text{Eq. 1.2}$$

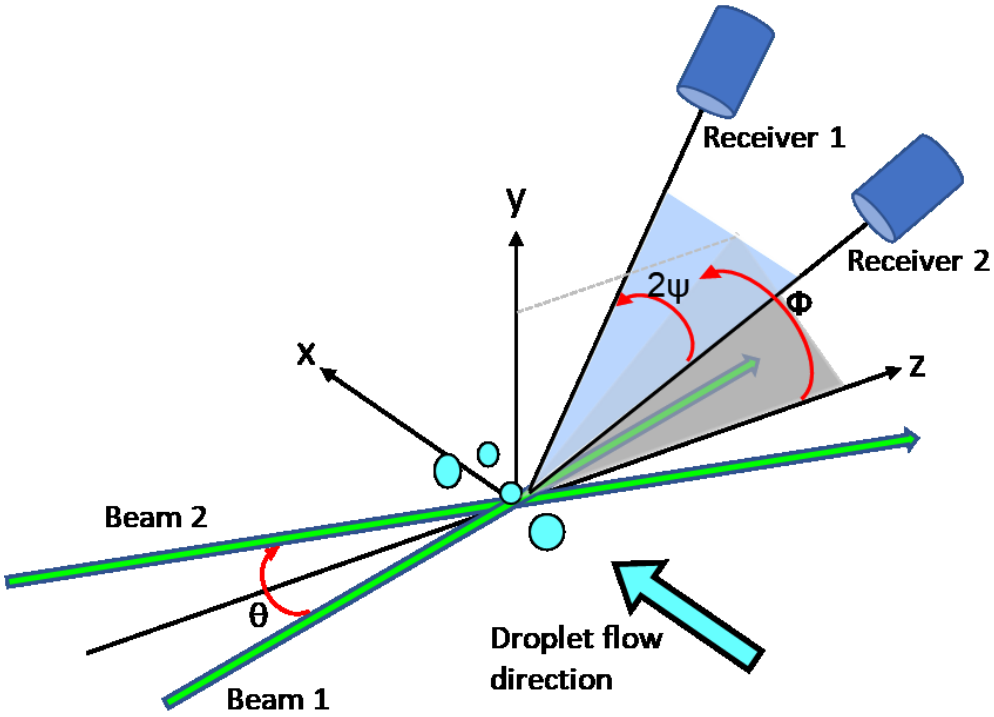

Figure 1.18 Schematics of optical component arrangements for phase Doppler method [93]

and n_p and n_m are indices of refraction for particles and medium, respectively. All the mentioned angles for studying water and suspension droplets were the same and the only difference was relative index of refraction. McClymer [94] provided a summary of literature for calculation of index of refraction for suspension.

1.4.2. Thermal Emission

The thermal radiation from a body is a function of wavelength, emissivity, and temperature as explained by Planck's law [95]. As shown in Figure 1.19, the radiation at each wavelength increases with increasing temperature. There is a peak of radiation at each temperature which moves to shorter wavelengths with increasing temperature.

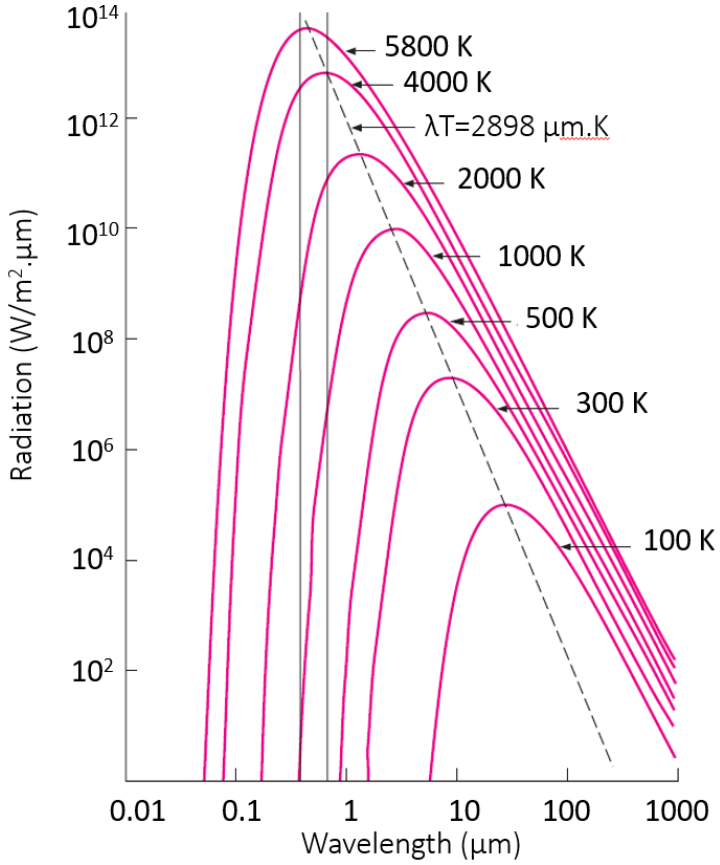

Figure 1.19. Radiation from the blackbody vs. wavelengths [96]

A real surface emits radiation equal to its emissivity times the radiation emitted by a blackbody. The spectral emissivity is generally a function of wavelength and temperature as given in Eq. 1.3.

$$\varepsilon_\lambda(\lambda, T) \equiv \frac{E_\lambda(\lambda, T)}{E_{\lambda,b}(\lambda, T)} \qquad \text{Eq. 1.3}$$

Where $E_\lambda(\lambda, T)$ and $E_{\lambda,b}(\lambda, T)$ are the emission of the real and blackbody surface, respectively. The temperature of particles can be measured by using a two-color pyrometer based on measurement of thermal radiation emitted at two distinct wavelengths. It is assumed that the target particle is a gray body which means that the emissivity is independent of the wavelength. Therefore, the term of emissivity is canceled in the Planck's law when it is written as the ratio of emission at two wavelengths at the same temperature. Figure 1.20 shows a schematic of the system to characterize target particles based on their thermal emission. The thermal radiation from the particles was divided in two parts. Each signal passes through a filter and finally reaches the

sensor. The transmission wavelengths of filters are different, and consequently the intensity of the signal in two detectors are different. As shown in Eq. 1.4 , the temperature of the target particles is calculated from the ratio of collected signals at the two wavelengths by applying Planck's law.

$$T = \frac{C_2(\lambda_1 - \lambda_2)}{\lambda_1 \lambda_2} \cdot \left[ln \frac{I_{\lambda_1}}{I_{\lambda_2}} + 5 ln \frac{\lambda_1}{\lambda_2} \right]^{-1} \qquad \text{Eq. 1.4}$$

Where C_2 is constant and $I_{\lambda 1}$ is the intensity of the signal at wavelength λ_1. Generally, the target particle is assumed to behave as a gray body to use the Planck's law.

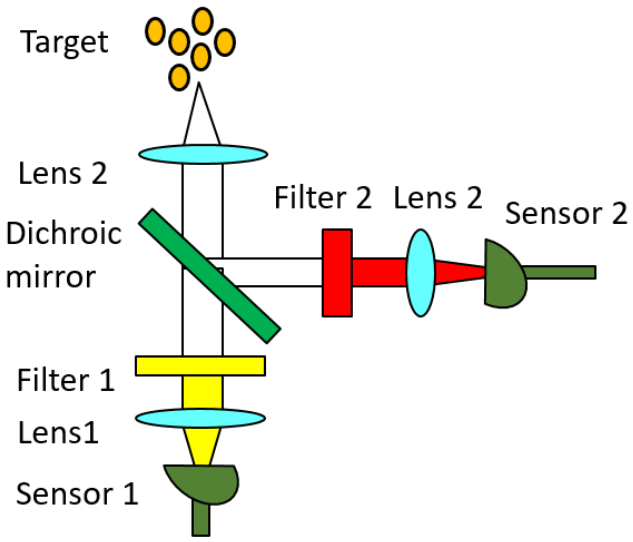

Figure 1.20. Schematics of thermal emission method for characterization of in-flight particles in plasma spray

There is an uncertainty in the measurement of temperature by a two-color pyrometer. A fundamental assumption for temperature measurement is that in-flight particles are gray bodies. However, emissivity at two wavelengths are not necessarily equal for real materials. Mauer et al. [97] studied temperature errors by deviations from the gray-body assumption in terms of temperature as shown in Figure 1.21. For example, 7.5 % difference between emissivity at two wavelengths ($\varepsilon_{\lambda 1}/\varepsilon_{\lambda 2} = 0.925$) results around 200 °C error for a measurement at 3000 °C. Touloukian and DeWitt [98] studied the thermal properties for a wide range of materials. Manara et al. [99] reported emittance of YSZ as a function of wavelengths which is a common material in

SPS. Therefore, deviation from gray-body assumption can be further studied by considering emissivity ratio at two wavelengths ($\varepsilon_{\lambda 1}/\varepsilon_{\lambda 2}$).

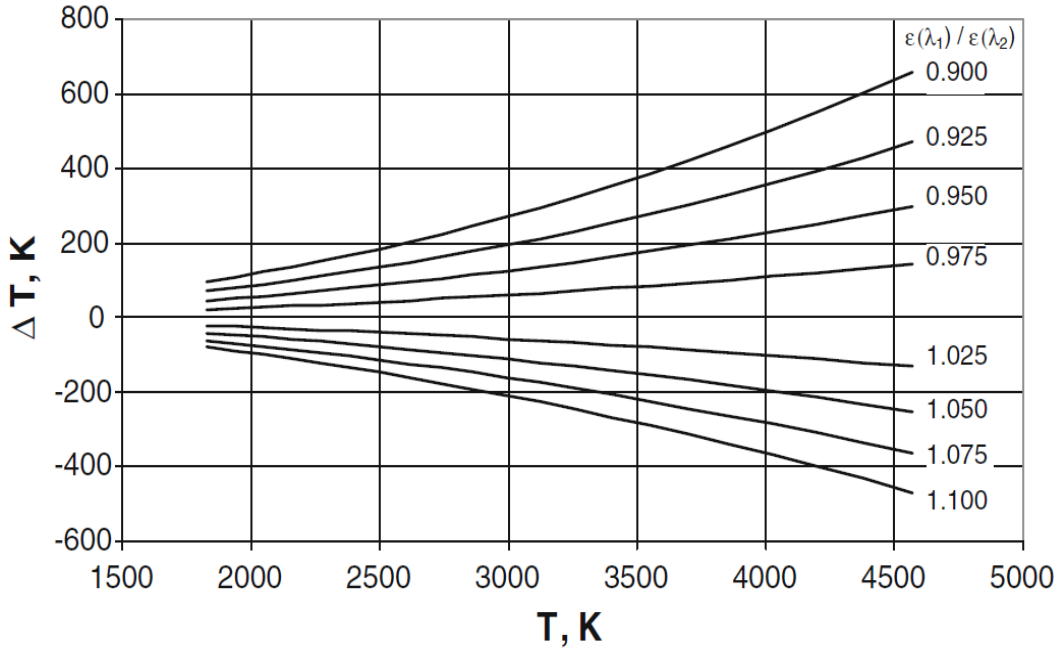

Figure 1.21. Temperature measurement error as function of emissivity ratios and absolute temperature [97]

The uncertainty of temperature measurement (ΔT) [100] arising from the unequal emissivity of $\varepsilon_1$and ε_2 at two wavelengths λ_1 and λ_2 is given according to Eq. 3.3.

$$c_2 \frac{\Delta T}{T^2} = \left(\frac{1}{\lambda_2} - \frac{1}{\lambda_1}\right)^{-1} ln\frac{\varepsilon_2}{\varepsilon_1} \qquad \text{Eq. 1.5}$$

where c and T are a constant and temperature, respectively. The uncertainty is minimum when the two wavelengths are close, and it increases as the separation between the two wavelengths increases. However, minimizing the uncertainty by choosing closer wavelengths reduces the sensitivity of a two-color pyrometer. Therefore, the wavelengths are selected in order to have a reasonable sensitivity to temperature variations with a reasonable level of uncertainty. It should be mentioned that the uncertainty which exists for the absolute temperature is much smaller for measuring relative temperatures (temperature variations). Therefore, the pyrometer based on the gray body assumption still provides a reliable relative temperature of in-flight particles.

1.4.3. Light Diffraction

Particle size measurement by the light diffraction approach [101] works based on Mie scattering theory [102], which states that the intensity of scattered light from a particle is a function of the particle size, shape, refractive index, wavelength and polarization of incident light, and observation angle (scattering angle) [103]. For known optical properties of the particles and surrounding medium, the size of the particles is calculated from measured scattering intensity by solving an inversion problem [104,105]. Figure 1.22 shows components of a light diffraction system composed of a laser and a detector array. The small particles in the measurement volume scatter the light mostly to the detectors at larger angles from the direction of the laser beam. Conversely, large particles scatter the light to the detectors at smaller angles close to zero degree from the laser beam. Thus, the distribution of scattered intensity as a function of angle is available. To find out the size distribution of particles, an intensity distribution for a given particle size distribution, as an initial assumption, is compared to the measured intensity. The distribution is corrected iteratively from the error between the measured intensity and the initial assumption. It continues to find the particle size distribution who has the best fit of intensity compared to the measured intensity.

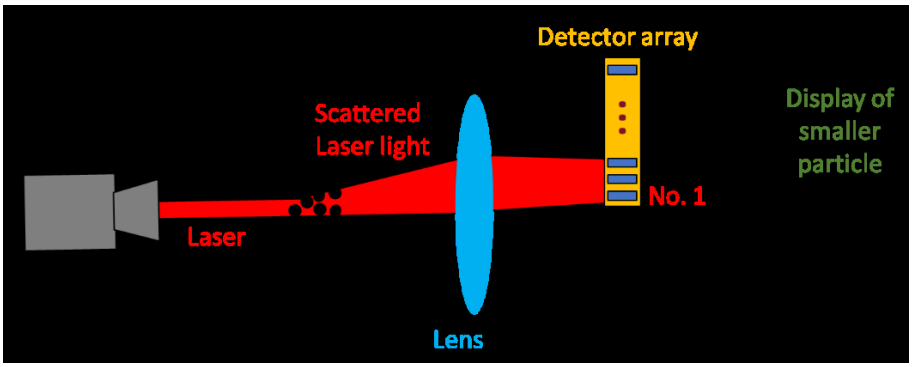

Figure 1.22. Schematics of light diffraction method for characterization of droplets and particles

Figure 1.23 depicts a particle of radius *a* illuminated with plane wave of light at wavelength λ. The light intensity *I* is scattered at an angle of *θ*. The scattering intensity can be calculated by solving the equation of electromagnetic fields in and around the particle [106] and it is represented by a Stokes matrix. The Stokes parameters for an unpolarised beam of incident light scattered by a spherical particle are given by Eq. 1.5:

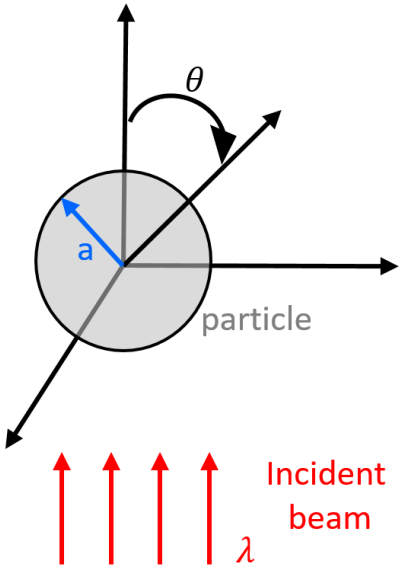

Figure 1.23. Polar coordination for studying scattering of a spherical particle of radius r exposed incident beam of wavelength λ [106]

$$I_s = S_{11} I_i \qquad Q_s = S_{12} I_i \qquad U_s = V_s = 0 \qquad \text{Eq. 1.6}$$

where I_s represents scattering intensity, Q_s and U_s shows linear polarization, and V_s shows circular polarization. I_i is the incident light and S_{11} and S_{12} are elements of Stokes parameters matrix which are calculated by Eq. 1.6:

$$S_{11} = \frac{1}{2}(|S_2|^2 + |S_1|^2) \qquad S_{12} = \frac{1}{2}(|S_2|^2 - |S_1|^2) \qquad \text{Eq. 1.7}$$

And S_1 and S_2 are elements of the amplitude scattering matrix which are calculated through Eq. 1.7:

$$S_1(\theta) = \sum_{n=1}^{\infty} \frac{2n+1}{n(n+1)} [a_n \pi_n + b_n \tau_n] \qquad S_2(\theta) = \sum_{n=1}^{\infty} \frac{2n+1}{n(n+1)} [a_n \tau_n + b_n \pi_n] \qquad \text{Eq. 1.8}$$

In these equation, a_n and b_n are the scattering coefficients and π_n and τ_n are the angle-dependent functions given in Eq. 1.8 and Eq. 1.9:

$$a_n = \frac{m\psi_n(mx)\psi_n'(x) - \psi_n'(mx)\psi_n(x)}{m\psi_n(mx)\xi_n'(x) - \psi_n'(mx)\xi_n(x)} \qquad b_n = \frac{\psi_n(mx)\psi_n'(x) - m\psi_n'(mx)\psi_n(x)}{\psi_n(mx)\xi_n'(x) - m\psi_n'(mx)\xi_n(x)} \qquad \text{Eq. 1.9}$$

$$\pi_n(cos\,\theta) = \frac{1}{sin\,\theta} P_n^1\,(cos\,\theta) \qquad \tau_n(cos\,\theta) = -\,sin\,\theta\,\frac{P_n^1(cos\,\theta)}{d(cos\,\theta)} \qquad \text{Eq. 1.10}$$

where ψ_n and ξ_n are Riccati-Bessel functions and P_n is Legendre polynomials. x and m are the size parameter and relative refractive index, respectively and are given by Eq. 1.10 and Eq. 1.11:

$$x = \frac{2\pi n a}{\lambda} \qquad \text{Eq. 1.11}$$

$$m = \frac{n_1}{n} \qquad \text{Eq. 1.12}$$

where n and n_1 are the refractive indices of medium and particle, respectively. All equations illustrate how the scattering intensity (I) is related to the size a of the scattering particle. The size distribution of an ensemble of particles can be calculated from angular scattering intensity profile by solving an inversion problem [104,105].

1.5. Thesis Organization

This thesis is divided into five chapters. The first chapter is an introduction to known elements and phenomena involved in SPS, to distinguish the outstanding characteristics of particles and importance of online monitoring of these characteristics, to recognize challenges for online monitoring, and to explain briefly the technique of characterization of droplets and in-flight particles. Finally, the objectives and organization of the thesis are presented. The main domains of study in the chapters two to four are shown in Figure 1.24.

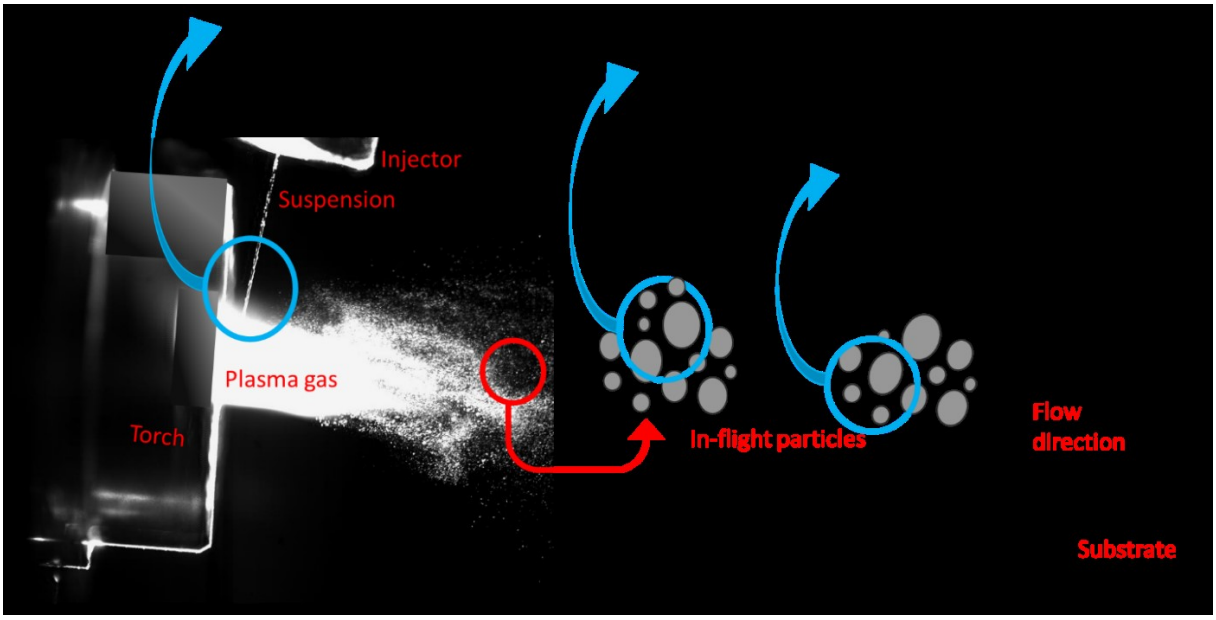

Figure 1.24. Domains and parameters to investigate in the thesis organized in each chapter

Chapter 2 presents a study on the suspension injection in a crossflow in standard condition. An effervescent atomizer was used to spray suspension in transverse flow to air to measure size and velocity of droplets by PDPA. Besides, the shape of spray in the crossflow was captured by shadowgraph. This fundamental study under room condition provided a base to investigate spray of suspension to plasma flow.

Chapter 3 provides a work to investigate temperature and velocity of in-flight particles in SPS by a newly developed system. The principle of measurement for characterization of particles in APS and modifications to adopt the system to fine particles in SPS is explained. For validation, the result of online readings is compared to result of offline measurement. Finally, the capability of the system to measure temperature of velocity of in-flight particles in different spray processes was evaluated.

Chapter 4 focuses on size measurement of in-flight particles in SPS. Light diffraction method is suggested for measurement and it is adjusted to spray condition by eliminating plasma radiation, reducing the turbulent flow in measurement volume, and sampling properly signals from particles. The result of online measurement is verified by result of offline measurement from collecting sample particles.

Chapter 5 summarizes the main achievements, conclusions, and contributions of this work in research conducted in the domain of thermal spray. At the end, a list of recommendation and future works are disclosed.

1.6. Objective

This work focuses on online characterization of particles and droplets in the SPS process. The global objective is to use and develop on-line optical diagnosis systems for optimization and control of SPS. Most of the previous works investigated the injection of suspension focused on visualizing liquid jet in the process. In this research, a fundamental study of suspension spray by an effervescent atomizer in crossflow was investigated at room temperature to find out size, velocity, and shape of spray. Result of measurement at room temperature (no plasma) is a preliminary step before studying the process under the plasma condition and it can be used for developing a new injection method in SPS. However, this study can provide a standalone overview for the general application of using an effervescent atomizer in a crossflow configuration regardless of SPS. Moreover, temperature measurement was investigated by a new diagnostic system for different materials and spray conditions. This research was as a part of the work to develop the first prototype for the temperature measurement in SPS. After the development of the system, effect of conditions and components on the temperature measurement was investigated for the new system. Finally, this work is a pioneer to measure size of in-flight particles in SPS. Challenges of size measurement in SPS were identified and strategies to eliminate these challenges were developed.

The main objectives of this research are summarized as follows:

- To study the spray of an effervescent atomizer in a crossflow configuration at room temperature by using PDPA as a base for a further development of SPS
    - To investigate spray of suspension by the effervescent atomizer in a crossflow configuration and compare results with those is obtained in quiescent air
    - To investigate spray of suspension by the effervescent atomizer in quiescent air and compare of droplet characteristics for pure water and suspensions with different concentrations of the particles
- To develop and investigate the temperature measurement system in the SPS process

    - To investigate the reliability of temperature measurement by the available diagnostic system for the SPS process
    - To improve measurement of temperature by revising components of a measurement system and developing a new system.
    - To investigate capability of the new system to measure the temperature of in-flight particles in SPS
- To investigate the potential of using light diffraction methods to measure size of in-flight particles in the SPS process
    - To identify the main sources of noise for the measurement and specify the limitation of the method for characterization of in-flight particles in the SPS process
    - To develop strategies to minimize the noises which affect the measurement and to remove limitations of previous methods

CHAPTER 2. ARTICLE 1: Characterization of a Suspension Spray from an Effervescent Atomizer in a Crossflow

A. Akbarnozari, S. Amiri, C. Moreau, and A. Dolatabadi [a]

Department of Mechanical, Industrial, and Aerospace Engineering, Concordia University, Montreal, Quebec, H3G 1M8, Canada

This article will be submitted in the journal of Atomization and Sprays.

Abstract

Suspension sprays and its transport phenomena by a gaseous cross flow have many natural and industrial applications. For example, injection of suspension jet in a high-speed flow is used in the emerging surface engineering process called suspension plasma spray (SPS). Typically, submicron ceramic oxide particles are mixed with water or ethanol to form a suspension that is injected in the plasma jet using different types of injectors. Injection parameters such as the type of injector and momentum flux ratio influence the size, velocity, and trajectory of suspension

[a] Ali Akbarnozari conceived of the idea, developed the plan of research, performed the calculation, carried out the experiments, analyzed the result, and wrote the manuscript. Shahin Amiri helped to develop the plan of research. Christian Moreau and Ali Dolatabadi helped to discuss the results, reviewed and commented on the manuscript, and supervised the project.

droplets in the plasma and the microstructure of the deposited coatings. Using an effervescent atomizer, due to its capability in transporting flows with various rheological properties is promising for injection of suspension in SPS. In this study, a custom-made effervescent atomizer was employed to introduce suspension radially into the flow of gas at room temperature. Spray of suspensions with different concentrations of glass particles in water was investigated in the crossflow air by PDPA. The results were validated and supported by studying the spray by the shadowgraph and the light diffraction method. The results of this study provide a better understanding of the spray of the suspension by the effervescent atomizer in the crossflow. Furthermore, it shows the concentration of the suspension has a slight influence on size and penetration of the suspension in the gas flow.

Keywords: Suspension spray, Crossflow spray, Effervescent atomizer, Droplet characterization, Phase Doppler particle analysis (PDPA), Laser diffraction, Shadowgraph.

2.1. Introduction

Suspension plasma spray is an emerging coating deposition method [107] in which ceramic particles suspended in a liquid are injected into a hot plasma jet issued from a plasma spray torch. The injected suspension is finely atomized by the high-speed crossflow plasma flow. The solvent (water or ethanol) is then evaporated, consequently the ceramic particles that are melted and deposited on a substrate to form a coating. This coating process is mainly studied for producing advanced thermal barrier coatings for aerospace and energy applications [108], but also for other emerging applications such as durable superhydrophobic coatings [109] and electrode coatings for hydrogen production [110]. Figure 2.1 shows the injection system in the SPS process. In this configuration, the suspension is introduced as a radial jet that, after interacting with the plasma, is atomized to suspension droplets. Size, velocity, and trajectory of the droplets influence characteristics of the molten ceramic particles and consequently the microstructure and physical properties of the deposited coatings.

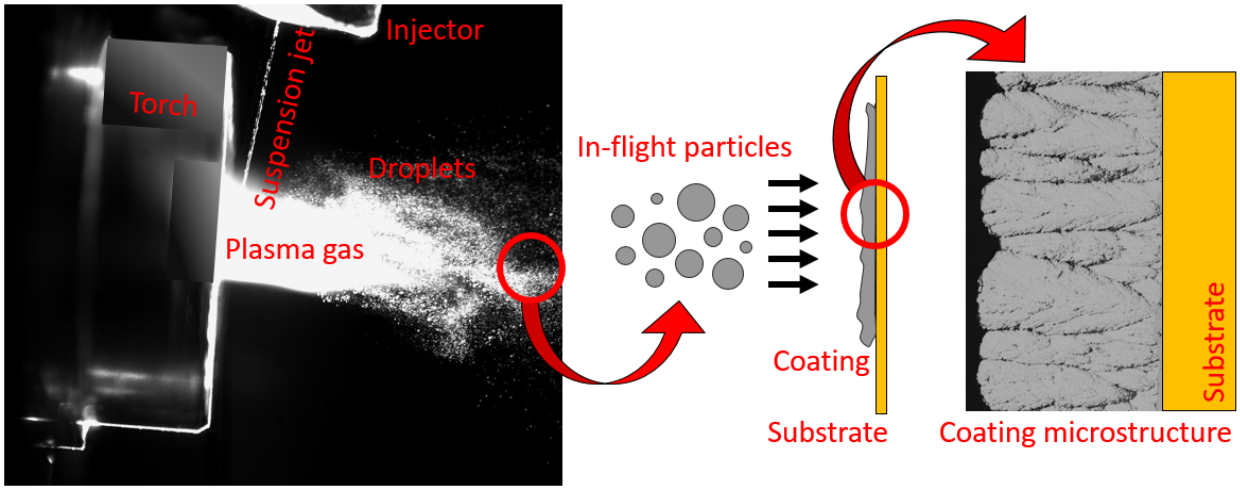

Figure 2.1. Suspension plasma spray process; injection of a suspension jet into a plasma plume, breakup of the jet and droplets, heating and acceleration of in-flight particles, formation of a coating, and illustration of a typical coating microstructure [111]

Instead of injecting a continuous suspension jet, the suspension can be atomized before penetrating to the plasma jet. In fact, the atomizer provides an additional tool to control the initial size of droplets while avoiding excessive plasma momentum dissipation for the jet break up. The atomizer enhances the heat transfer from the plasma flow to the spray of droplets. For example, Toma et al. [112] compared a jet injector and an atomizer used to make coating and they observed different coating microstructures. It is expected that using the atomizer can provide the spray to make a nanostructure. As another example, Aubignat et al. [84] performed velocimetry and shadowgraph to characterize an air-blasted atomizer for SPS process. It was observed linear correlation between the gas to liquid ratio (GLR) and median size of the droplets for a suspension of 20 wt % alumina.

Effervescent atomizer was suggested as an alternative injector to introduce suspensions in the SPS. Lefebvre et al. [19] explained the effervescent atomizer as a twin-fluid atomizer in which the liquid and air (or a neutral gas) are injected into a mixing chamber as shown in Figure 2.2. Bursting of air bubbles at the discharge of the injector shapes ligaments that eventually form liquid droplets after primary and secondary breakup. The gas to liquid ratio (GLR) is one of the main parameters controlling the characteristics of the formed droplets.

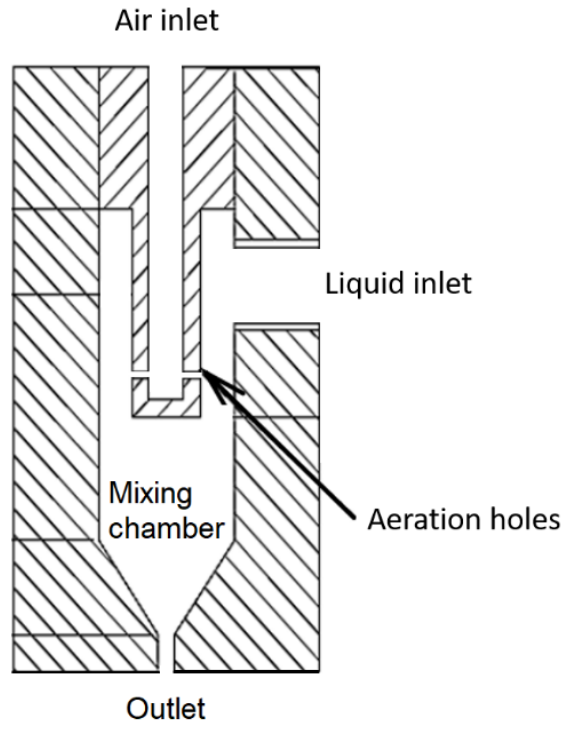

Figure 2.2. Cross-section of the effervescent atomizer shows the air and liquid inlets and the mixing chamber

One of the advantages of using an effervescent atomizer is the formation of a rather small cone angle spray with large momentum flux. In fact, this spray eliminates the possibility of dispersion of suspension outside the plasma plume which eventually can increase the deposition efficiency. Hrishikesh et al. [46] studied the mass distribution of a spray from the effervescent atomizer and showed that mass distribution was the maximum at the centerline. In fact, the maximum mass distribution at the centerline is favorable for SPS applications. In addition, the performance of the effervescent atomizer is almost independent of viscosity of the suspension [47]. The other advantage of effervescent atomization is consumption of less amount of gas as compared to other types of atomization processes [50]. Furthermore, the risk of clogging at the exit of the atomizer during the injection of suspension is considerably reduced because of its large orifice size. As an example, Ochowiak et al. [48] used the effervescent atomizer to spray the solutions of a polymer having non-Newtonian characteristics. Moreover, as the penetration length is concerned, Fan et al. [49] showed that suspension atomized with an effervescent nozzle can efficiently penetrate into a high-velocity crossflow.

The majority of the studies on characterization of the effervescent atomizer were carried out with water, or in a mixture of two or more liquids [50]. There were limited studies on the spray of suspension created by an effervescent atomizer in crossflow. In this area, Sinha et al. [51] and Saleh et al. [20] investigated trajectory and penetration of suspension in terms of gas to liquid ratio and momentum flux ratio in room temperature near the exit of the atomizer.

One of the main challenges for analysis of suspension spray is the inhomogeneous droplets containing nano- or micro-size solid particles. Wriedt et al. [113] used PDPA to characterize a spray of optically inhomogeneous suspensions such as milk and coffee. The inhomogeneous droplets showed a broad size distribution. However, they observed that the mean value of the size distribution was not affected by the optical inhomogeneity. They concluded that droplet size distribution broadens, and to compensate that, they suggested applying two strategies of deconvolution method [114] or iterative inversion [115]. In addition to post processing technique to improve the result, raw signal provides additional information about target droplets if the mode of scattering is considered. Onofri et al. [116] studied reflected and refracted signals (dual burst technique, DBT) of inhomogeneous suspension droplets to measure size, velocity, and concentration in suspension. They used the signal of reflection to measure size of suspension droplet. The novelty of the present work is that a spray of suspension of glass particles up to 10 wt.%, produced by the effervescent atomizer in the crossflow at room temperature is investigated by PDPA. The shape of spray, size and velocity of the droplets far from the exit of the atomizer in the quiescent and the crossflow air were characterized by PDPA. The results obtained by PDPA were validated compared to those results measured by shadowgraph and light diffraction methods. Finally, effect of particle concentration on characteristics of atomized droplets is studied.

2.2. Methodology

2.2.1. Material

The experiments were carried out for distilled water and two water-based suspensions. The suspensions were made by adding glass particles (Coespheric, USA) with a median diameter of around 4 microns in distilled water. Figure 2.3 shows a scanning electron microscope (SEM) image of the glass particles at a magnification of 1K taken by SEM (Hitachi S3400, Japan). The suspensions were stirred and mixed by an ultrasonic liquid mixer (QSonica, USA) to uniformly disperse the glass particles in the liquid phase. Surface tension, viscosity, and density of the

suspensions, as dominant parameters for spray formation, were measured and calculated. The viscosity of the suspension was calculated by the semiempirical model called Krieger-Dougherty equation ($\mu_s = \mu_w(1 - \emptyset/\emptyset_c)^{-B\emptyset_c}$) [117], where μ_s and μ_w are viscosity of suspension and water, Φ is the particle volume fraction, and Φc and B are constant 0.64 and 2.5, respectively. The density was calculated by the equation for slurry ($\rho_s = (1 - \emptyset)\rho_w + \emptyset\rho_p$), where ρ_s, ρ_w, and ρ_p are density of suspension, water, and particles. Table 2.1 shows the properties of suspension with different particle concentrations. The concentration of particles in suspension varied between 0 and 10 wt.%. The surface tension was measured by a Du Nouy tensiometer (Fisher Scientific, USA). Increasing the concentration of particles caused the surface tension to decrease and density and viscosity to increase.

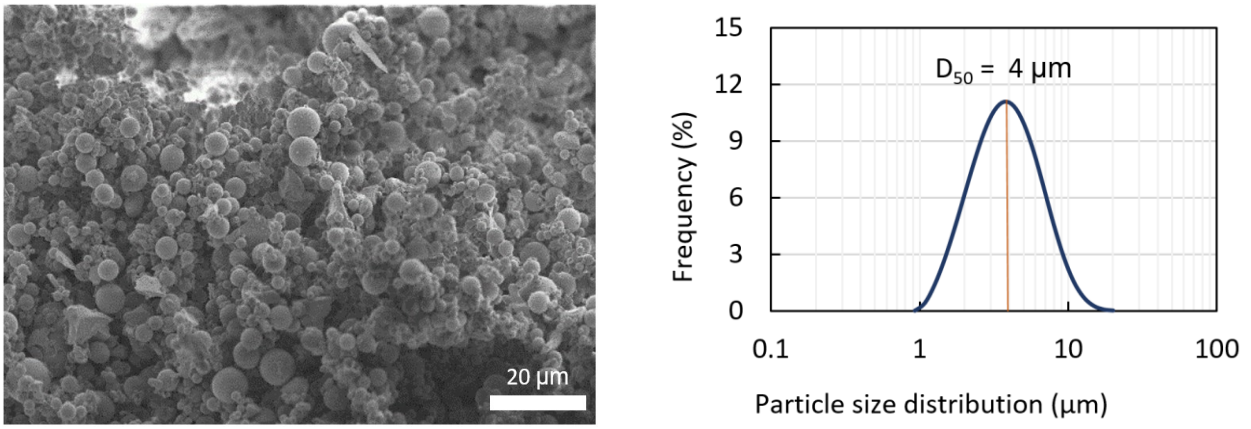

Figure 2.3. Glass particles used in the suspension (left) morphology of particles from a scanning electron microscope (SEM) image and (right) particle size distribution of feedstock

Table 2.1. Distilled water and suspension properties

Liquid	Particle (wt.%)	Density (g/cm^3)	Viscosity (Pa.s)	surface tension (N.m)
Distilled water	0.0	1.000	8.9×10^{-4}	0.072
Suspension No.1	5.0	1.031	9.5×10^{-4}	0.069
Suspension No.2	10.0	1.063	1.0×10^{-3}	0.066

By using Arogo-Biot, Lichtenecker, and Newton's equations, summarized by McClymer et al. [94], real part of index of refraction for suspensions with the weight fractions of 0, 5, and 10 wt.% of glass particles (should be converted to the volume fraction for the calculation) were 1.340,

1.338, and 1.339, respectively. Compared to the index of refraction of water (1.335), theoretically, changes in index of refraction was negligible. In fact, it could not cause significant changes in measurement by PDPA. On the other hand, Reyes-Coronado et al. [118] provided an equation to calculate the imaginary part of index of refraction of suspensions. At the wavelength of 514 *nm* for scatterers of glass particles of 4 μm in diameter, and laser power of 400 mW/mm^2, the imaginary part of refractive index was 1.25×10^{-8}i. The imaginary part of refractive index of water is 1.18×10^{-9}i. In fact, that means the suspension droplets had more extinction of light compared to the water droplets. In fact, the extinction of the light reduced the intensity of scattered light from the particles that should be received in the detectors.

2.2.2. Experimental Setup

The measurements were conducted for two spray configurations; in quiescent air and crossflow air. For the crossflow air, the tests were carried out in an open-loop subsonic wind tunnel which had a plexiglass square test section. The cross-section was 10 × 10 cm and it was connected to a blower fan which provided nominal air velocity up to 50 m/s. For a turbulent air crossflow, the velocity is minimum near the wall and it quickly increases to an almost constant value by moving toward the center of the tunnel. Therefore, the velocity profile is almost flat in the measurement region. The effervescent atomizer was installed from the top surface at the mid-plane of the test section. The exit of atomizer was situated 1 cm below the top wall of the wind tunnel. Droplet size and velocity distributions were acquired by the PDPA (TSI, USA) used in a forward scattering configuration. The transceiver was positioned at 30 degrees of the transmitter as shown in Figure 2.4. For spraying in both quiescent and crossflow air, a plane was identified to measure the size and velocity of droplets situated at 12 cm downstream of the atomizer. For quiescent air, the plane was perpendicular to the centerline of the spray. For crossflow, the plane of study was perpendicular to the direction of crossflow air (see Figure 2.4). The data of the droplets at each point was obtained from 1000 valid measurements or 30 seconds carried out by the Flowsizer software (TSI, USA). The distance between each two consecutive points was 5 mm. The software was set to measure the droplet size considering the refracted light from particles. Information about the PDPA system and the number of measurement points in each plane are given in Table 2.2 and Table 2.3.

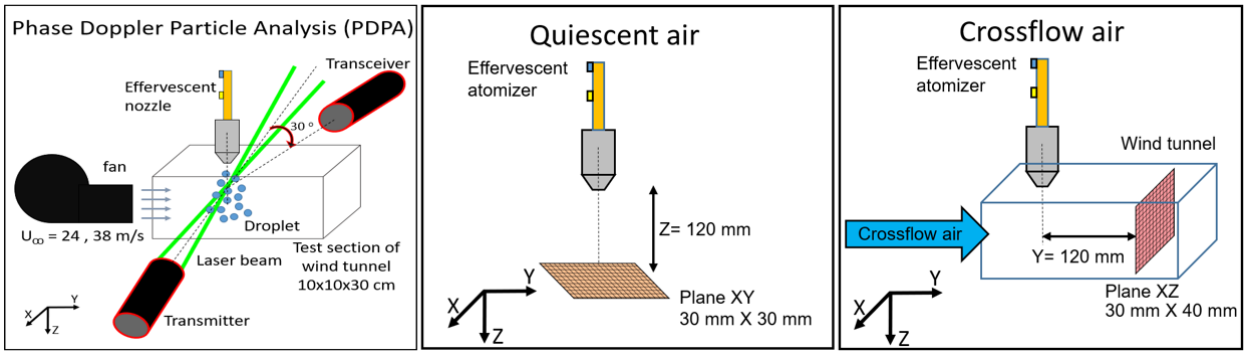

Figure 2.4. The experimental setup for the PDPA measurements including planes of study for quiescent and crossflow air

Table 2.2. Characteristics of the PDPA system

Diagnostic system parameters	Value
Type of laser	Argon Ion
Maximum Laser power (mW)	400
Azimuthal angle (degree)	30
Laser light wavelength(nm)	488 - 514
Number of samples per point	1000

Table 2.3. Size and number of measurement points in the planes for the characterization of spray by PDPA with measurement at every 5 mm

Ambient air	Plane of measurement	Number of measurement points	Field of interest (mm x mm)
Quiescent	Perpendicular to the centerline of spray	49	30 x 30
Crossflow	Perpendicular to the crossflow air	63	30 x 40

2.2.3. Operating Conditions

Table 2.4 shows the test conditions to characterize the effervescent atomizer. The experiments were carried out at fixed GLR of 7 %, which is also the optimum working conditions for this atomizer. Saleh et al. [20] showed the increase in GLR more than 7 % did not provide advantages for this atomizer. Similarly, Sinha et al. [51] confirmed that the size of droplets produced by an effervescent atomizer did not change after increasing GLR to a certain level. They reported the penetration length increased by increasing the GLR up to 7 %. Mass flow rate of liquid was adjusted according to spraying constraints for SPS applications. In this study, the crossflow air velocity and mass flow rate of suspensions were kept constant for testing with the different suspensions. The crossflow air velocity was measured by a pitot tube and it was adjusted at 24 and

38 m/s for two sets of experiments with each suspension. In fact, the spray dominantly overpenetrated the crossflow for the crossflow velocity less than 24 m/s. Also, the wind tunnel limited the maximum crossflow velocity to 38 m/s. As the velocity changes, the volume per unit of time (CFM) for the crossflow changes compared to the volume per unit of time for the spray. However, parameters related to volume of the spray and the crossflow are not interesting in analysis of the phenomena in continuous flow in the measurement volume of the open-loop wind tunnel. Instead of the volume fraction of spray and crossflow, the momentum flow ratio was calculated and considered. The spray condition gives the momentum flux ratio for each test as shown in Table 2.5.

Table 2.4. Spray condition for the measurement in the quiescent and crossflow air

Injection parameters	Value
GLR (%)	7
Liquid flow rate (g/s)	1.32
Air flow rate in atomizer (g/s)	0.09
Crossflow air velocity (m/s)	24 – 38

Table 2.5. Dimensionless numbers for three testing liquids

crossflow velocity (m/s)	Momentum flux ratio		
	Water	Sus 5 wt.%	Sus 10 wt.%
24	3.8	3.9	4.0
38	1.4	1.5	1.5
crossflow velocity (m/s)	Reynolds Number		
	Water	Sus 5 wt.%	Sus 10 wt.%
24	2.7×10^4	2.6×10^4	2.5×10^4
38	4.3×10^4	4.2×10^4	4.1×10^4
Quiescent air	Weber Number		
	Water	Sus 5 wt.%	Sus 10 wt.%
	648	716	773
Quiescent air	Ohnesorge Number		
	Water	Sus 5 wt.%	Sus 10 wt.%
	0.0033	0.0036	0.0038

2.2.4. Experimental Validations

Characterization of spray by PDPA was validated by three supporting experiments explained as follows. Attenuation of light passing through a thin film of the suspension was determined to choose the scattering mechanism of particles (reflection or refraction) in the PDPA. To elaborate more, for suspension droplets formed of nanoparticles, the reflection signal in the

perpendicular polarization was expected to be stronger than the refraction signal. In fact, for the mentioned case, the reflection signal contains more reliable information of the droplet size. However, validity of using refraction signal of suspension droplets contained micro-size particles was investigated. Figure 2.5 shows the test setup to measure attenuation of laser power when it passed through a film of the suspension, which represents a droplet, by using a power-meter. To understand attenuation of a suspension droplet, the thickness of the suspension film was adjusted 60 µm. For this purpose, a rectangular gasket frame (empty at the center) of around 60 µm was placed between two layers of plexiglass. Testing liquid was deposited on one plexiglass and it was spread on empty space of the gasket and covers by the second plexiglass.

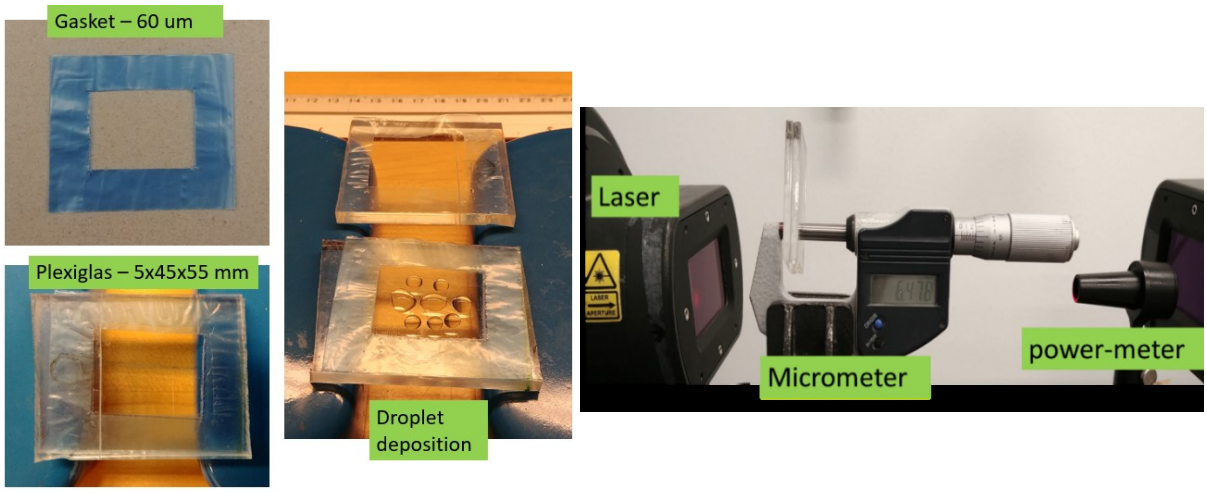

Figure 2.5. The experimental setup to measure attenuation of the laser beam passes through a 60 µm film of suspension

The shadowgraph was used to characterize the spray to validate and support the result of measurement by PDPA. For the shadowgraph experiments, a high-speed camera (Photron SA1.1, USA) and a light source with a diffuser sheet were mounted on two sides of the test section as shown in Figure 2.6. The images were taken with a frame rate of 5400 fps and a resolution of 1024 × 1024 pixels for a field of view of 10 × 10 cm. For each testing condition, 500 frames were recorded and superimposed in the ImageJ image analysis software (National Institute of Health, USA) as shown in Figure 2.6 (middle). Then, the background image was subtracted from the superimposed image of spray. A threshold of 91% was applied to the images to have a sharper boundary between the spray and the surroundings. In fact, the threshold divided the image to background and spray [119]. Around 10 % cut-off of the light as the threshold does not have a

significant effect on analysis and it is common value for similar studies [52]. The result is Figure 2.6 (right) which shows the shape of the spray from the effervescent atomizer in the crossflow. In addition to the shape of spray, the shadowgraph was employed to measure the size of the droplets in the quiescent air for the validation purpose. The camera and the resolution were the same, however, the field of view was decreased to 20 × 20 mm by using a AF-S VR micro lens (Nikon, Japan) to find more detail information about objects. Size of a droplet was calculated from the number of pixels and the pixel size. The objects composed of more than 3 pixels were considered as droplets.

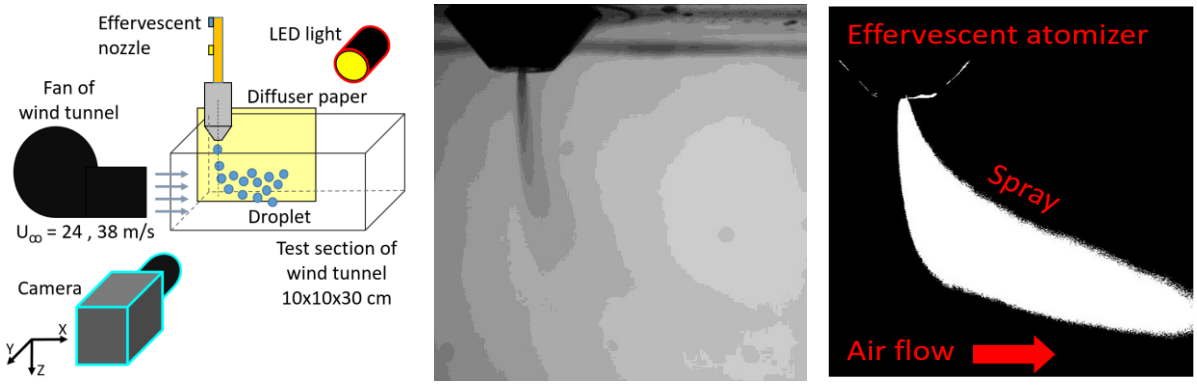

Figure 2.6. (Left) experimental setup for the shadowgraph of the suspension in the crossflow injected by the effervescent atomizer in the wind tunnel (middle) a shadowgraph image of the suspension in the air crossflow in the wind tunnel (right) and the result of superimposed 500 images

As an alternative method, size of the suspension droplets was measured based on light diffraction method by Spraytec (Malvern analytical, UK) for global validation purpose. Detail of the light diffraction system is available in literature [120] which is based on the fact that scattering intensity of a droplet at each angle depends on size of the droplets. Size distribution of droplets along a line of measurement was calculated from measuring the scattering intensity from droplets and solving an inversion algorithm. In this study, the light diffraction system measured size of droplets in a cylinder of laser light with a diameter of 1 cm and length of 10 cm in the test section at 12 cm downstream the atomizer as shown in Figure 2.7. The laser beam of light diffraction system passed through the xz plane which contained the measurement points of PDPA.

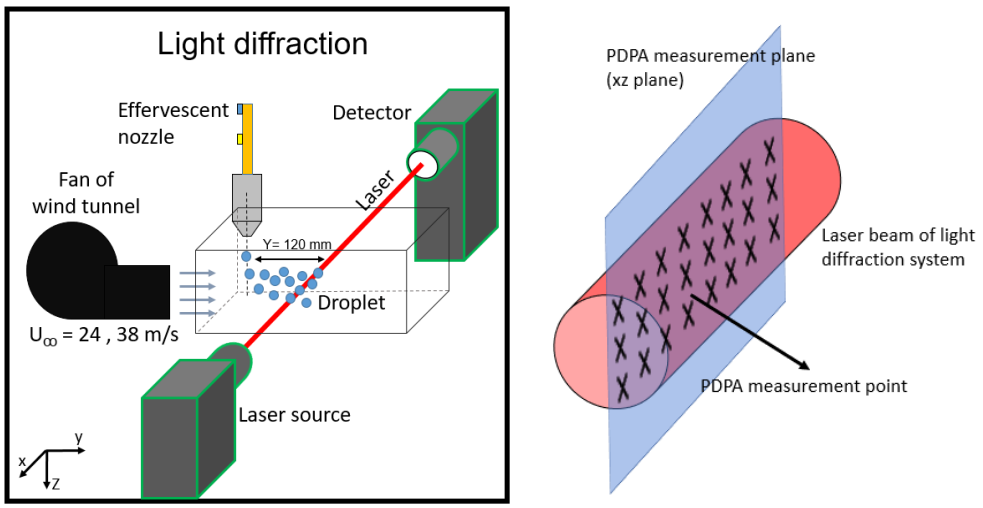

Figure 2.7. (left) light diffraction system used to measure the size of droplets at 12 cm downstream the nozzle exit (right) position of the laser beam of the light diffraction system relative the measurement points by PDPA

The presented droplet size distribution for each point was an average of 1000 validated independent measurements. Validation of the size measurement was based on adjustment of a parameter called the diameter difference which was set at 7 % in this study as suggested in the manual of the PDPA [121]. Figure 2.8 shows diameter difference as a function of the particle diameter which was an average of measurements. Measurement was accepted for the points shown in green where the diameter difference was less than 7 % of the average diameter. The white line at 7 % in the graph distinguishes rejected data points in red color where the measured diameter was outside the acceptable limit.

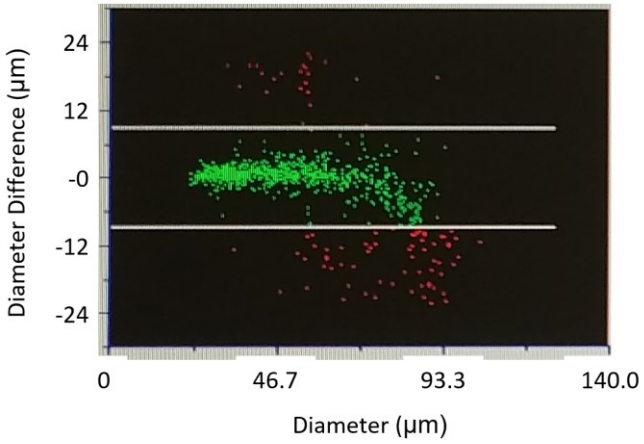

Figure 2.8. Diameter difference as a function of particle diameter

2.3. Results and Discussion

Suspension droplets sprayed by the effervescent atomizer were characterized by PDPA in the quiescent air and the crossflow air. The measurements were validated through the evaluation of light attenuation in suspension and later through the characterization of the spray and droplets by the shadowgraph and the light diffraction techniques. Evaluation of light attenuation by the film of suspension validated the measurement of the suspension droplets by PDPA based on the refraction signal. The attenuation was measured for plexiglass without any liquid. Later, the attenuation was measured for water and for the suspension of 10 wt.%. The suspension attenuated the laser power by nearly 75% at around zero degree which means the laser light around zero degree was scattered in all angles by glass particles. The attenuation of the laser light could be compensated by increasing the laser power for the experiments. To summarize, the PDPA is capable of characterizing droplets of suspension containing up to 10 wt.% glass particles of 4 μm in average with the index of refraction 1.5 in the refraction mode. Validity of suspension characterization by PDPA method cannot be generalized and in case of suspensions with different materials and particle sizes, the validity of measurements should be evaluated.

2.3.1. Spray in Quiescent Air

Contours of droplet size and velocity in the plane perpendicular to the spray centerline for the water and suspension of 5 and 10 wt.% glass are given in Figure 2.9. It was verified by the experiments that size of droplets did not change in the axial direction from around 10 cm downstream of spray. Therefore, the measurement in this work was conducted at 12 cm away from the exit of the atomizer. Although there were some investigations in a similar configuration, for example, Lin et al. [122] which reported the size of droplets increased by increasing the distance from the atomizer because of coalescence of droplets and formation of larger droplets, it was not observed in this research around a distance of 12 cm away from the atomizer. As shown in Figure 2.9, at this offset distance, the smallest droplets were at the center of spray and larger droplets were positioned away from the center. This distribution was as a result of relative position of the liquid and the air at the exit of the atomizer. The liquid sticks to the wall of the atomizer in form of a thin rim and the air (bubbles) occupies the center of the exit channel. At the exit, the bubbles expand, burst, and cause that relatively smaller droplets are generated at the center of

spray and relatively larger droplets are distributed at a farther radial distance from the center. In this work, the dimensionless numbers of x/d, y/d, and z/d were made of the coordination in x, y, and z direction divided by the diameter of the injector *(d)*. It is noteworthy to mention that droplet size reduced as the concentration of the particle in the suspension increased. This may be explained by reduction in surface tension with increasing glass wt. %. Because of a lower surface tension, smaller droplets were generated in the secondary breakup. Similar result was achieved by Qian et al. [47] that illustrated droplet size was reduced by decrease in surface tension. Furthermore, our results confirmed their observation that the viscosity has a slight effect on droplet size. The result showed as the surface tension decreased the size of suspension droplets reduced. This result is in a good agreement with previous research was Ejim et al. [123] reported the droplet size depending more on surface tension than the viscosity.

Figure 2.9 (bottom images) shows the velocity of droplets measured at 12 cm offset from the exit of the atomizer. The velocity of water droplets was around 16.5 m/s at the centerline of spray where it reduced monotonically to less than 12 m/s at 15 mm away from the centerline of spray by moving in the radial direction. Velocity of droplets at the centerline for the suspension of 5 wt.% reduced to around 13.5 m/s. However, the velocity of suspension droplets was almost the same as velocity of water droplets at the periphery of spray. For the suspension of 10 wt.%, the velocity at the centerline of spray was measured around 15 m/s and gradually, the velocity reduced to less than 12 m/s at 15 mm from the centerline of spray. Relatively higher velocity of the water droplets was consistent with the analytical calculation. In fact, the mass flow rate of the liquid kept constant for all tests and the density of the suspension increased by adding more particles to liquid. Therefore, the velocity of suspension droplets should be lower than the velocity of water droplets.

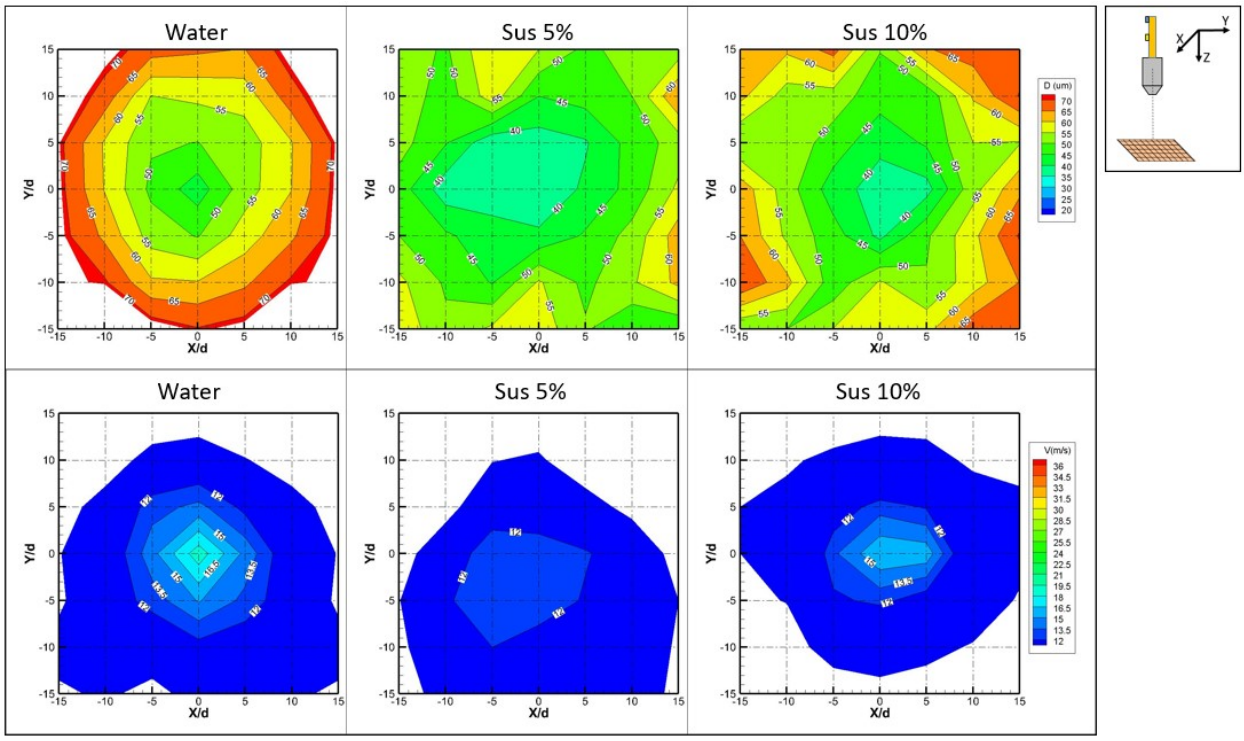

Figure 2.9. Contours of droplet size (top) and contour of velocity (bottom) by PDPA measurement for water and suspensions in the plane perpendicular to spray centerline at 12 cm offset from the exit of the atomizer in the quiescent air

Figure 2.10**Error! Reference source not found.** shows a shadowgraph image of water droplets at 12 cm offset from the exit of the atomizer in the quiescent air. Average size of droplets of water, suspension of 5 and 10 wt.% was 46.1, 46.0, and 43.1 μm, respectively. Difference between the average size of droplets in terms of concentration of the glass particles was not significant. It was observed a spray of suspension of 10 wt.% glass particles had the finest droplets. The decrease in the average size of the droplets, from the water to the suspensions, was expected to be related in a more effective breakup for suspension which generated finer suspension droplets. However, attenuation of light in the suspension droplets could eliminate the number of small suspension droplets to be captured in the shadowgraph images. Generally, these results provided a visually proven benchmark for size of droplets which was comparable with measured size by PDPA.

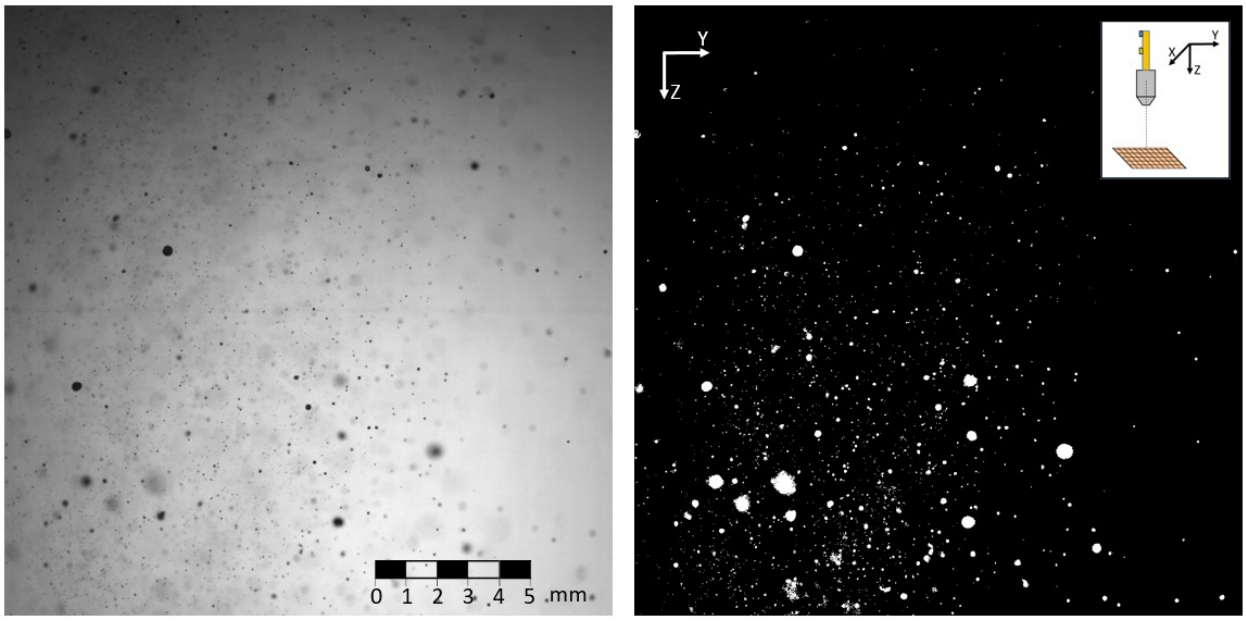

Figure 2.10. The shadowgraph of suspension droplets for size measurement at 12 cm offset from the exit of the atomizer in the quiescent air for a field of view 20 × 20 mm, (left) raw image and (right) background-removed image

2.3.2. Spray in Crossflow Air

Spray shape of three suspensions in the crossflow air was achieved through shadowgraph imaging. Figure 2.11 shows a comparison of spray shape for the transverse air velocity of 24 and 38 m/s. Since the far field of spray was the target of this study, the general shape of spray, especially at downstream, was considered for analysis. The liquid kept moving in the downward direction for 1 to 2 cm depending on the liquid and velocity of crossflow. After that, the liquid droplets dragged toward downstream of flow by the crossflow and they traveled mainly along the flow of the air. At crossflow velocity of 24 m/s, the water droplets dispersed on the leeward (close to the top of the channel) while the suspension droplets showed more effective penetration to the crossflow. When the crossflow velocity was increased to 38 m/s, the shape of spray for all the liquids was quite similar. This is an interesting observation that the suspension penetrates effectively in the crossflow. It will practically be beneficial for SPS that all the tested suspension effectively penetrates into the crossflow.

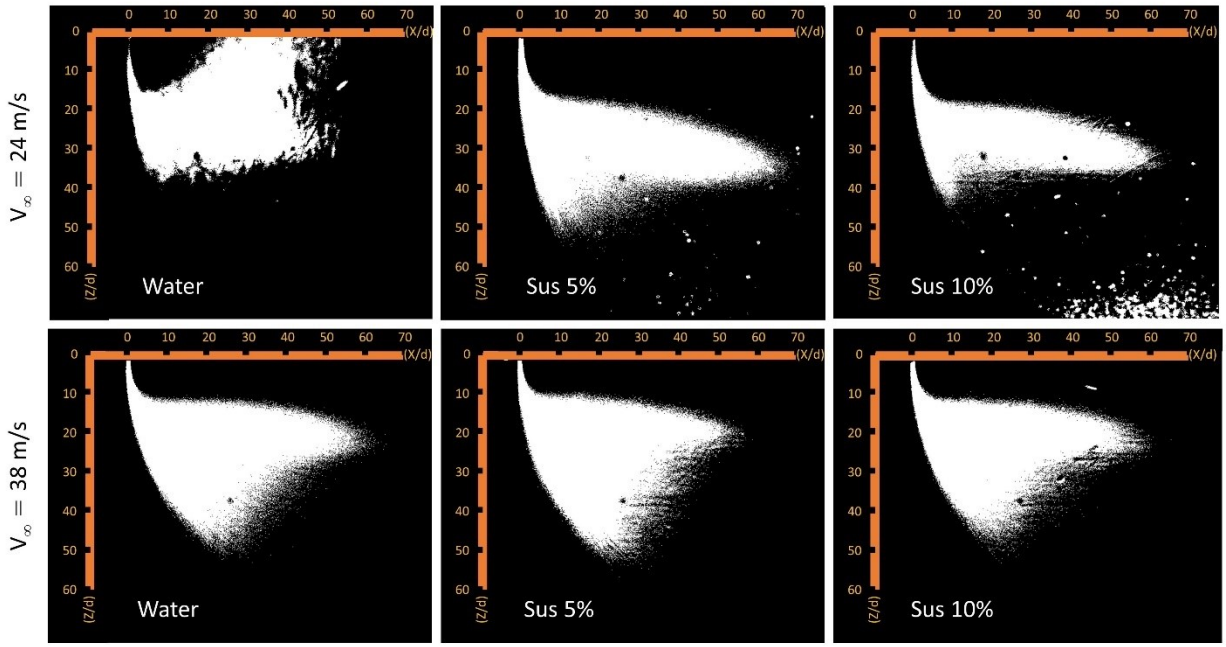

Figure 2.11. The shadowgraph images of spray of liquids for two crossflow velocities

Data rate of PDPA system is an indicator of the number of particles which is counted for size and velocity measurements. Generally, increasing of the laser power leads to increase in data rates. For example, the data rate increases 20 times or more as the power of laser is doubled. In this work, the laser was adjusted to levels for different experiments that the data rate of measurements was kept almost in the same order. Data rate was varied between 1000 and 7000 Hz depending on the measurement location. Generally, at the periphery of spray data rate is the lowest and it is increased toward the center of spray and finally the maximum near the center of spray in downstream. As shown in Figure 2.12 at a crossflow velocity of 24 m/s, the maximum data rate for the spray of water was observed at z/d of 20. The maximum of data rates shifted down to z/d of 30 and 35 for the suspensions of 5 and 10 wt.%, respectively. The droplets of suspension had a higher density, they penetrated more the crossflow, and they moved toward farther z/d in downstream. This is in a good agreement with the slight changes in the momentum flux ratio (Table 2.5). In the case of crossflow 38 m/s, the situation was different from crossflow velocity of 24 m/s. Data rate was maximum between z/d 25 to 30 for all three fluids at 38 m/s crossflow velocity. This observation shows the droplets effectively penetrated to the crossflow. Moreover, the crossflow was the dominant factor in the trajectory of the most droplets. It means the droplets followed the crossflow air and they did not shift to a farther z/d.

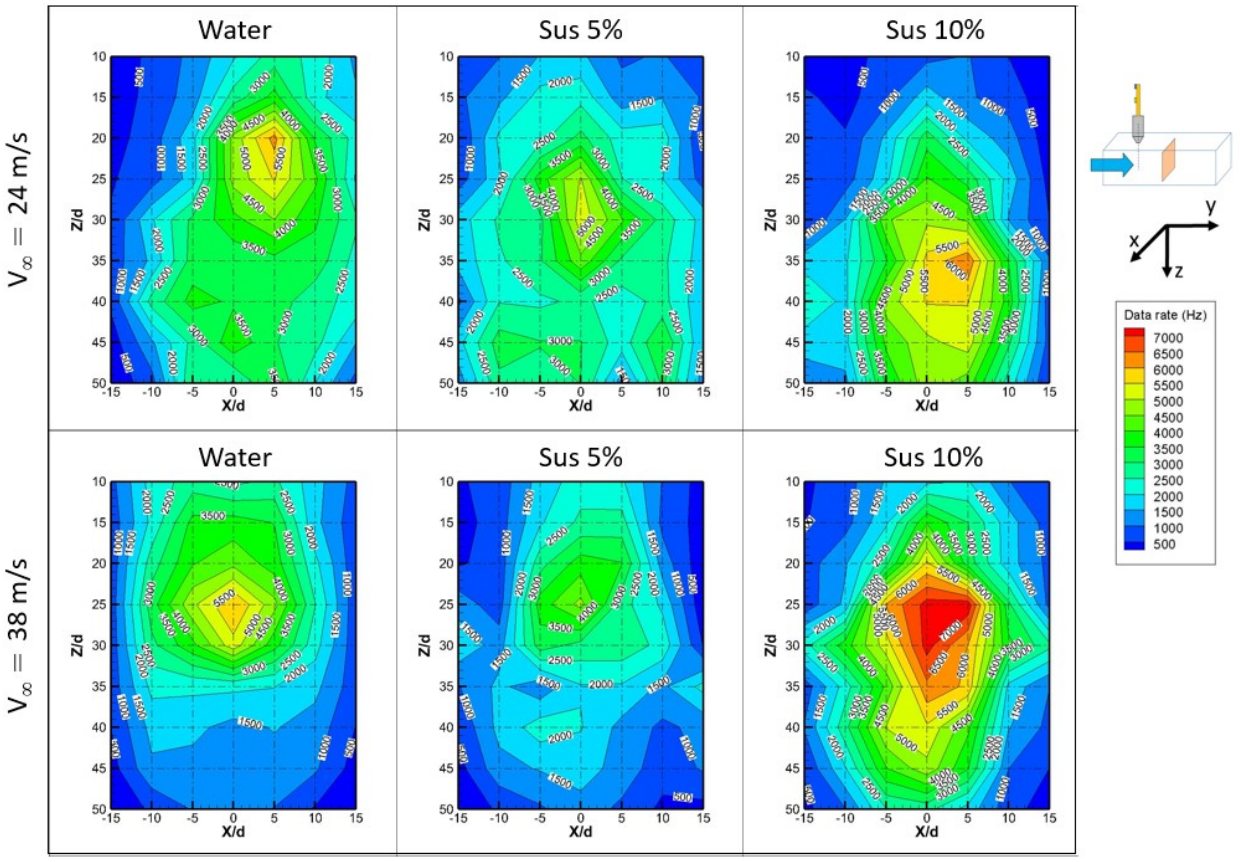

Figure 2.12. Contours of data rates by PDPA measurement in the plane perpendicular to the crossflow air with offset of 12 cm from the centerline of spray for water and suspensions at the crossflow velocities 24 m/s(top) and 38 m/s (bottom)

Figure 2.13 shows the contour of droplet size in the plane perpendicular to the transverse flow at 12 cm downstream the injection point for crossflow velocities of 24 and 38 m/s. The cross-section of spray (patternation) in the offset plane in the direction of the transverse flow resembled the cross-section of spray in the quiescent air. This pattern was always observed for both crossflow velocities. For the 3 liquids, the droplet size was the minimum at the center of the spray cross section, around 20 µm, and it increased gradually by moving towards the periphery where reached around 50 µm. The smallest particles were at vertical distance (z/d) of 35 – 40 at the transverse velocity of 24 m/s where the smallest particles moved to z/d of 30 – 35 at the transverse velocity of 38 m/s.

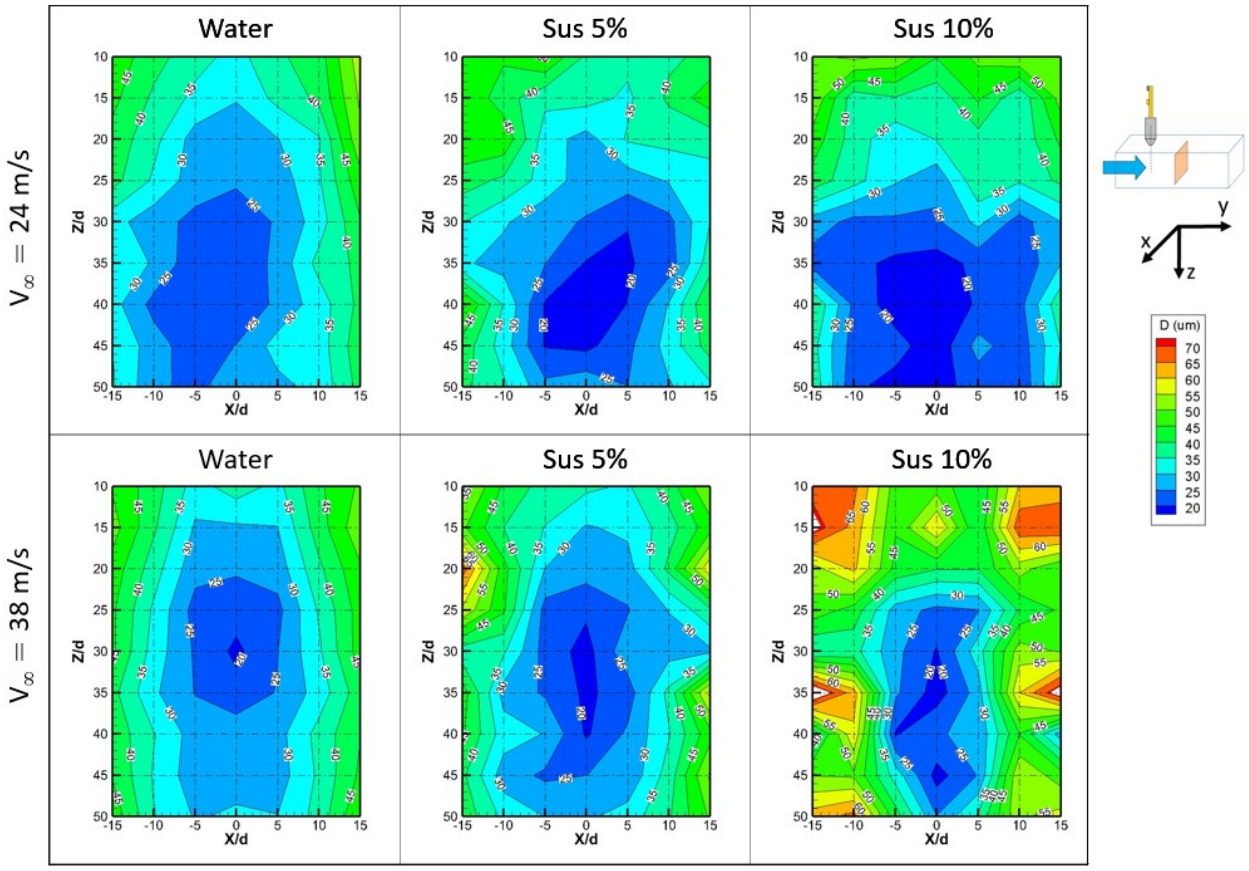

Figure 2.13. Contours of droplet size in the plane perpendicular to the crossflow air with offset of 12 cm from the centerline of spray

Figure 2.14 shows the results of droplet size measurement by the light diffraction (LD) method. The D_{10}, D_{50}, and D_{90} values of the droplets were plotted for water and suspensions with 24 and 38 m/s crossflow velocity. For suspension of 10 wt.%, D_{10} was quite identical which means the minimum size of particles could not physically decrease less than 13 µm. D_{50} and D_{90} of suspension of 10 wt.% for crossflow velocity of 24 m/s were more than the case of 38 m/s. In fact, the crossflow broke up the larger droplets to smaller one at higher crossflow velocity. The same trends were observed for the water and suspension of 5 wt.%. By increasing the concentration of particles for the 3 liquids, the droplet size was decreased. For example, D_{50} of water was 32 µm at crossflow velocity of 24 m/s. D_{50} was 32 and 29 µm for the suspension of 5 and 10 wt.% relatively. In fact, changes in size of droplet was not significant for D_{10}, D_{50}, and D_{90}. The droplet size of all suspension was quite similar to the crossflow velocity of 38 m/s. However, for all the cases the value of size parameters for the velocity of 38 m/s were less than representative parameters at the crossflow velocity of 24 m/s. Comparing the results of measurement by the PDPA and the laser

diffraction confirmed that there was not a significant difference between the droplet size of water and suspension at the same crossflow velocity.

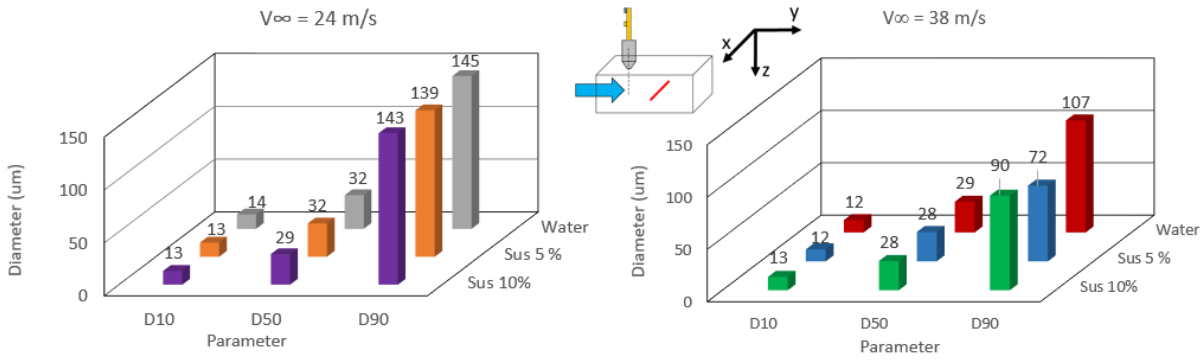

Figure 2.14. Statistical analysis of particle size (D_{10}, D_{50}, and D_{90}) by the light diffraction method along a line of measurement at 12 cm offset of spray centerline for water and suspensions at crossflow 24 and 38 m/s

The velocity component along the crossflow for the droplets at 12 cm offset of spray centerline was measured by PDPA. In general, the velocity all over the plane of scanning was almost uniform. Figure 2.15 shows the velocity contour of droplets in X/d and Z/d positions for the air crossflow at 24 and 38 m/s. For both cases, most of the droplets reached the velocity of crossflow or slightly lower. In all cases, a horseshoe shape was recognized in the contour of velocity where the velocity of droplets was almost the same inside this region. The velocity of droplets was maximum (the same as the velocity of crossflow) inside the horseshoe and the velocity was reduced by moving to the periphery and center bottom of the contour. Compared to the quiescent air result where the droplets of the same speed formed a complete ring shape, in the crossflow, the shape of the region of droplets with a same speed turned to horseshoe shape. These changes were expected to be as a result coalescence of droplets and formation of larger droplets with lower velocity along the crossflow. The velocity was measured for water, suspension of 5 wt.%, and suspension of 10 wt.%. The spray of droplets kept the same shape as the concentration of particles in droplets changed. At the crossflow velocity of 38 m/s, the most of water droplets traveled at velocity of 34.5 m/s and less whereas the most of suspension droplets traveled at velocity of 36.0 and higher. The suspension droplet reached higher momentum which was predicable according to their higher viscosity and density.

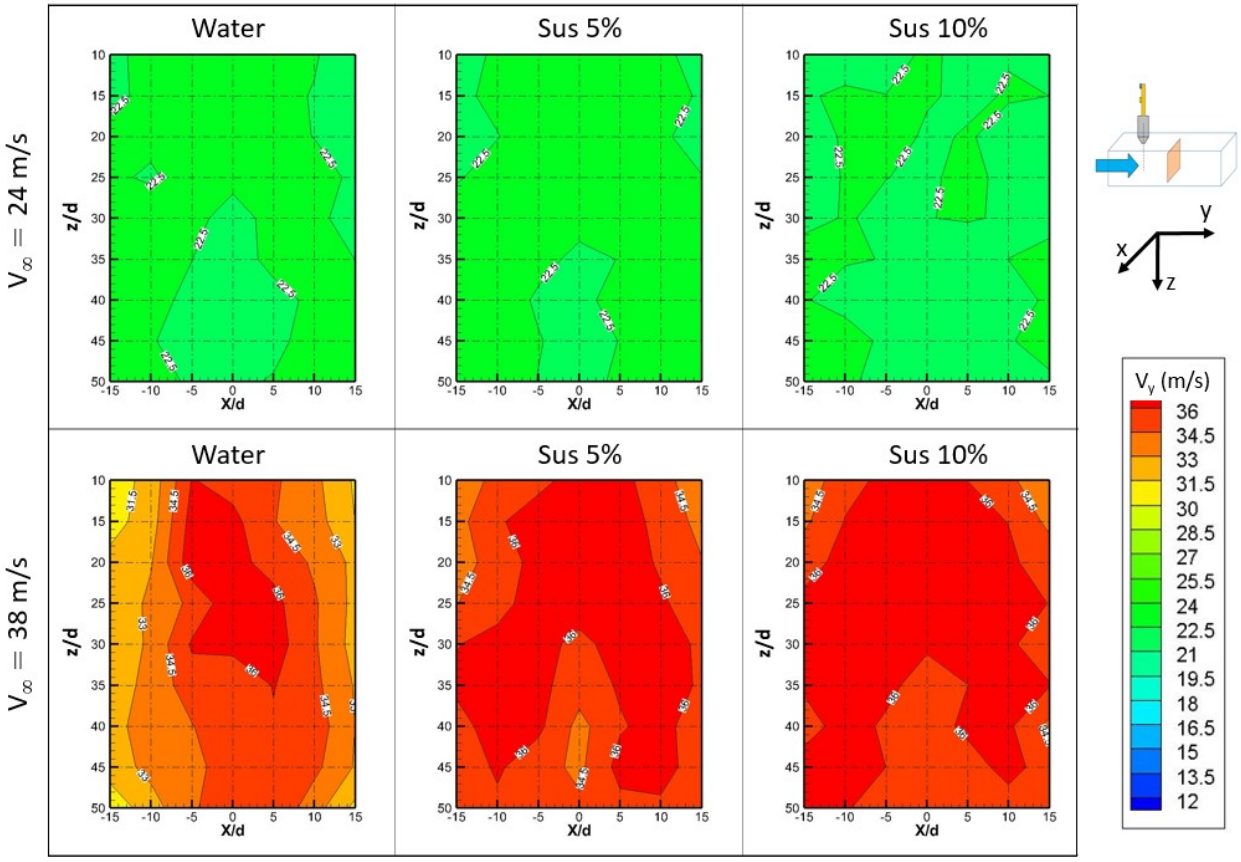

Figure 2.15. Contours of the velocity component at the direction of the spray centerline in the plane perpendicular to the crossflow air and at the 12 cm offset from the nozzle by the PDPA measurement for water and suspensions at the crossflow velocities 24 m/s (top) and 38 m/s (bottom)

Figure 2.16 shows contours of volume flux at offset plane of 12 cm downstream for all cases calculated based on V_y. Volume flux could be as an indicator that the most of spray passes from which regions of a cross-section. The volume flux was not monotonic. It was relatively higher at the center and lower at the periphery of the measurement section. In fact, high volume flux could result from parameters such as large droplet size, high velocity, and high number count in a region. In the cases of the crossflow velocity of 24 m/s, the maximum volume flux was observed at z/d around 20 for water, at z/d around 30 for the 5 wt.% suspension, and at z/d around 25 for the 10 wt.% suspension. The volume flux reduced gradually by moving from the center toward the periphery. Although the shape of contour was not like a well-defined shape, it is more or less was an oval shape. The volume flux of droplets had more similarity to the number count of droplets at crossflow velocity of 24 m/s. In the other half of the tests where the crossflow velocity was around

38 m/s, the maximum volume flux was shifted about 10 units in z/d toward the top. As an example, in the case of water, the maximum volume flux was placed at z/d around 10. Similar to the other case, it was hard to find a well-define shape for the contour of volume flux. However, it was slightly similar to the horseshoe shape which was the shape of the velocity contour. It can be speculated that a higher velocity of droplets changes the pattern of volume flux dominantly.

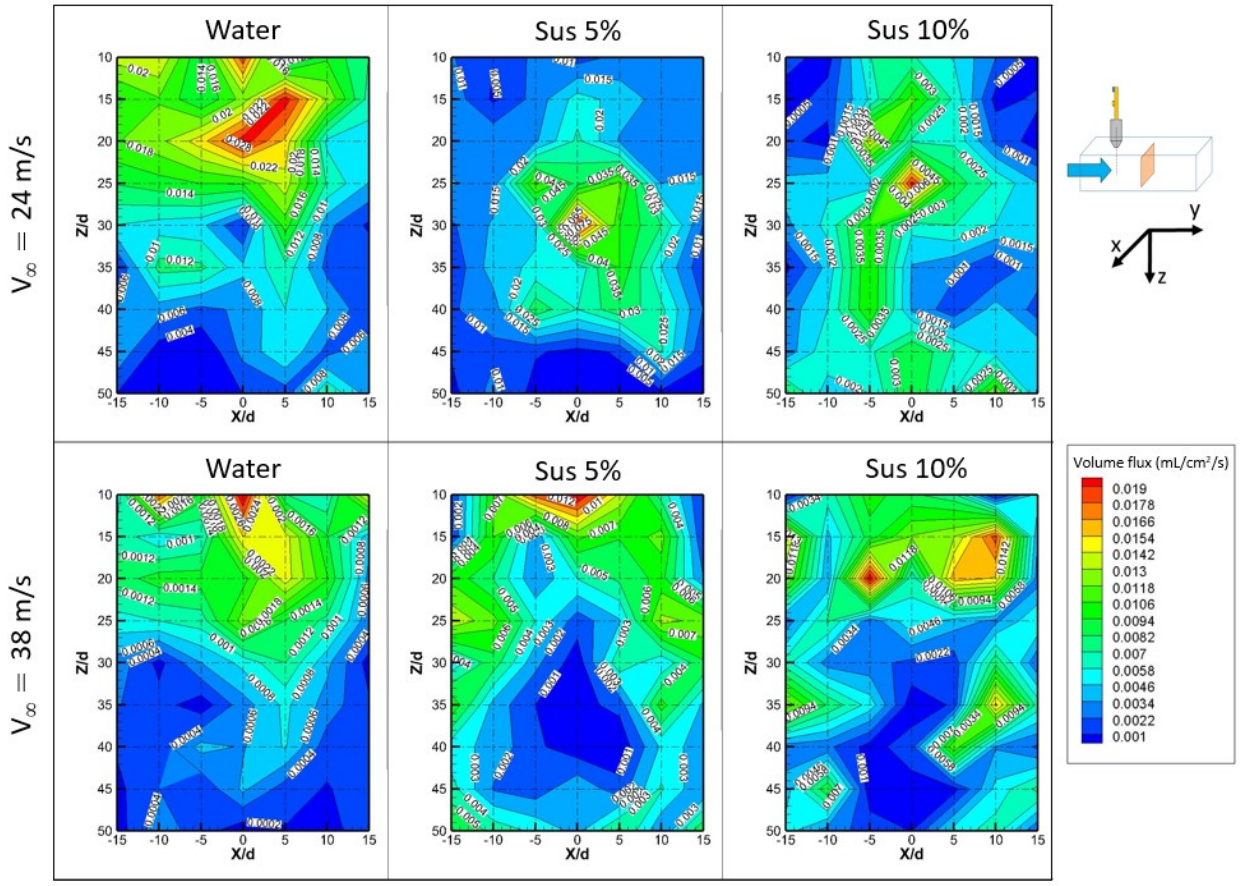

Figure 2.16. Contours of volume flux in the plane perpendicular to the crossflow air with offset of 12 cm from the centerline of spray for water and suspensions at the crossflow velocities 24 m/s (top) and 38 m/s (bottom) considering the scale of cases are different

2.3.3. Uncertainty Analysis

Statistical analysis of the measurements was conducted for the water droplet size in the quiescent air. Measurements were repeated six times along the radial direction of spray at 12 cm offset from the exit of the atomizer. Figure 2.17 the average diameter and the standard deviation of water droplet size as a function of the radial distance from the center of spray. The average diameter of droplets was 41 µm at the center of spray and the standard deviation was 1 µm. Moving

toward the periphery of the spray, the average size of droplets and standard deviation continuously increased. At the radial distance of 5 mm from the center of spray, the average diameter of droplets and the standard deviation were around 46 and 2 µm, respectively. Reaching the 15 mm away from the centerline of spray, the average diameter and the standard deviation increased to 65 and 3 µm, respectively. The increase in the standard deviation at the periphery of the spray can result from the stronger effect of turbulence that generates droplets with a wider range of diameters.

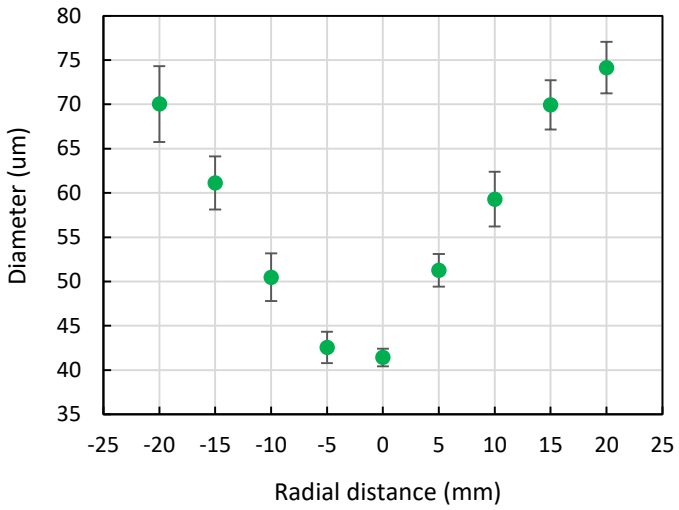

Figure 2.17. Average diameter and standard deviation along the radial direction from the center of spray for water droplets at the offset distance of 12 cm from the atomizer

2.4.Conclusions

The complexity of atomization phenomena by an effervescent atomizer and effect of diverse parameters made it necessary to perform the experimental characterization for specific applications and conditions. In addition to spray characterization, validity of characterization of suspension droplets with the diagnostic system based on phase Doppler should be investigated. In this study, the atomization was investigated in the quiescent and crossflow air. To recognize the influential parameters and proper adjustment of those parameters in SPS application, the effect of crossflow velocity and the concentration of particles in the testing liquid were investigated at room temperature (no plasma) in a wind tunnel. From the executed study, it was concluded that the concentration of particles in the suspension slightly changed the size of the droplets in quiescent

air. Size of droplets of suspension was less than size water droplets in the quiescent air. For crossflow, the spray almost saved its circular shape and the smallest droplets at the center of spray were enveloped by larger droplets. The shape of spray was conserved independent of the crossflow velocity. Regarding the effect of the crossflow, the size of droplets in crossflow was reduced significantly compared to the size of droplets in the quiescent air for the three liquids. It is noteworthy to recall that for the measurement at the offset distance from the spray centerline where the spray was completely steady and uniform, size of droplets at downstream was independent of particle concentration in the liquid phase. Furthermore, the transverse velocity of air in the wind tunnel had a major influence on the final velocity of droplets. Most droplets in the spray reached the velocity close to the velocity of the transverse flow at downstream. The large droplets either broke up into smaller droplets or followed the crossflow, or they overpenetrated and did not transfer downstream. Contours of volume flux showed most of liquid travel at z/d level close to the exit of the effervescent atomizer. This means that for a more effective penetration of suspension and a more uniform spatial distribution of the suspension, it must reach a higher momentum of the injection. It was speculated the large droplet as a result surface breakup from suspension close to the exit of the injector had also an effect in the volume flux distribution. Attenuation and a broader scattering of light in spray of suspension is inevitable, however, these phenomena did not compromise results of measurement based on the phase Doppler analysis for mentioned suspension.

Acknowledgement

The authors gratefully acknowledge Dr. Amr Saleh for his kind help and advice for the test setup preparation. This project was funded by the Natural Sciences and Engineering Research Council of Canada (NSERC) and Canada Research Chair.

.

CHAPTER 3. ARTICLE 2: Online Diagnostic System to Monitor Temperature of In-flight Particles in Suspension Plasma Spray

A. Akbarnozari[1], F. Ben Ettouil[1], S. Amiri[1], O. Bamber[2], J-D. Grenon[2], M. Choquet[2], L. Pouliot[2], C. Moreau[1 b]

[1] *Department of Mechanical, Industrial, and Aerospace Engineering, Concordia University, Montreal, Quebec, H3G 1M8, Canada*

[2] *Tecnar Automation Ltée, Saint-Bruno-de-Montarville, Quebec, J3V 6B5, Canada*

This article has been published in the proceedings of the International thermal spray conference (ITSC) 26th – 29th may, Yokohama, Japan 2019 and it was selected to be published in the *Journal of Thermal Spray Technology.*

Abstract

[b] Ali Akbarnozari conceived of the idea, developed the plan of research, performed the calculation, carried out the experiments, analyzed the result, and wrote the manuscript. Christian Moreau helped to discuss the results, reviewed and commented on the manuscript, and supervised the project. Shahin Amiri helped to develop the plan of research as the postdoctoral fellow. Fadhel Ben Ettouil helped to carry out the experiments as the postdoctoral fellow. Olivier Bamber, Jean-David Grenon, Marc Choquet, and Luc Pouliot fabricated the measurement prototype.

Suspension plasma spray (SPS) is going through a transition phase from research and development to daily use on the production line. Improving of repeatability and reproducibility of coating elements and parameters makes SPS a replacement of former well-developed processes. This transition can be achieved by using a diagnostic system to monitor and control key parameters that influence the coating microstructure. Temperature and velocity of the in-flight particles are among the most critical parameters that should be monitored. However, the small size of coating particles, limitations of previous measurement systems, and harsh spray conditions do represent significant challenges in characterizing accurately the in-flight particles in SPS. In this study, different strategies were investigated to improve the accuracy of temperature measurements of particles in SPS. Two light collection configurations (double-point and single-point measurement) as well as the influence of plasma radiation were investigated. The results were evaluated by collecting and studying splats. The size and shape of splats were correlated with the temperature of in-flight particles. The sensitivity of temperature measurement to the optical filtering, reflection of plasma radiation from the surrounding booth and direct radiation from plasma were investigated. It showed that the single-point measurement system was well adapted for SPS.

Keywords: Suspension plasma spray, Online measurement, In-flight particle temperature, Thermal emission, two-color pyrometer, Diagnostic system,

3.1. Introduction

Suspension plasma spray (SPS) produces coatings with unique microstructures by injecting submicron ceramic particles through a liquid carrier in a high temperature plasma jet. The coating profits from superior chemical, mechanical, and thermal properties which opens opportunities for numerous applications [14]. Temperature and velocity of in-flight particles in SPS are among the main parameters controlling the coating microstructure and, consequently, properties of the surface. The condition of the in-flight particles before impingement on a substrate has a direct impact on the coating characteristics [124]. Therefore, to control hardness, thermal conductivity and other properties of the final coating, temperature and velocity of in-flight particles are key parameters that should be monitored and controlled [125]. Regarding the importance of on-line monitoring systems, on the one hand, these tools have become an important component for developing, understanding, and optimizing new processes in research, and on the other hand, they have been crucial for the advancement of automation in industrial production lines. In short,

monitoring tools facilitate understanding the process-property correlation [126]. Development of diagnostic tools and measurement setups for different thermal spray processes has been investigated by several authors including Solonenko [58], Boulos [53,127], Fincke [128,129], and Vardelle [54]. Moreau et al. [60-62,66,130] developed integrated velocity and temperature measurement systems that led to the commercialization the DVP-2000 and AccuraSpray sensors (Tecnar, Canada). The DPV-2000 was the first commercial diagnostic system for using in thermal spray processes. The AccuraSpray was designed as an industrial diagnostic tool to use in atmospheric plasma spray (APS) and high velocity processes (HVOF) to measure temperature and velocity of the in-flight particles. However, each process requires a customized sensor head because of different filtering requirements. The AccuraSpray helped in research to investigate and optimize spray distance for SPS process [72]. Mauer et al. compared AccuraSpray with the DPV-2000 (Tecnar, Canada) for APS powders and they found good agreement between the measured temperatures of in-flight particles by both systems [71]. Furthermore, McDonald et al. [80] carried out splat studies and temperature measurement for the APS process. They related the online measured temperature of in-flight particles to characteristics of the collected splats which confirmed the validity of measurement for APS.

To monitor the in-flight particles, there are some challenges that are unique to the SPS process. Small size of particles, rapid temperature change of the particles along the spray axis, thermal and non-thermal radiation from plasma [131] are some challenges of in-flight particles measurement in the SPS process. The AccuraSpray G3 (and earlier versions) is an ensemble particle diagnostic system relying on a double-point measurement configuration that was designed for conventional thermal spray processes and not for SPS process. The double-point measurement configuration consists in collecting the thermal radiation emitted by the in-flight particles at two different wavelengths at two locations spaced by a few millimeters along the particle jet. When it applied to SPS, the sensor could lack accuracy especially for temperature measurement. Despite this fact, this system has been used to characterize spray parameters such as temperature and velocity of the in-flight particles in SPS and the results were reported by Tarasi et al. [82]. Vaβen et al. [132] reported the temperature measurement of yttria stabilized zirconia (YSZ) in-flight particles in SPS.

The main objective of this paper is to assess the reliability of temperature measurement of in-flight particles in SPS. To so do, comparison between double-point and single-point measurement configurations was carried out. Furthermore, effects of optical filtering, surrounding radiation reflection and plasma radiation on raw signals and temperature measurement in the SPS process were investigated. Finally, the overall performance of the new AccuraSpray 4.0 using the single-point measurement configuration in SPS processes was evaluated.

3.2. Theory and Background

3.2.1. Temperature Measurement

The temperature measurement using the AccuraSpray sensor is carried out by detecting the thermal emission from in-flight particles. The sensor provides an ensemble average data from particles that pass through its measurement volume which is roughly 200 mm^3. The minimum measurable temperature for this apparatus is around 900 $^{\circ}C$. It has a camera and an alignment beam to place the measurement volume at a target point. It measures the temperature by using a two-color pyrometer based on the Planck's law. Briefly, the thermal radiation from a body is a function of wavelength, emissivity, and temperature as given in Eq. 3.1.

$$I_{em}(\lambda, T) = \varepsilon \frac{C_1}{\lambda^5} \frac{1}{\left\{exp\frac{C_2}{\lambda T} - 1\right\}} d\lambda \qquad \text{Eq. 3.1}$$

where I_{em} is the intensity emitted by a black body in W/Sr in an interval of wavelength $d\lambda$ centered at a wavelength λ in meter, T is the particle's surface temperature in Kelvin, C1 =9.352 x10-17 $W.m^2$, C2 =1.439 x10-2 m.K and ϵ the emissivity. A two-color pyrometer measures the intensity of radiation I_{λ_1} and I_{λ_2} in two wavelengths λ_1 and λ_2 . For this purpose, a bandpass filter is placed in front of each of two detectors to block other wavelengths. Generally, the radiant source is assumed to behave as a gray body. The temperature is calculated from Eq. 3.2.

$$T = \frac{C_2(\lambda_1 - \lambda_2)}{\lambda_1 \lambda_2} \cdot \left[ln\frac{I_{\lambda_1}}{I_{\lambda_2}} + 5ln\frac{\lambda_1}{\lambda_2} \right]^{-1} \qquad \text{Eq. 3.2}$$

Generally, temperature and velocity of in-flight particles together provide key characteristics of a spray condition. In the AccuraSpray system, the particle velocity is measured by a time-of-flight technique [60]. Each particle in the measurement volume radiates a signal that passes through 2 adjacent measurement points located along to the general motion of the particle

in the spray plume. Knowing the distance between the measurement points, the particle speed is calculated from the time difference between the radiation peaks measured in each detector.

There is an uncertainty in the measurement of temperature by a two-color pyrometer. A fundamental assumption for temperature measurement is that in-flight particles are gray body. According to definition, emissivity of surface is independent of wavelengths for the gray body. However, emissivity at two wavelengths are not necessarily equal for real materials. Mauer et al. [97] studied temperature errors by deviations from the gray-body assumption as a function of temperature as shown in Figure 3.1. For example, 7.5 % difference between emissivity at two wavelengths ($\varepsilon_{\lambda 1}/\varepsilon_{\lambda 2} = 0.925$) results around 200 °C error for a measurement at 3000 °C. Touloukian and DeWitt [98] studied the thermal properties for a wide range of materials. Manara et al. [99] reported emittance of YSZ as a function of wavelengths which is a common material in SPS. Therefore, deviation from gray-body assumption can be further studied by considering emissivity ratio at two wavelengths ($\varepsilon_{\lambda 1}/\varepsilon_{\lambda 2}$).

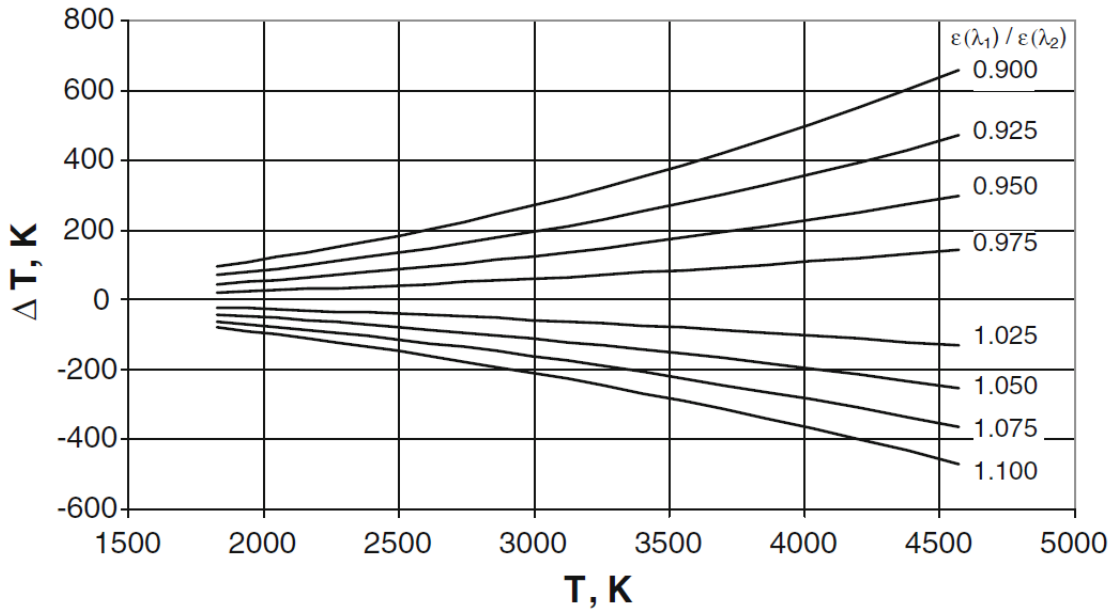

Figure 3.1. Temperature measurement error as function of emissivity ratios and absolute temperature [97]

Gray body assumption causes an uncertainty in temperature measurement of in-flight particles by the two-color pyrometer. The uncertainty of temperature measurement (ΔT) [100] arising from the unequal emissivity of $\varepsilon_1$and ε_2 at 2 wavelength of λ_1 and λ_2 as shown in Eq. 3.3.

$$c_2 \frac{\Delta T}{T^2} = \left(\frac{1}{\lambda_2} - \frac{1}{\lambda_1}\right)^{-1} ln \frac{\varepsilon_2}{\varepsilon_1} \qquad \text{Eq. 3.3}$$

where *c* and *T* are a constant and temperature, respectively. The uncertainty is minimum when the two wavelengths are close, and it increases as the separation between the two wavelength increases. However, minimizing the uncertainty by choosing closer wavelengths in the spectrum costs a loss in sensitivity of two-color pyrometer. Therefore, separated wavelengths are selected to have an effective sensitivity to measure temperature which has a higher level of uncertainty. It should be mentioned, the uncertainty which exists for the absolute temperature does not exist for the relative temperature. Therefore, the pyrometer based on the gray body assumption still provides a reliable relative temperature of in-flight particles.

3.2.2. Single-point Measurement vs. Double-point Measurement

Figure 3.2 shows a schematic diagram of a two-color pyrometer used in a double-point measurement configuration as implemented in the AccuraSpray G3C (and earlier versions) versus a single-point measurement configuration studied in this work and implemented in the new AccuraSpray 4.0. Contrary to the double-point measurement system, where I_{λ_1} and I_{λ_2} are measured at two distinct points along the spray axis (almost 3 mm apart from each other), in the single-point measurement system, the signal is captured from one point in the measurement volume and the collected radiation is divided in two parts using a dichroic mirror. The signals are then passed through the filters at two distinct wavelengths and finally reach the detectors. Aziz et al. investigated the effect of plasma radiation on the accuracy of temperature measurements [133]. Based on their finding, the bandpass filters were readjusted and optimized for more effective elimination of the plasma radiation. It is worth mentioning that double-point measurement system has some practical advantages in terms of robustness of measurement, relative simplicity of the configuration, and cost efficiency. In fact, the double-point measurement is a robust system that provides reliable result for APS and HVOF processes. Furthermore, it does not require a dichroic mirror in the configuration which makes it simpler while the results are still reliable. Finally, from a commercial aspect, a double-point measurement system is less expensive to manufacture which was more favorable for customers and the developer.

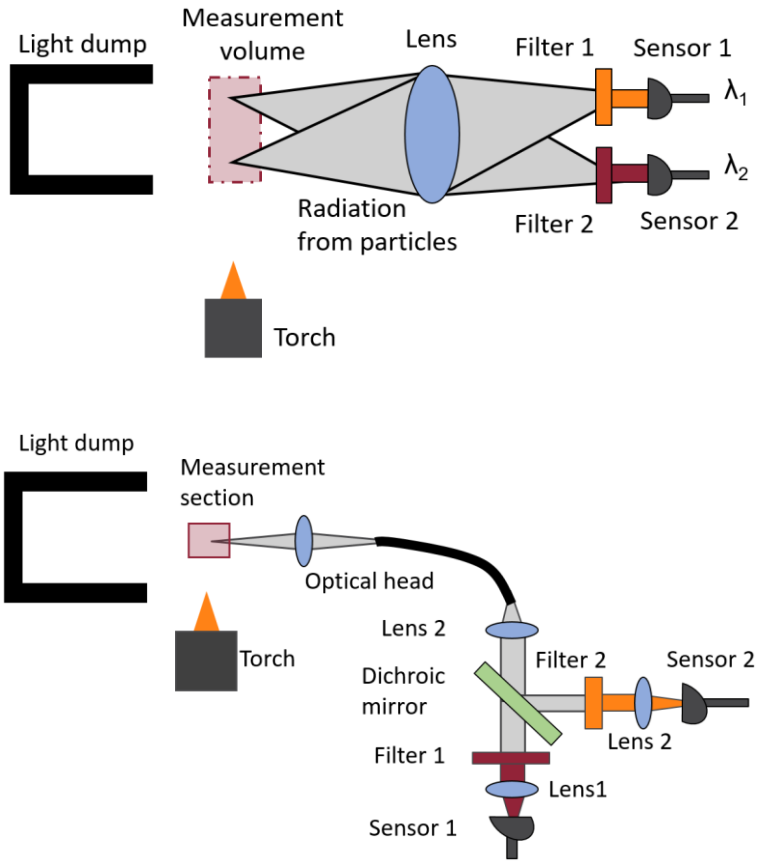

Figure 3.2. Schematic diagram of the pyrometer for characterization of the particles configured with (top) double-point measurement of AccuraSpray G3C (bottom) single-point measurement of the prototype and AccuraSpray 4.0

3.2.3. Velocity Measurement

For more extensive characterization of in-flight particles, temperature and velocity of particles are studied together. Velocity measurement was not the focus of this part and the principle is explained in general terms. Velocity of in-flight particles is calculated by using a time-of-flight approach. Each particle in the measurement volume radiate a signal that passes through 2 adjacent measurement slits located parallel to the general motion of the particles in the spray plume. Knowing the distance between the measurement points and magnification of optics, the particle speed is calculated from the time difference between the radiation peaks measured in each detector.

3.3. Experimental Methodology

Three distinct diagnostic apparatuses used in our experiments were the double-point measurement AccuraSpray G3C, a new prototype of single-point measurement, and AccuraSpray 4.0 developed based on the prototype with improved filtering. This paper reports two main sets of experiments. In the first part, temperature of the in-flight particles in SPS process was evaluated by both the double-point measurement system and single-point measurement prototype. This prototype was used to assess the gain in accuracy of the single-point measurement approach in the development of the new AccuraSpray 4.0. In the second part, the SPS process was characterized by the single-point measurement system (AccuraSpray 4.0) developed based on the prototype equipped with an optimized filtering. Furthermore, the sensitivity of measurement to the testing conditions were analyzed.

3.3.1. Comparison of AccuraSpray G3C and the Prototype in SPS

The double-point measurement system and the single-point prototype were compared to measure temperature of in-flight particles related to changes of plasma power and standoff distance. The center wavelength (CWL) of the transmission window of the filters of the double-point measurement system were 785 and 995 nm and the full width at half maximum (FWHM) of the window was around 50 nm. The CWL of sensor 1 and its FWHM for the single point measurement system was readjusted at 787 and 40 nm. The powder was 8 mol% YSZ (ZiBo.V.Gree. Trading, China) with an average particle size 0.4 µm. A suspension of 1 wt.% polyvinylpyrrolidone (Sigma-aldrich, USA) as a surfactant and 20 wt.% powder in ethanol, was radially injected into the plasma jet originated from a 6 mm nozzle of a 3MB torch (Oerlikon Metco, Switzerland). At a constant suspension flow rate of 25 mL/min, the experiments were repeated for three different plasma powers which adjusted by controlling the gas composition, gas flow rate, and electrical current of plasma. Table 3.1 shows the variables and spray conditions for the tests.

Table 3.1. Plasma conditions for spraying the YSZ suspension with the 3MB torch

	Gas flow rate			Current	Power
Test #	(L/min)			(A)	(kW)
	Ar	He	H2		

1	45	0	5	600	34
2	25	25	0	700	27
3	25	25	0	600	23

3.3.2. Measurement by the Prototype and Splats Sampling

Validity of the temperature measurement was indirectly investigated by studying the splats obtained in different spray conditions. The suspension was prepared as described above but the powder concentration was set to 10 wt.%. Lower suspension concentration was used to reduce the density of splats collected on glass substrates. For the purpose of validation, the temperature was measured using the prototype at 5 spray distances and splat samples were collected on a glass substrate at the same distances. The spray parameters of these experiments were those identified as Test # 3 in Table 3.1. The collected splats were studied by using a scanning electron microscope (SEM) S3400 (Hitachi, Japan) at accelerating voltage of 5 kV. Then, links between measured temperatures of in-flight particles and micrographic information of collected splats were studied.

3.3.3. AccuraSpray 4.0 for SPS

Single-point measurement system, developed based on the validated prototype, was employed to characterize first the in-flight particles under plasma conditions of Test # 3 in Table 3.1 for spray of 20 wt.% YSZ suspension. In a second series of experiments, temperature and velocity of in-flight alumina particles spray with an axial injection plasma torch (Northwest Mettech Corp., Canada) a 3/8-inch nozzle diameter. An alumina powder (ZiBo.V.Gree. Trading, China) with an average particle size of 0.4 μm was put in suspension in ethanol with a concentration of the 20 wt.% powder with 1 wt.% polyvinylpyrrolidone (Sigma-aldrich, USA) as a surfactant. The flow rate of alumina suspensions was kept constant at 45 mL/min for each set of experiments. Nitrogen with a flow rate of 15 mL/min was employed to atomize the suspension before entering the plasma. Table 3.2 shows spray conditions for these tests.

Table 3.2. Plasma conditions for spraying the alumina suspension with the Mettech torch

Test #	Gas flow rate (L/min)			Current (A)	Power (kW)
	Ar	N_2	H_2		
4	184	23	23	180	90

3.3.4. Temperature Sensitivity to Measurement Conditions

Effect of optical filtering, reflection from surrounding walls, and direct plasma radiation were investigated for the spray of a YSZ suspension with the 3MB torch operated in Test #3 conditions (Table 3.1). The raw signal at the detector and measured temperature were compared for three conditions. To understand the effect of optical filtering, the signal and temperature were recorded by using regular filters of the AccuraSpray 4.0 compared to an enhanced filter configuration. The enhanced filter was composed of two customary filters with OD 6 which they were stuck together for more effective blockage of the rejected wavelengths. To investigate effect of the reflection from surrounding walls in the spray booth, a light beam dump was employed. The beam dump was a mat black closed-end cylinder of 10 cm in diameter. The beam dump was placed in front of the diagnostic system to prevent reflection of radiation from the plasma or other sources on the surrounding booth walls from entering the diagnostic system. The raw signal and temperature were recorded in the presence and absence of the beam dump. Finally, to understand the effect of direct plasma radiation on the measurement, a shield was placed between the plasma and the diagnostic system. The signal and temperature were recorded with and without the shield.

3.4. Results and Discussion

3.4.1. Characterizing YSZ in SPS by AccuraSpray G3C and the Prototype

AccuraSpray G3C and the prototype were used to measured temperature of in-flight particles in SPS. Figure 3.3 shows the temperature of in-flight YSZ particles as a function of plasma power at 60 mm from the torch exit as measured with the double-point measurement system and single-point prototype. The double-point measurement system displayed significantly higher temperature readings, reaching 3457 °C at a plasma power of 34 kW while the single-point measurement prototype measured 3140 °C for the same condition. The difference between two readings was 317 °C and it stayed as high as 262 °C for the lower plasma power (23 kW).

Figure 3.4 presents the temperature readings from the double-point measurement system and single-point measurement prototype at three different spray distances for the 34 kW plasma power. Temperature readings of the single-point measurement system at standoff distances from 60 mm to 100 mm show a continuously decreasing trend with the spray distance as expected. For the double-point measurement apparatus, the temperature decrease was observed up to 80 mm and then the temperature starts to increase at a larger standoff distance. This increase can be explained in terms of rapid cooling rate of particles. In-flight particles are cooled by the surrounding air as

they exit the plasma and their temperature decrease as they move from the torch. On the same figure, the measured temperature with the same system was always higher than the temperature measured by the single-point measurement prototype. This difference was around 317 °C at a standoff distance of 6 cm and around 95 °C at the 8 cm. Briefly, the double-point measurement overestimated the temperature of in-flight particles and the single-point measurement prototype provided a more realistic result. In-flight particles in SPS were more sensitive to the steep temperature gradient of plasma. The slope of changes in the temperature of in-flight particles measured by the prototype is slow. This can be because of a bias towards the relatively larger and hotter particles. These particles have stronger radiation and slower cooling rates and they have a noticeable influence on the average temperature recorded by the system.

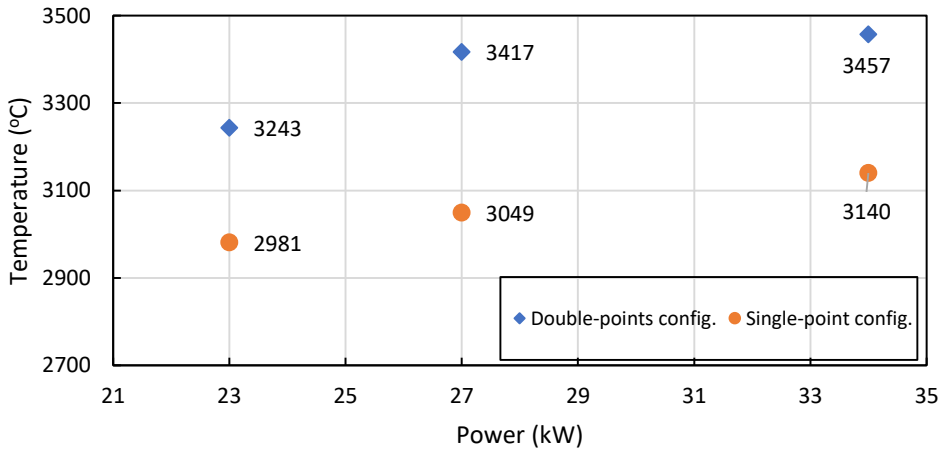

Figure 3.3. Temperature of YSZ in-flight particles measured by the double-point measurement system and single-point measurement prototype in SPS process at 60 mm standoff distance of the 3MB torch

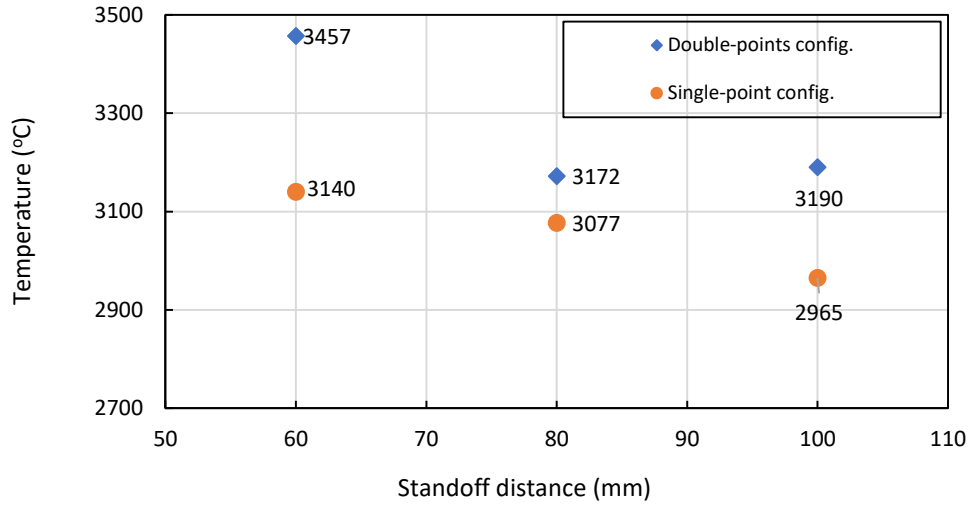

Figure 3.4. Temperature of YSZ in-flight particles measured by the double-point measurement system and single-point measurement prototype in SPS process for the condition of high power (Test # 1) with the 3MB torch

3.4.2. Analyses of Collected YSZ Splats From SPS

Figure 3.5 shows the particle temperature as a function of standoff distance from the torch exit in the Test 3 condition (Table 3.1). This low power condition was selected to avoid large overheating of the particles so that it was possible to collect splats at different standoff distance where particles temperature was expected to be above the melting point for the shorter spray distance and below the melting point for the farthest standoff. The measurement showed that the most noticeable temperature changes were between the standoff distances 30 and 40 mm where the temperature dropped by around 200 °C. The rapid initial temperature drop can be associated more to the stray radiation than the natural temperature decrease of the particles. Fazilleau et al. [22] showed the temperature of plasma drops considerably (independent of gas type) at close axial distances. However, it remains as high as 4000 °C at standoff distance of around 5 cm. Therefore, the particles cannot experience a sharp temperature drop because of the plasma cooling. Delbos et al. [23] studied heat transfer for the particles. Assuming the radiative heat transfer between the plasma and particles was in balance as far as 4 cm, convection heat transfer was the dominant mechanism for cooling down of particles. This means than the temperature drop should be linked to the convection which changes linearly with temperature. On the other hand, the level of stray radiation from the plasma was higher close to the torch. Spectroscopic measurements [133] showed that the irradiance from free charges and ions in the plasma covers the whole spectrum in the visible and near-infrared (NIR) ranges. This irradiance was higher closer to the torch, and it

diminished with the measurement distance from the torch. Therefore, it is concluded that the reading of a high temperature at 30 cm was due to the stray radiation which added to the thermal radiation from particles. At a standoff distance of 40 cm, the rate of cooling was around 25 ˚C /cm. The cooling rate decreased as the measurement volume was farther from the torch and it increased for a higher power plasma. The results obtained using the single-point measurement prototype seemed promising, nevertheless, it required to be verified indirectly through the splats studies.

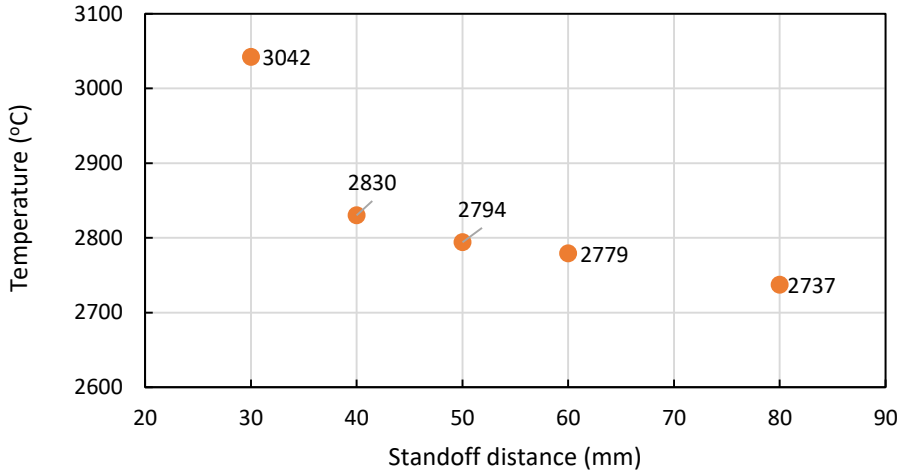

Figure 3.5. Temperature of YSZ in-flight particles measured by prototype in SPS process for the condition of low power (Test # 3) with 3MB torch

Figure 3.6 depicts the SEM images of splat samples collected at different spray distances. At 30 mm, the glass substrate was totally covered with the splats which meant relatively high deposition efficiency. The number of splats was countless, and the shape of splats illustrated that most particles were entirely molten at the impact. At this point, the device recorded the temperature of 3042ºC which was more than the melting point of the YSZ. At 40 mm, the glass substrate was more visible which indicates that a smaller number of particles had enough energy to successfully impact and attach to the substrate. Furthermore at 40 mm, fewer number of splats smaller than 1 µm was observed compared to the spray distance of 30 mm. The temperature measured by the sensor at 40 mm was 2830 °C which was very close to the YSZ melting point (2800 °C) [134]. As the spray distance increased to 50 and 60 mm, the deposited area on the glass substrate reduced and the shape of splats tended towards thicker well-developed discs. Moreover, number of spherical particles with diameter ranging between 0.5-1 µm was observed at 60 mm. These spheres were partially resolidified in-flight particles which reached the substrate. However, the impact did

not deform their shapes as they were partially solid. The minimum diameter of the splats at 50 mm was around 1 μm. At that distance, the diagnostic device measured temperatures around 2779 °C which is marginally below the melting point of the material. At 80 mm, most of the particles reached the substrate in the form of resolidified spheres except relatively large particles. At this distance, no flatten splats smaller than 1.5 μm can be observed and the number of collected splats was countable. Tendency of splats to conserve their spherical shape supported this idea that they were semi-molten. The temperature of in-flight particles was 2737 °C at 80 mm from the torch.

As discussed above, the density of collected splats on the glass plates decreases rapidly with the spray distance. Comparison between the number of particles observed on the glass substrate at 8 and 5 cm proved that the large number of particles were not molten, and they did not have enough momentum to be collected at 8 cm. It is a reasonable assumption to consider particles as a point source which are distributed uniformly. The number of particles per unit of the surface area counted on the glass substrate depends on the distance from the source. For a stationary torch and a fixed sampling glass substrate, the number of particles on the substrate is reduced proportional to the inverse of the squared distance. However, as the torch scanned the substrate in our case, the number of particles on the substrate should be reduced proportional to the inverse of the distance. The ratio of the particle number at 8 and 5 cm was calculated by counting the number of particles in the same area of interest at the two distances. It was found that the number of particles counted at 8 cm was much less than the number of particles calculated from the number particles at 5 cm times the ratio of distance. In short, this was an indication that fewer particles could reach and stick to the substrate because of cooling down and velocity reduction. Moreover, the diagnostic device makes ensemble measurements which covers the full range of particle size and temperature distributions. In fact, it gave an average temperature value of all the particles that passes through its measurement volume with a bias towards hotter and larger particles as they emit higher intensity of thermal radiation. Observation of few small splats collected on the substrate confirmed that the smaller particles of the distribution were at lower temperature than the melting point. At an impact to the substrate, these smaller particles were resolidified and they consequently bounced back. At spray distance of 80 mm, the double-point measurement system showed a temperature around 2886 °C which was considerably higher than the melting point of the material. The physical reason that the double-point measurement overestimates the temperature is $I_{\lambda 2\, measurement}$ was less than $I_{\lambda 2\, real}$ and this resulted that $(I_{\lambda 1}/I_{\lambda 2})_{measurement}$ was larger than

$(I_{\lambda1}/I_{\lambda2})_{real}$. Consequently, the temperature calculated from Equation 3.2 by a larger emission ratio at two wavelengths overestimated the real temperature. Therefore, the result of the double-point measurement system was in contradiction to the information achieved from studying of splats through the SEM. To summarize, evolution of temperature along the spray was consistent with the evidence achieved from analysis of the micrographs. The splat analysis confirmed credibility of temperature reading by the single-point measurement prototype.

30 mm

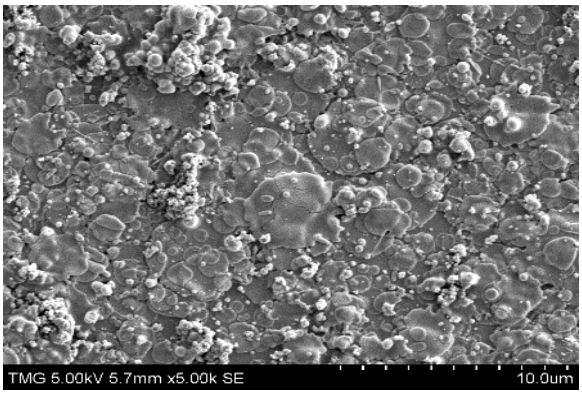

40 mm

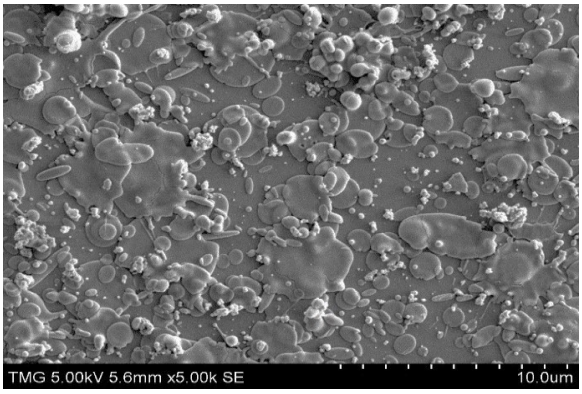

50 mm

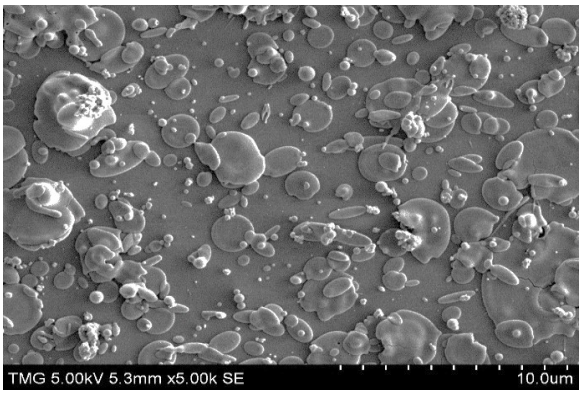

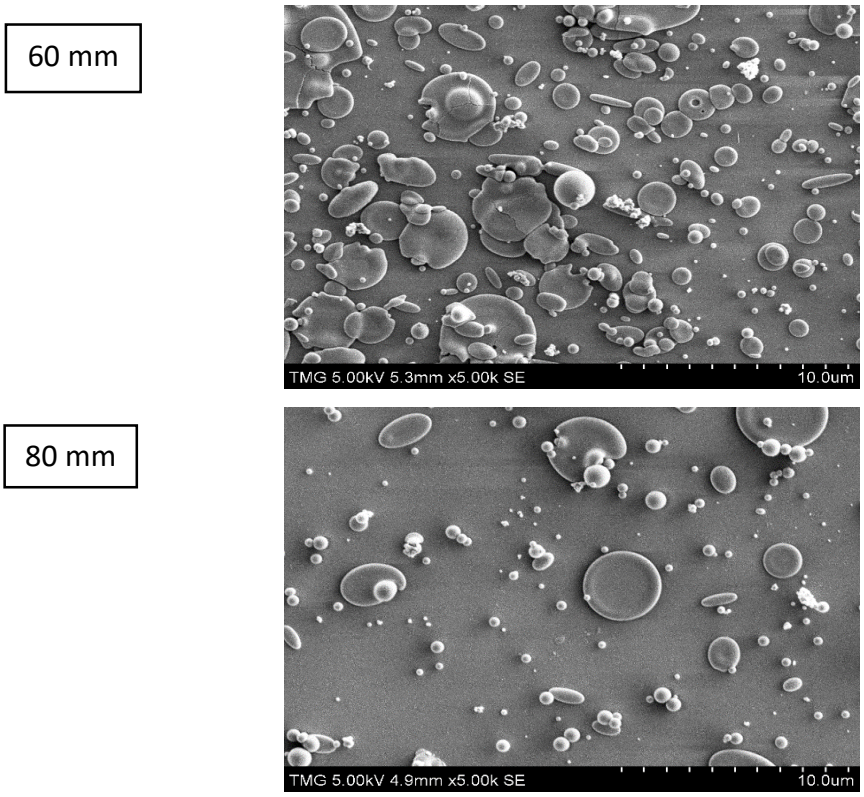

Figure 3.6. The SEM images of YSZ splats at the glass substrates for 5 spray distances from 30 to 80 mm for condition of low power (Test # 3) in SPS process with 3MB torch

3.4.3. Characterizing YSZ in SPS by AccuraSpray 4.0

In this experiment, the temperature and velocity of in-flight particles were measured by the integrated single-point measurement system AccuraSpray 4.0 as a function of standoff distance. Figure 3.7 shows that the velocity of in-flight YSZ particles constantly decreased as the standoff distance increased. The velocity decreased from 496 m/s at 30 mm from the torch to around 221 m/s at 60 mm. The trend of changes was as expected and within a common range of velocity for typical plasma conditions in SPS. The result showed the velocity dropped around 100 m/s per 10 mm for standoff distance from 30 to 50 mm. Effect of plasma at this range of distance was noticeable.

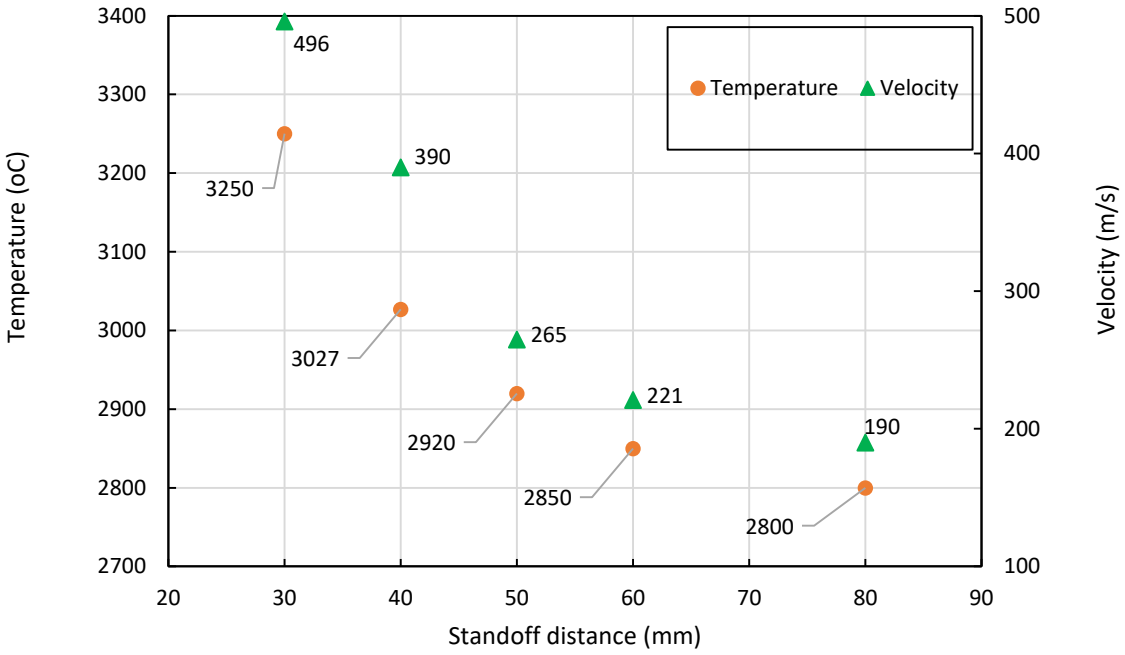

Figure 3.7. Temperature and velocity of YSZ in-flight particles measured by the single-point measurement system in SPS process for the condition of low power (Test # 3) with the 3MB torch

3.4.4. Sensitivity Analysis of Temperature to Measurement Conditions

The objective of this section is to report on the sensitivity of temperature measurements on the spray environment and improved filtering used in the diagnostic system. Figure 3.8 shows the raw signals from the temperature detector of λ_1 at six different measurement conditions collected in the same spray conditions (Test 3). Depending on the measurement condition, the voltage amplitude was different. In other words, the surrounding booth and stray radiation could have an impact on the detected signals. A more detailed analysis was carried out by looking at the root mean square (RMS) value of the signals to better understand the effects of measurement conditions.

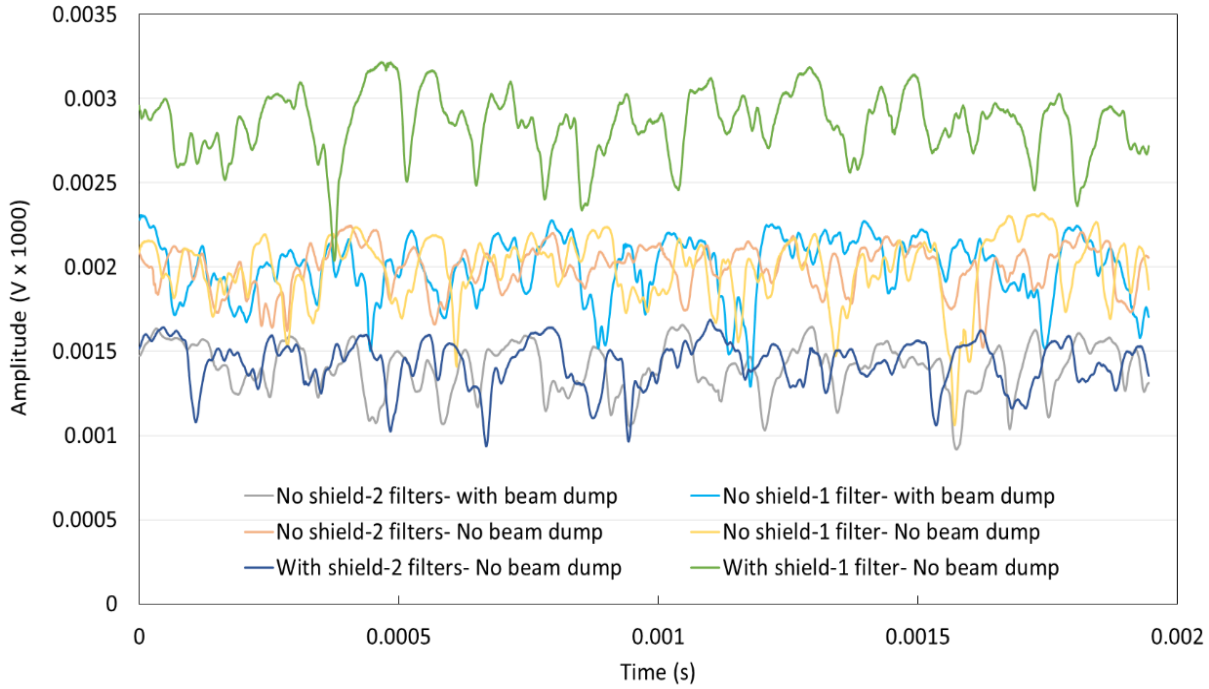

Figure 3.8. Voltage amplitude at the temperature detector for the 6 measurement conditions at spray condition test #3

Figure 3.9 shows n RMS signal value for each case. The reference condition was Case 4 without the shield, the light dump, and the enhance filtering. Table 3.3 reveals percentage of changes in the RMS values when each of three mentioned options were added to the test setup. The enhanced filter reduced the RMS value between 20 and 30 % compared to the ordinary filter of the diagnostic system. The reduction in the RMS could be as a result of an unfavorable signal attenuation of the in-flight particles in the transmission band of the filter and as a result of more effective blockage of the stray radiation out of the transmission band. Between these two, higher blockage of unwanted wavelengths of the spectrum by the filter reduced the RMS value more significantly. In the other case, employing the light beam dump reduced the RMS value between 4 and 5 % which means the reflection from the booth had a small effect the signal. Finally, using the shield between the plasma and the diagnostic system reduced the RMS by 1 %. Analysis of RMS value provided an indicator to assess the effects of measurement conditions on the measured temperature. This analysis is more tangible when measured temperature was considered for each measurement conditions.

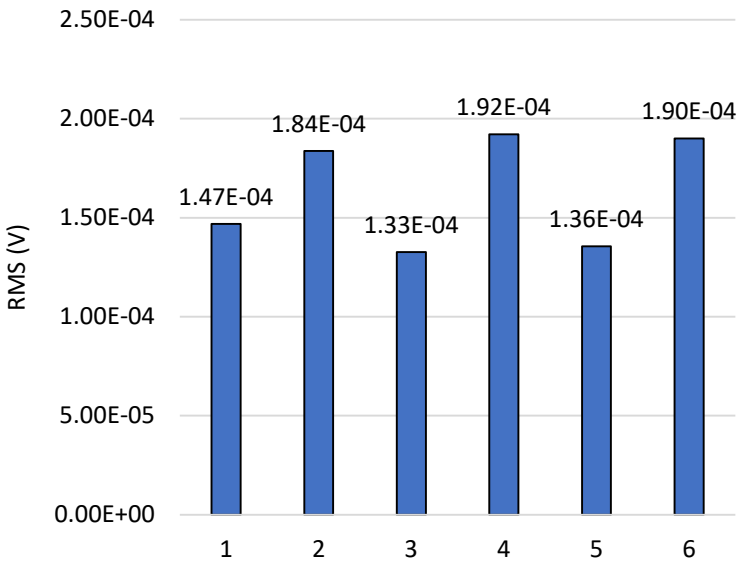

	Measurement condition		
Condition No.	Plasma shield	Enhanced filter	Beam dump
1	No	Yes	Yes
2	No	No	Yes
3	No	Yes	No
4 (reference)	No	No	No
5	Yes	Yes	No
6	Yes	No	No

Figure 3.9. RMS of signal amplitude for 6 measurement conditions at the spray condition #3

Table 3.3. Reduction of RMS value for each of three added elements to the test setup

Effect	RMS reduction (%)
Enhanced filter	20 – 30
Beam dump	4 - 5
Plasma shield	1 - 2

Figure 3.10 shows the temperature for the measurement conditions as a function of the standoff distance. The trend of changes for all the standoff distances was the same. To elaborate more, the temperature at standoff distance of 50 mm is discussed in more detail below. The temperature at the reference condition was 2855 ºC which was the highest of all measurement conditions. Temperature in the case of using the enhanced filter reduced it to 2816 ºC. The measured temperature by the enhanced filter was 39 ºC less which correspond to the 20 % lower RMS value. Regarding reflection effect, the temperature was 2843 ºC (12 ºC less than the reference condition) when the beam dump was employed. In the previous analysis, it was understood that the beam dump reduced the RMS value by 4 %. If the plasma direct radiation was concerned, the temperature was 2832 ºC when the shield protected the diagnostic system from the direct plasma radiation. In this case, a lower temperature of 22 ºC was corresponded to 1 % lower RMS value of the signal. Effect of the enhanced filter was more significant when the standoff distance was shorter as expected. At 30 mm from the torch, temperature of the reference condition was 2994 ºC

whereas the temperature was 2870 °C for the case of using the enhanced filter. It is helpful to mention, although the temperature varied around 124 °C at 30 mm of the torch, the velocity had insignificant variation as the measurement condition changed as shown in Figure 3.11. Similarly, the variation of velocity for different measurement conditions at the further standoff distances was insignificant. To summarize, the measurement condition changes the recorded temperature to a certain extent. Undesirable spectrum has the major effect on temperature, and it can be eliminated by using a filter with the more effective blockage.

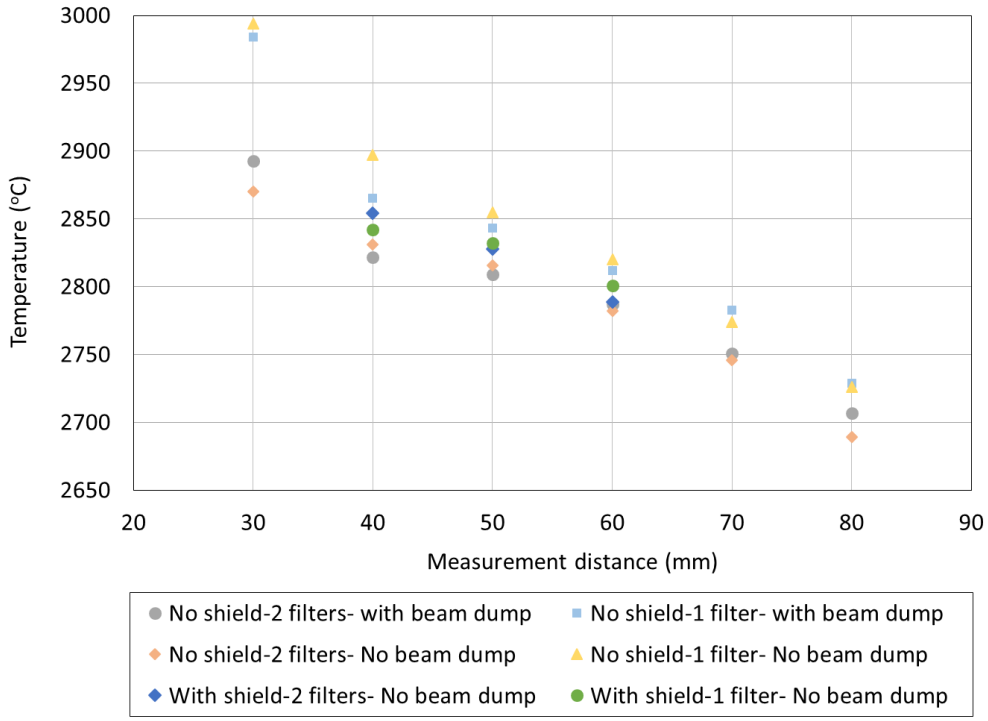

Figure 3.10. Temperature of in-flight particles as a function of standoff distance 6 measurement conditions for the spray condition test #3

3.4.1. Characterizing Alumina in SPS by AccuraSpray 4.0

Performance of the single-point measurement system was investigated for a higher power plasma which causes more intense plasma radiation and consequently more challenges for characterization of in-flight particles. Temperature of alumina powder, injected to the plasma from the Mettech torch, was measured in the SPS process by the single-point measurement system. The Mettech torch can be operated at very high power. Figure 3.12 shows that the particles temperature decreased from 2700 to 2670 ºC by sampling at two different standoff distances (50 and 75 mm). It means the particles experienced a drop of temperature around 30 ºC by moving 25 mm.

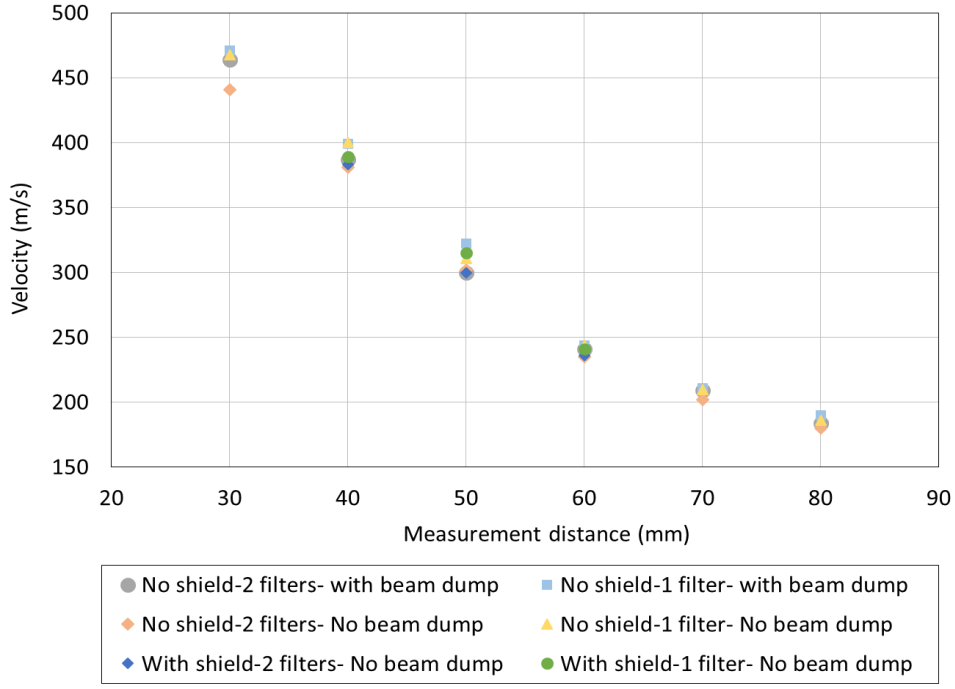

Figure 3.11. Velocity of in-flight particles as a function of standoff distance 6 measurement conditions for the spray condition test #3

It was predictable that temperature of particles would be lower at the farther distance, however, this drop was relatively small. This result can be explained by considering the melting point of alumina and plasma power at the measurement points. In fact, the melting point of alumina is around 2070 °C which is considerably lower than the plasma temperature in this experiment. Therefore, most of the axially injected particles got fully molten in the heat of plasma. On the other hand, the length of the plasma plume from the exit of the torch was over 75 mm. It was an indicator that both measurements were conducted in the hot zone which had a small temperature gradient along the plume. This was in an agreement with the measurement. Velocity of in-flight particles drops from 669 to 643 m/s which was expected for the spray condition. Tarasi et al. [82] reported a temperature around 2900 °C and a velocity around 610 m/s for a similar spray condition of alumina and YSZ mixture measured by the double-point measurement system, AccuraSpray G3C. The temperature measured by the single-point measurement system was more realistic than the one measured by the double-point measurement system.

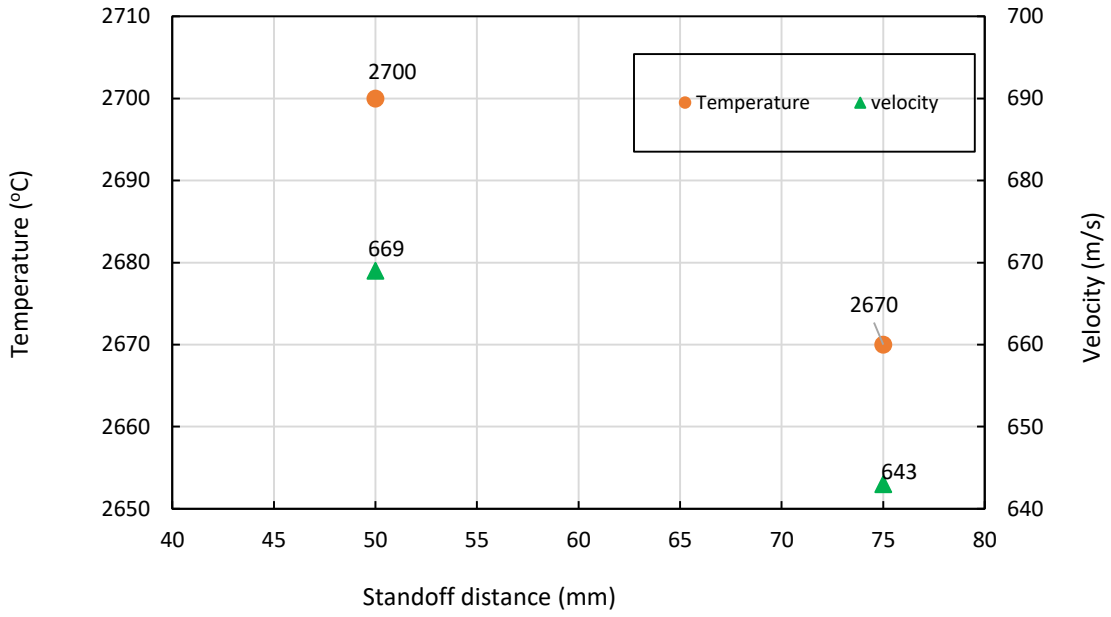

Figure 3.12. Temperature and velocity of alumina in-flight particles measured by the single-point measurement system in SPS process for the condition of Test # 4 with the Mettech torch

3.4.2. Uncertainty Analysis of Temperature Measurement

Figure 3.13 shows standard deviation (STD) for temperature measurement with the single-point measurement system. STD temperature was reported for 50 seconds measurement at 6 points from 30 to 80 mm from the torch. The STD at 30 mm from the torch was maximum between all the measurements and the average STD over time was 45 °C. At 40 mm from the torch, the STD reduced, and the average STD was 29 °C. This decreasing trend in the STD and average STD continued at the next measurement points. However, at 80 mm from the torch the average STD slightly increased. It can be due to the required higher amplification of the signals to have a temperature measurement of relatively cold particles at the long standoff distance. Table 3.4 shows the average STD of temperature for different standoff distances.

Table 3.4. Average STD of temperature over a period of time for standoff distances between 30 and 80 mm for the double-point measurement system

standoff distance (mm)	30	40	50	60	70	80
Average STD of temperature (°C)	45	29	21	13	13	15

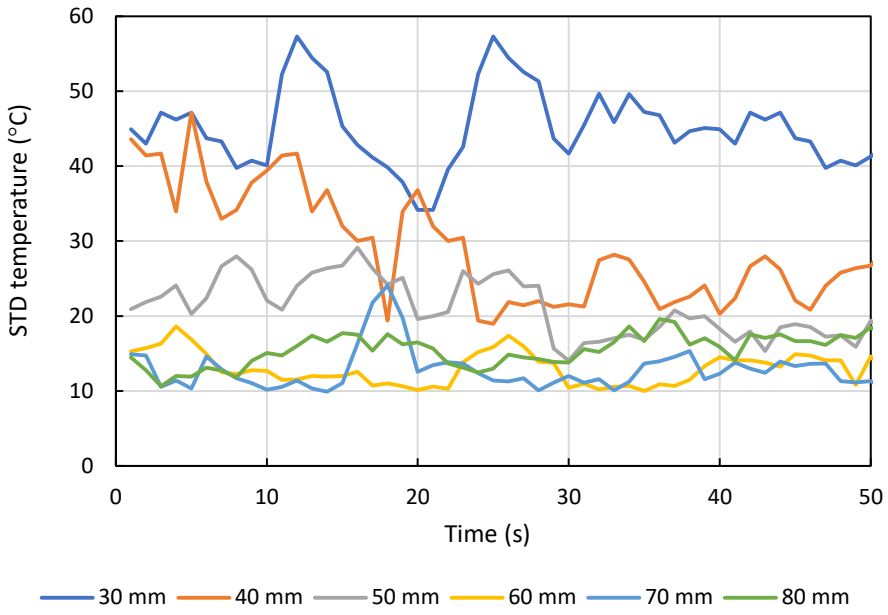

Figure 3.13. Standard deviation (STD) of temperature measurement during a period of time for standoff distances between 30 and 80 mm for the double-point measurement system

3.5. Conclusions

The main objective of this work for development of a reliable system to measure temperature of in-flight particles in SPS and evaluation of the system was successfully achieved. Diagnostic system for the APS process known as AccuraSpray G3C, the double-point measurement system, can provide an estimation of temperature of in-flight particles in SPS for spray distance between 50 mm to 80 mm and it shows some deviation from expected temperature after a spray distance. The deviation exists regardless of the plasma power. Furthermore, the double-point measurement system always overestimates the temperature of in-flight particles in SPS. Therefore, this system was further developed and adjusted exclusively for SPS to improve the accuracy of temperature measurement. A single-point measurement configuration and an improvement of the signal filtering were applied in the new system. The result of temperature measurement in SPS was indirectly verified through the splat analysis. The splat analysis is consistent with the evolution of temperature measured by the single-point measurement prototype. The SEM images of splats showed that most of the particles were resolidified and they didn't flatten nor stuck to the substrate when the measured temperature of particles was below the melting point. Moreover, effect of measurement conditions on temperature of particles was investigated.

The study showed the stray radiation has limited influence on the temperature measurement in the condition of this work. Elimination of stray radiation with using components such as an enhanced filter, a beam dump, and a shield provide more realistic temperature of in-flight particles particularly at a shorter spray standoff distance. Applying these components can be necessary to avoid significant bias on the measurement of temperature for some spray and measurement conditions. In short, due to reduction in the measurement volume and optimized filtering, the single-point measurement AccuraSpray 4.0 successfully measured the temperature of the in-flight particles in SPS.

Acknowledgements

The authors gratefully acknowledge Dr. Fadhel Ben Ettouil, Morvarid Mohammadian, and Saeid Garmeh for their kind help to carry out the experiments and for their fruitful discussion on the topic. This project was funded by the Natural Sciences and Engineering Research Council of Canada (NSERC), Canada Research Chair, and Mitacs program.

CHAPTER 4. ARTICLE 3: Analysis of Scattering Light from In-flight Particles in Suspension Plasma Spray for Size Measurement

A. Akbarnozari, S. Amiri, A. Dolatabadi, C. Moreau [c]

Department of Mechanical, Industrial, and Aerospace Engineering, Concordia University, Montreal, Quebec, H3G 1M8, Canada

This article has been published in the *Journal of Thermal Spray Technology*, First online 22 March 2019, DOI: 10.1007/s11666-019-00852-6

Abstract

Suspension plasma spray (SPS) is an emerging coating process for making surfaces with superior properties. In this process, in-flight spray particle characteristics (such as size, velocity, and temperature) have a direct influence on the properties of the deposited coatings. Accordingly, online diagnostic tools to characterize the in-flight particles in the SPS are sought by research laboratories and industrial centers for process optimization and control. However, small particle size, high temperature, and radiation of the plasma make it challenging to carry out these measurements. In this study, we used a light diffraction (LD) approach to measure online the size of in-flight particles sprayed from a well-predefined size distribution. Refraction of the laser beam

[c] Ali Akbarnozari conceived of the idea, developed the plan of research, performed the calculation, carried out the experiments, analyzed the result, and wrote the manuscript. Christian Moreau and Ali Dolatabadi helped to discuss the results, reviewed and commented on the manuscript, and supervised the project. Shahin Amiri helped to carry out the experiments, discussed the results, and reviewed the manuscript as the postdoctoral fellow.

by the hot plasma/gas jet is one of the main sources of noise for such size measurement. Successful measurements were achieved by shielding the measurement section and filtering the plasma radiation to reduce the influence of the laser refraction and plasma radiation. Results showed that the LD method has the potential to be used to monitor online the size distribution of in-flight particles in the SPS process.

Keywords: Particle size distribution, Online measurement, In-flight particle characterization, Light scattering, Diagnostic system, Suspension plasma spray. Laser diffraction

4.1. Introduction

Suspension plasma spray (SPS) is a coating process in which feedstock particles of submicron size are introduced to high temperatures and high velocity plasma by a liquid carrier [135]. As shown in Figure 4.1, a plasma torch provides the heat and momentum to melt and direct the particles toward a substrate to produce a coating layer. In comparison, in atmospheric plasma spray (APS), the feed particles are around 10 to 100 μm in size and are injected into the plasma by a gas carrier. Undoubtedly, the use of finer particles in SPS compared to APS provide unique morphological, chemical, thermal, and mechanical properties to the SPS coatings [136-138]. SPS coatings have been developed for a range of applications. For example, SPS has been studied by Jaworski et al. [139] for depositing hydroxyapatite coatings on biomaterial substrate. Thermal barrier coatings (TBC) for gas turbine blades were reviewed in works of Vassen et al. [140] and Fan et al. [141], more recent application, Sharifi et al. [7] sprayed titanium oxide to make a durable anti-icing surface for an aircraft; and finally, by Aghasibeig et al. [6] produced an electrocatalytically active surface by SPS. Detailed description on the SPS process and its applications have been published in [142,143]. Accordingly, the growing application of SPS requires a more precise understanding and control over the process which depends on capacity of diagnostic systems.

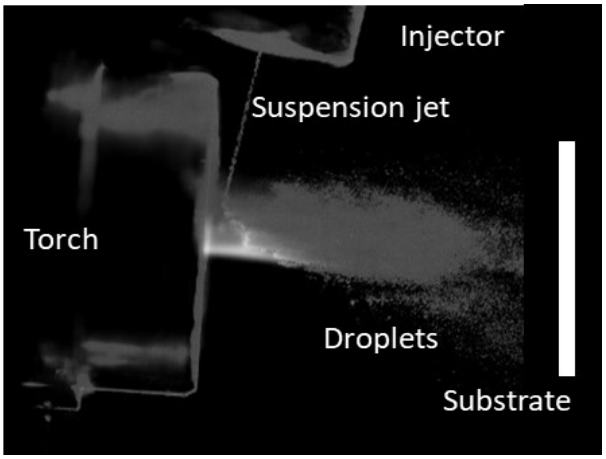

Figure 4.1. Suspension plasma process, the injection of suspension jet in the plasma and generating droplets

4.1.1. Particle Trajectory and Size Changes

Measuring particle size in the SPS process is particularly important as compared to the APS process for two primary reasons: First, the trajectory of particles near the substrate depends on their size; Second, particle size is prone to changes during the spray process. Berghaus et al. [144] modeled the velocity of particles near the substrate based on particle size. They noticed that both particle trajectory and velocity varied noticeably with size. Likewise, Crowe et al. [145] explained that trajectory of particles depends on the interaction of particles and the gas which quantified by Stokes number (*St*). *St* is defined as the ratio of the response time of the particle over the characteristic time of the flow. That is to say, for $St<<1$, a particle has sufficient time to respond to flow deviation, therefore following the fluid. This is the case for fine particles in spray when approaching the substrate. On the other hand, for the $St>>1$ a particle does not have enough time to respond to the change of flow direction and therefore leaves the flow. The latter scenario corresponds to relatively larger particles, which get deposited on the substrate and contribute to building the coating. Altogether, Figure 4.2 shows schematically particle trajectories in terms of size near the substrate. This phenomenon has a strong influence on the coating microstructure and consequently coating properties. Additionally, VanEvery et al. [24] explained that when small particles moved almost parallel to the substrate, they stuck to asperities of the substrate surface or already deposited particles. This phenomenon, which causes the coating to have a columnar porous microstructure, has been named the shadow effect.

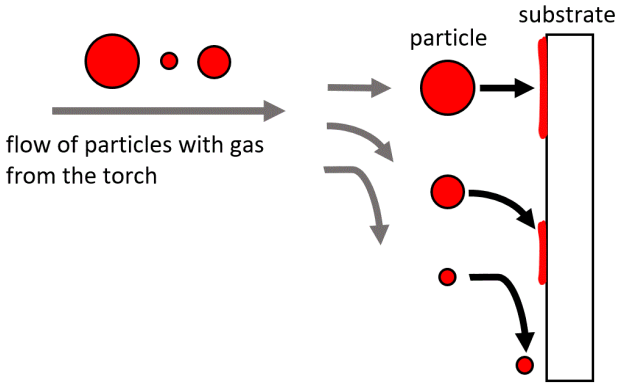

Figure 4.2. Schematic showing the effect of size on the trajectory of particles near the substrate. Large particles flow straight to the substrates, while tiny particles deviate and move parallel to the substrate. Particles with intermediate size stay in between these two conditions

Pawlowski [31] described that particle size through the SPS process is prone to remarkable changes because of the agglomeration and evaporation of particles. Consequently, the size of particles close to the substrate is different from the size of feedstock particles. Figure 4.3 shows how the SPS process can cause changes in the size of particles. In this case, being exposed to plasma for a short time, the suspension jet interacted with the hot gas flow, breaking up into smaller droplets. The liquid phase of the suspension is then evaporated, and feedstock particles get closer to each other in droplets. At this time, adjacent particles start melting and get agglomerated in the heat of the process. On the other hand, the agglomerated and molten particles can undergo size decrease on their path toward the substrate because of evaporation. Therefore, the size of the in-flight particle near the substrate is not the same as the feedstock and depends on the actual spray conditions. In particular, Pourang et al. [146] modeled the SPS process and showed that, at a 6 cm standoff distance from the torch, the feedstock particles of a few hundred nanometers were agglomerated and formed particles averaging 1.0 to 1.5 μm in size. It is noteworthy to highlight that, throughout this paper, the word "droplet" is used to designate a droplet of atomized suspension while the word "particle" designates a solid or molten particle of coating material as illustrated in Figure 4.3.

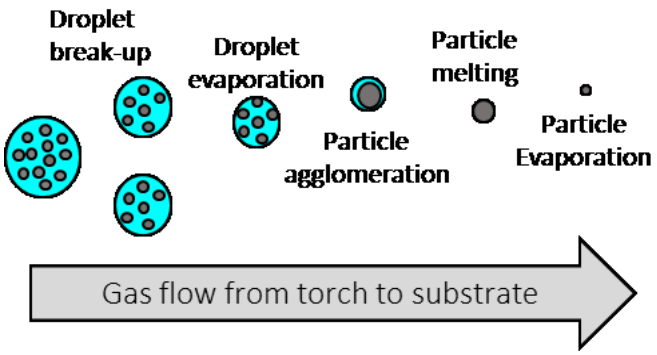

Figure 4.3. Schematic showing the phenomena involved in the suspension plasma spray process

4.1.2. Online Measurement

Online monitoring of spray parameters is used in industry to control and guarantee the quality of deposited coatings and reduce the number of rejected parts [147]. More than fifty parameters determine the actual plasma and injection conditions that affect the coating properties. Nonetheless, instead of monitoring each of these spray parameters, the characteristics of in-flight particles near the substrate can be monitored and provide the information required for adjusting the injection and plasma parameters. Fincke et al. [148] explained that supplying the result of online monitoring in a spraying process equipped by a real-time feedback control improves the repeatability, reliability, and reproducibility of coatings.

4.1.3. Diagnostic System

Fauchais et al. [149] reviewed the available diagnostic systems for thermal spray processes. Among the pioneers, Fincke et al. [55] measured size of particles from magnitude of scattered light. The first commercial diagnostic system for online characterization of in-flight particles was developed in the 1990s based on works by Moreau et al. [150-155] and commercialized under the names DPV 2000 and DPV evolution (Tecnar, Saint-Bruno-de-Montarville, Canada). It measured the size, velocity, and temperature of in-flight particles in thermal spray processes. Later, Blain et al. [59] introduced an optical device that characterized online the particles during the APS process. Moreau et al. [74] explained how the monitoring the spray process provided a tool to control coating properties in research centers and on the production floors. Moreover, Cetegen et al. [76] measured the size of the particles by Phase Doppler Particle Anemometer (PDPA). In addition to optical method mentioned already, there were some research to measure the size of in-flight particles through imaging techniques such as: Particle Shape Imaging (PSI) based on works by Zimmermann et al. [77] and Landes [78]. In another example, Wroblewski et al. [70] claimed to

estimate the size of particles by using CCD arrays and applying topological criteria. In all available diagnostic systems except for PDPA, particles with a diameter larger than 5 μm were detectable [156] and fine particles of SPS were not able to be recognized. For a particular case, Rampon et al. [79] reported the use of a Laser Diffraction (LD) method to measure the droplet size of the YSZ suspension and the in-flight particles. Their results of size distribution required to be validated.

The main objective of this study is to investigate the capabilities and limitations of the laser diffraction technique to measure online size distribution of in-flight particles in SPS process. To do so, approaches for reducing the influence of plasma radiation and laser refraction are discussed and implemented. Spray experiments were carried out with glass particles with a known particle size distribution to validate the online measurements.

4.2. Theory and Background

4.2.1. Light Scattering

Particle size measurement by the light diffraction approach works based on Mie scattering theory, which states that the intensity of scattered light from a particle is a function of the particle size, shape, refractive index, wavelength and polarization of incident light, and observation angle (scattering angle) [103]. Figure 4.4 depicts a particle of radius a received plane incident light of wavelength λ and it scattered the intensity of I at scattering angle of θ. The scattering intensity was achieved from solving the equation of electromagnetic fields around the particle [106] and it is represented by Stokes matrix. For scattering of a spherical particle from receiving an unpolarized beam of incident light, the Stokes parameters were given in Eq. 4.1:

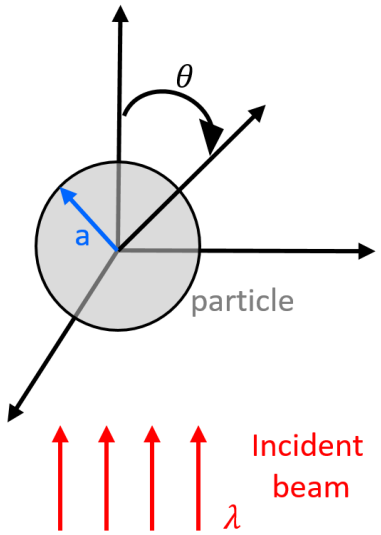

Figure 4.4. Polar coordination for studying scattering of a spherical particle of radius r exposed incident beam of wavelength λ [106]

$$I_s = S_{11} I_i \qquad Q_s = S_{12} I_i \qquad U_s = V_s = 0 \qquad \text{Eq. 4.1}$$

where I_s represents scattering intensity, Q_s and U_s shows linear polarization, and V_s shows circular polarization. I_i is the incident light and S_{11} and S_{12} are elements of Stokes parameters matrix which are calculated by Eq. 4.2:

$$S_{11} = \frac{1}{2}(|S_2|^2 + |S_1|^2) \qquad S_{12} = \frac{1}{2}(|S_2|^2 - |S_1|^2) \qquad \text{Eq. 4.2}$$

And S_1 and S_2 are elements of the amplitude scattering matrix which are calculated through Eq. 4.3:

$$S_1(\theta) = \sum_{n=1}^{\infty} \frac{2n+1}{n(n+1)} [a_n \pi_n + b_n \tau_n] \qquad S_2(\theta) = \sum_{n=1}^{\infty} \frac{2n+1}{n(n+1)} [a_n \tau_n + b_n \pi_n] \qquad \text{Eq. 4.3}$$

In this equation, a_n and b_n are scattering coefficients and π_n and τ_n are angle-dependent functions given in Eq. 4.4 and Eq. 4.5:

$$a_n = \frac{m\psi_n(mx)\psi_n'(x) - \psi_n'(mx)\psi_n(x)}{m\psi_n(mx)\xi_n'(x) - \psi_n'(mx)\xi_n(x)} \qquad b_n = \frac{\psi_n(mx)\psi_n'(x) - m\psi_n'(mx)\psi_n(x)}{\psi_n(mx)\xi_n'(x) - m\psi_n'(mx)\xi_n(x)} \qquad \text{Eq. 4.4}$$

$$\pi_n(\cos\theta) = \frac{1}{\sin\theta} P_n^1(\cos\theta) \qquad \tau_n(\cos\theta) = -\sin\theta \frac{P_n^1(\cos\theta)}{d(\cos\theta)} \qquad \text{Eq. 4.5}$$

where ψ_n and ξ_n are Riccati-Bessel functions and P_n is Legendre polynomials. x and m are the size parameter and relative refractive index respectively as are shown in Eq. 4.6 and Eq. 4.7:

$$x = \frac{2\pi n a}{\lambda} \qquad \text{Eq. 4.6}$$

$$m = \frac{n_1}{n} \qquad \text{Eq. 4.7}$$

where n and n_1 are the refractive indices of medium and particle respectively. All equations illustrate how the scattering intensity (I) is related to the size of particle (a). For example, Figure 4.5 shows the scattering intensity from a laser beam at λ = 633 nm by water droplets of 1, 4, and 10 μm in air. The scattering intensity is maximum at zero degree, however, it reduces up to ninety degrees and afterward it increases again. The changes in scattering intensity as a function of the angle reduce as the size of the particles decrease.

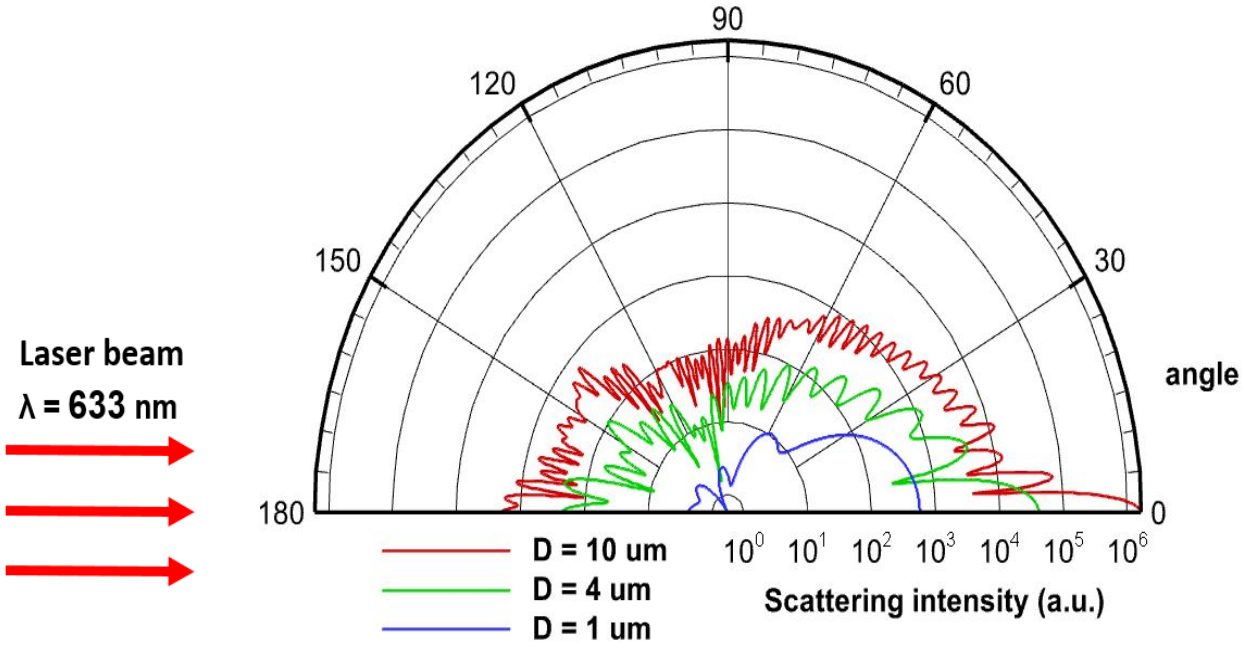

Figure 4.5. Scattering intensity as a function of the angle and size around a spherical droplet [157]

Size of the particles is calculated from scattering intensity by solving an inversion problem [104,105]. In brief, the inversion problem starts by assuming a size distribution for the particles

and calculates the scattering intensity for that distribution. In the second step, the calculated scattering intensity was compared to the experimentally acquired scattering intensity to correct the assumed size distribution. Iteration of correcting the size distribution and calculating the scattering intensity leads to find the particle size distribution. The inversion problem finds size distribution of particles for a known wavelength and given scattering intensity at a scattering angle. Substantially, the smaller particles mainly scatter light in a wide angle, while larger particles mainly scatter light in a low angle (close to zero degrees). Although LD is well-established measurement method, the SPS process introduced some challenges to be overcome. Mainly, the refraction of laser beams, plasma light, and minimum number of particles in the measurement volume were investigated in this study.

4.2.2. Laser Beam Refraction

Laser beam refraction means bending of light because of a change in the speed of light while the light goes across a medium. Fundamentally, a ray of light deviates when it leaves a medium of index of refraction n_0 and enters a different medium of index n_1. In this case, the angle of deviation is proportional to the ratio of refractive indices of two media. For a mixture of media (fluids), the refractive index of the mixture is a function of the refractive indices and volume fractions of pure components. In addition, refractive index depends on density, temperature, and temperature gradient of media [158-160]. Therefore, light refraction (beam steering) occurs when the medium of measurement is not uniform with respect to temperature, density or composition. For example, Dumouchel et al. [161] investigated the laser beam steering in a spray and they reported the beam steering caused overestimation of size distribution for drops.

Figure 4.6 illustrates schematically the beam steering when it passed through a hot gas. In other words, the gas in the measurement section was composed of several elements; hot gases (typically a mixture of neutral gases such as argon and/or helium, or combustion products like CO and/or CO_2), and the surrounding cold air with different volume fractions. When the hot gas gets mixed with the cool surrounding air in the turbulent flow, the mixture of the two gases did not have uniform temperature and density distributions. Therefore, the laser beam is refracted in a small angle and it does not have the so-called unperturbed trajectory. In other words, the figure schematically shows that instead of a sharp-tip red cone of light meets in zero degree, the light is spread like a truncated light-red cone in angles of around one degree.

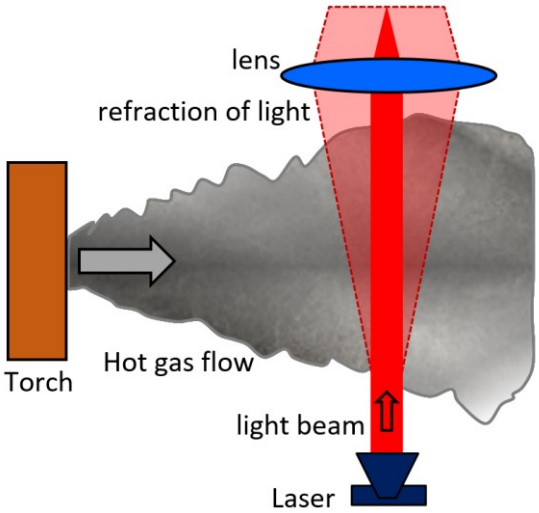

Figure 4.6. Laser beam steering, laser light refraction in the plasma and defocusing unscattered laser

4.2.3. Plasma Light

Plasma has radiation in a range from infrared to ultraviolet. The radiation of plasma is reflected from the surfaces and is refracted by the particles exist around the plasma. The radiation of plasma is measured by a spectrometer at different distances for different range of wavelengths. Seeing that, Gougeon et al. [162] and Aziz et al. [133] reported the plasma radiation in the range of visible and infrared wavelengths for plasma spray process. Plasma radiation causes some challenges to use optical diagnostic devices in the plasma spray process. Therefore, it is necessary to prevent or minimize the effect of plasma radiation and reflection on detectors of the optical diagnostic system. Using a shield and bandpass filter minimize the effect of plasma on the system.

4.2.4. Number of Particles

Success measurement depended on capturing signals from an adequate number of particles in measurement volume. Specifically, the small size of the target particles was one of the main measurement challenges in this study. In the extreme case of Mie scattering (close to the geometrical optics), when the ratio of particle size to the incident light wavelength is more than 10, the intensity of scattered signal by a particle changes proportional to a^2 where a is the radius [163]. Generally, this ratio varies between $0.55a^2$ and $1.90a^2$ in the region of Mie scattering. Therefore, as the size of particles in the SPS process reduces around one order of magnitude compared to the APS process, the intensity of their scattered signal reduces between *55* and *190*

times. Therefore, a minimum number of particles should present in the measurement volume to scatter enough stable light to stimulate the detector for a correct size distribution.

4.3. Experimental Methodology

4.3.1. Material

The testing material for the size measurement was glass particles (Cospheric, USA). The micrograph and size distribution of particles are illustrated in Figure 4.7 which confirms median size (D_{v50}) of 4 µm. There were several reasons for selecting this material; *(i)* its size distribution was quite close to the range of particle sizes which were expected to be observed near the substrate during the SPS process, *(ii)*, it had a narrow size distribution, *(iii)*, in terms of safety, it was neither toxic nor hazardous, *(iv)*, it was suspended in the water uniformly and did not agglomerate or sediment during preparation or injection. The particles were soda lime glass microspheres with an index of refraction 1.5 as specified by the supplier. Test of glass particles made it possible to perform the test of online size measurement and more important, to validate the result. To prepare suspension, 10 wt.% glass particles were mixed with distilled water by a mechanical stirrer and an ultrasonic liquid mixer (QSonica, USA) to have a homogeneous suspension.

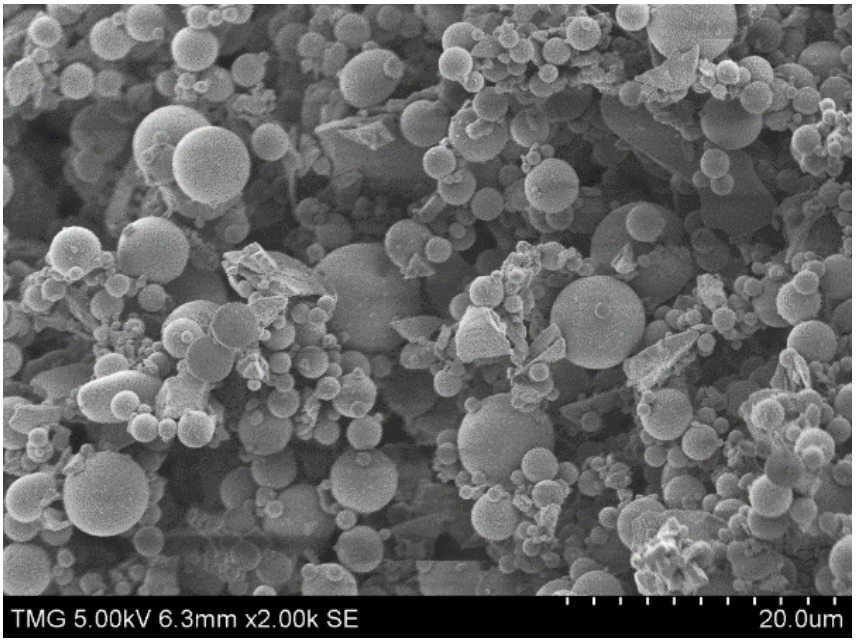

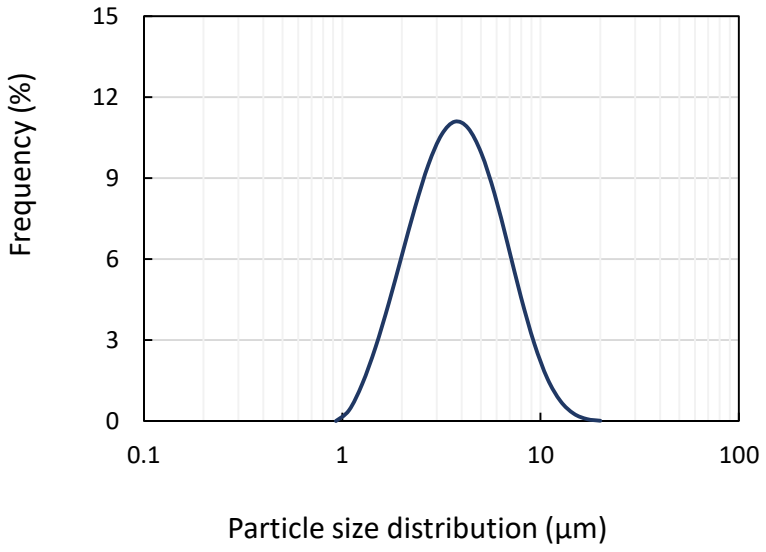

Figure 4.7. SEM microstructure of the glass particles (top) and their particle size distribution (bottom)

4.3.2. Plasma and Injection System

Figure 4.8 shows the plasma spray and the suspension injection systems. In detail, the suspension was injected to the hot gas flow by a homemade injection system composed of a pressurized suspension tank equipped with agitating device, a Coriolis flow meter, and an injector. The plasma torch was 3MB fed by argon gas with a flow rate of 60 SLPM and the plasma power around 16 kW. The suspension was injected at 60 mL/min (mLPM) from an orifice of 250 µm. Size of the in-flight particles measured at a standoff distance of 20 cm from the torch on the centerline of plasma. The effect of plasma radiation and light on measurement were reduced at 20 cm of the torch. This distance was more than usual spray condition which is between 4 and 6 cm. However, the size of in-flight particles does not change after 6 cm. By measurement at 20 cm, the size was the same as 6 cm and the effect of plasma noise was reduced. Choice of plasma conditions (such as argon gas and relatively low plasma power) and injection conditions were adjusted to prevent from melting and changing the size of the glass particles during the spray. Therefore, the result of online measurement could be validated by comparing with the size distribution of the feedstock particles. In other words, it was expected that the particle size distribution of the in-flight particles would be the same as particle size distribution of the feedstock material.

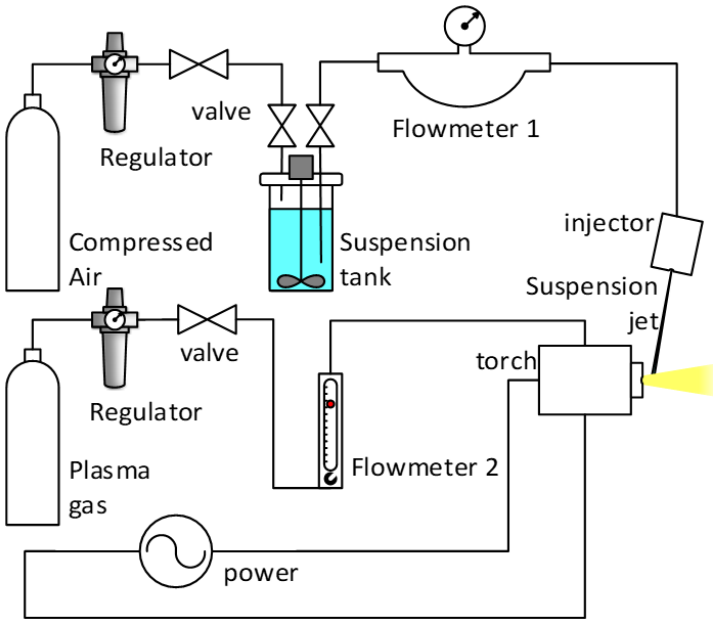

Figure 4.8. Plasma spray and suspension injection systems

4.3.3. Acquisition Apparatus

Diagnostic system was Spraytec (Malvern Panalytical, Grovewook, UK) which functioned based on the Mie scattering and was first introduced by Swithenbank et al. [164]. It had two configurations to characterize the samples: First, for a spray of particles in air which used for online measurement; Second, for the particles circulated in a liquid of a closed loop system (a wet dispersion unit). The latter configuration was used for offline measurement to validate the result and also to find the minimum number of particles. The diagnostic system had a helium neon laser of 2 mW at a wavelength of 633 nm and with a beam diameter of 10 mm. Moreover, its detector consisted of 36 concentric silicon diode array sensors situated between 0 and 18 degrees where detector zero was at zero angle and detector 36 was at the angle of 18 degrees of the unscattered laser. The data acquisition rate of the system was between 1000 Hz and 10 kHz. Also, effective range of size measurement for the system was 0.1 – 1000 µm. For measurement, the LD system captured background and raw signals. The background was obtained with the plasma and laser and without particles. The raw signal was obtained with plasma, laser, and particles. Finally, it calculated the scattering intensity of particles by subtraction the background signal from the raw signal. Briefly, the scattering intensity of the in-flight particles was calculated from Eq. 4.8:

$$I_p = I_{RS} - I_{BG} \qquad \text{Eq. 4.8}$$

where I_p , I_{RS} , and I_{BG} are scattering light intensity of particles, raw intensity, and background light intensity respectively. In SPS, the background was expressed as the measured intensity when the plasma was running and pure water (no suspension) was injected. In the same way, the raw intensity was declared a measured intensity when plasma was running at the time suspension was injected. Figure 4.9 shows the configuration of the diagnostic system in the SPS process, including the measurement section, laser, and the detector, two layers of shields, and bandpass filter. The emitted plasma light was prevented from reaching the detectors by the shields and a bandpass filter. For shielding, a plate of steel with an aperture of a few millimeters was placed in front of the torch. The size of aperture was optimized through experiments. A second shield from aluminum with an aperture of 10 mm was placed after the first shield to prevent the heat transfer of hot steel to the measurement volume and to direct the flow of gas through the laser of the diagnostic system. The deployment of the shields was for research studies, however, it could be replaced with a more practical configuration which is currently under development in our laboratory.

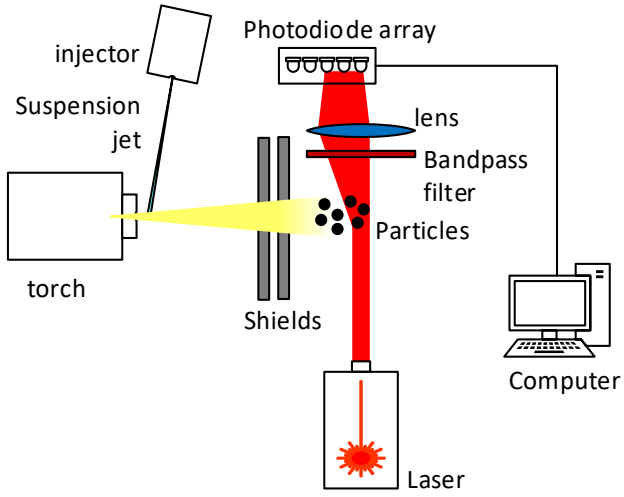

Figure 4.9. Schematics of test setup composed of a suspension injection, a plasma torch, and laser diffraction systems, two layers of shields were placed between the torch and the diagnostic system

Although the shield in the test setup blocked direct radiation from the plasma to the detectors, the reflected radiation from the spray booth reached the detectors. Under these circumstances, the bandpass filter, with transmission around the wavelength of the laser, was mounted in front of the detectors to eliminate the plasma light. Equally important, the range of transmissions of the selected filter was wide enough to accept tilted incident scattering after the

blueshift. Figure 4.10 illustrates that the filter had a transmission between 626 and 640 nm. Besides, for wavelengths less than 600 and more than 680 nm, the transmission was negligible.

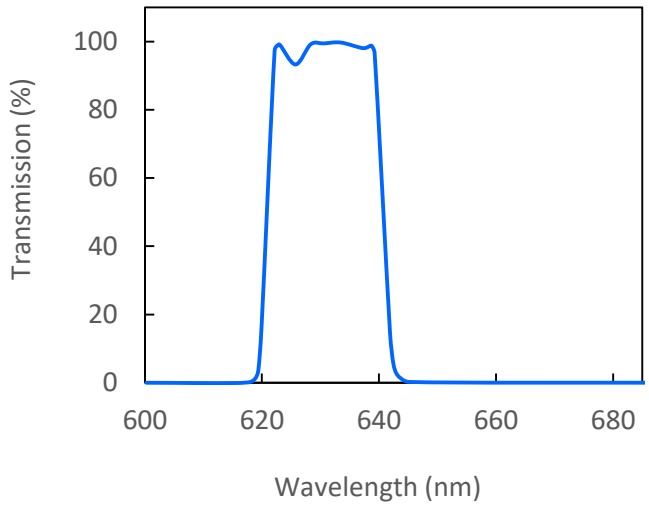

Figure 4.10. Transmission range of the bandpass filter for the detector

Scattering of particles from the plasma was eliminated for the measurement. In reality, the filter permitted the spectrum, within transmission range, to reach the detector regardless of the source of radiation. The particles scattered light from two sources: First, the laser light of the diagnostic system; Second, the radiation of the plasma. To understand the impact of these scattering signals on measurement, the irradiance of a particle distribution from these two sources was calculated based on Mieplot's (Philip Laven) [157] Mie theory. For this purpose, the scattering of glass particles with D_{50} of 4 µm and a standard deviation of 50% (similar to the testing powder) were studied. Figure 4.11 shows the calculation of the irradiance of the particles from laser sources compared to the calculated irradiance of a particle from plasma at spray distances of 4 cm (typical SPS standoff distance and without any bandpass filter in the diagnostic system) and 20 cm (suggested standoff distance for this study) with and without the bandpass filter. Altogether, the graph reveals that particle light scattering from plasma and laser was in the same order of magnitude at the spray distance of 4 cm without the filter. By using the filter and measurement in 20 cm, the scattered plasma reduced three orders of magnitudes compared to the scattered laser. Thus, using the bandpass filter for the detector and adjusting the measurement volume in right distance from the torch, minimized the effect of scattered plasma. Technically speaking, calculated scattering intensity by particles from the plasma source shows effect of filtering to reduce noise.

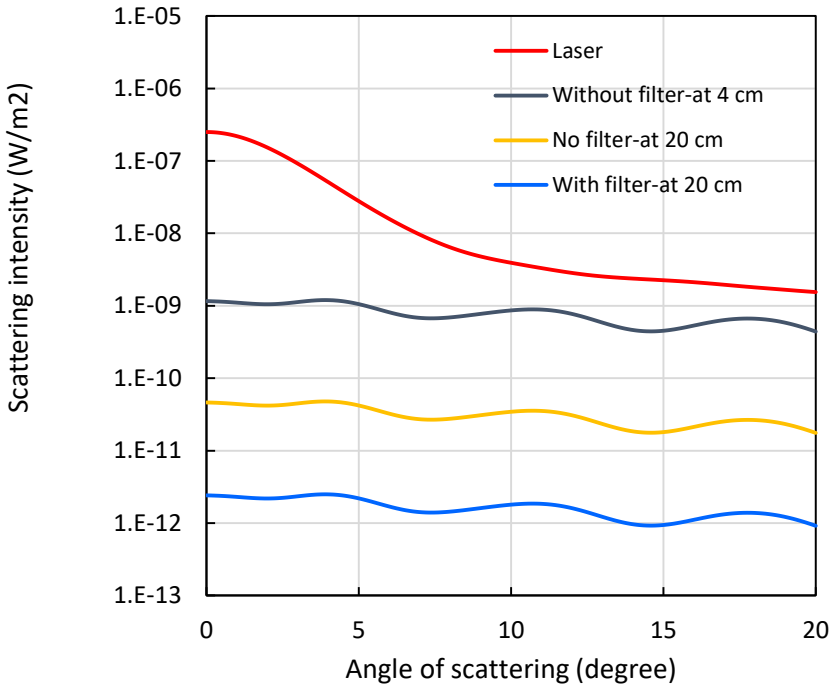

Figure 4.11. Calculated scattering intensity based on Mie theory for glass particles with a log-normal distribution around an average size of 4 µm and standard deviation of 50 %, from a laser source at a wavelength of 633 nm (red line), from a source of plasma at standoff distance of 4 cm without any filter (gray line), from the source of plasma at standoff distance of 20 cm without any filter (orange line), and from the source of plasma at standoff distance of 20 cm with a bandpass filter of 626-640 nm (blue line)

4.4. Results and Discussion

4.4.1. Minimum Number of Particles

Practically, in SPS, the number of particles was mainly controlled by the concentration of powder in suspension and the flow rate of injection. In this study, the minimum number of particles was measured from doing a set of experiments at the wet dispersion unit. According to the experiment, there was no measurable signal at a lower number of particles in the measurement volume. By adding more particles, scattering intensity became stable and size was measured correctly for the given particles. For the glass powder with an average diameter of 4 µm, the minimum number of particles was around 15,000, which corresponded to the peak intensity of 40 (a.u.) in the graph of scattering signal versus the detector. LD system calculates particle size distribution when ensemble measurement of scattering signals from all the particles in the measurement volume was above a minimum level of light intensity defined based on the sensor specification. Moreover number density of particles and size of measurement volume experienced

a constant change during the spray because of plasma condition and suspension injection. Therefore, the number of particles in measurement volume was a key parameter insured the response of the system for reliable measurement. Generally, the scattering intensity corresponded to the signal of the glass particles when the majority of water droplets were vaporized by adjusting the plasma power. However, the presence of the water droplets in the measurement volume had an impact on the raw signal. Ideally, the diagnostic system measured the size of in-flight particle when the liquid droplets fully evaporated. As one step in the SPS process, the liquid phase of suspension droplets was vaporized during their residence time in the hot gas. This step was mainly controlled by adjusting the power of the plasma system and injection conditions. Although, existence of droplets in measurement volume was inevitable because of the instabilities of both plasma and injection during spray. Therefore, it is necessary to understand the possible effect of the droplet signal on the measurement. For example, Marchand et al. [165] measured the droplet size for superpulsating atomization, where D_{50} was around 20 µm. In our case, the irradiance of water droplets of this size was calculated and compared to the irradiance of glass particles with D_{50} of 4 µm and standard deviation of 47%. Figure 4.12 reveals the irradiance for a water droplet at their peak was equaled the irradiance of 56 particles. Moreover, calculations showed the irradiance of one water droplet was around 12 times more than the irradiance of one particle in the angle of peak intensity of the particle (detectors 27 and 28). In other words, the scattering of one droplet was equivalent to the scattering of 12 particles. Therefore, the number of particles must be sufficiently more than the number of droplets to have reliable signal for particle size measurement. The calculations showed that presence of water droplets in the measurement volume results a bimodal graph. In our experiment, the measurement illustrated the scattering signal was unimodal and the peak belonged to the signal from the in-flight particles. This meant the number of droplets in the measurement section was quite low and it did not interfere in the measurement of particle size.

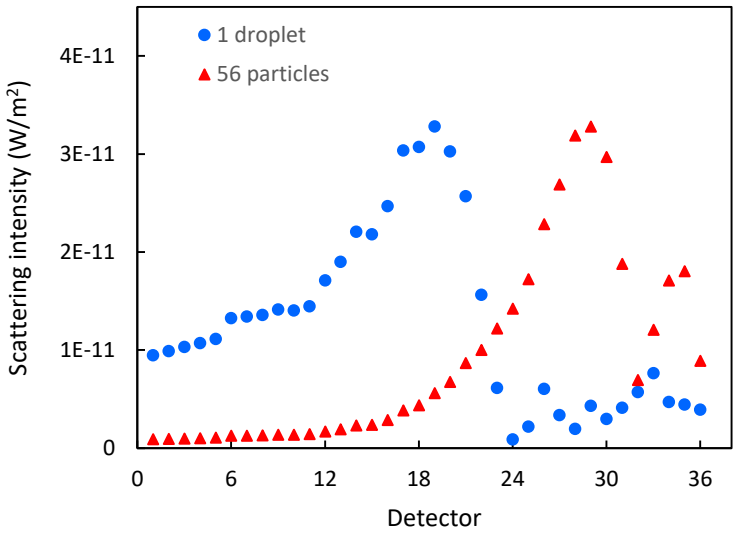

Figure 4.12. Calculated scattering intensity of one water droplet with an average size of 20 µm and standard deviation of 50%, compared to scattering intensity of 56 glass particles with average size of 4 µm and standard deviation of 50% to assess possible effect of droplets on the scattering signal

4.4.2. Influence of the Shields

Refraction of light caused that the laser was received in several detectors near the zero angle without scattering from any particles. This led to extensive light intensity in the background and the raw signal in the first detectors because of refraction in small angles. Figure 4.13 depicts the effect of the beam steering on the background intensity received in all detectors by comparing three measurement conditions; when the plasma was not running (the blue triangle), when the plasma was running without a shield (red circle), and finally, when the plasma was running and the shields were placed between the torch and the diagnostic system. In our experiment, refraction was within an angle of less than one degree; nevertheless, it was large enough to influence the first twelve detectors to different extents depending on spray conditions. Under the experiment circumstance, the intensity of the signal in the first twelve detectors for the plasma condition was three orders of magnitude greater than the time the plasma was off. The effects of laser refraction were partially eliminated from the background and the raw signal by mounting the shields between the torch and the diagnostic system. In comparison, the shields reduced the background signal for plasma by at least one order of magnitude in the first detectors. From detector 12 to the last one, there were no significant differences between measurements of background for three cases. In

brief, experimentally measured background light shows the effect of plasma on diagnostic system when there were no particles to scatter light from plasma and laser.

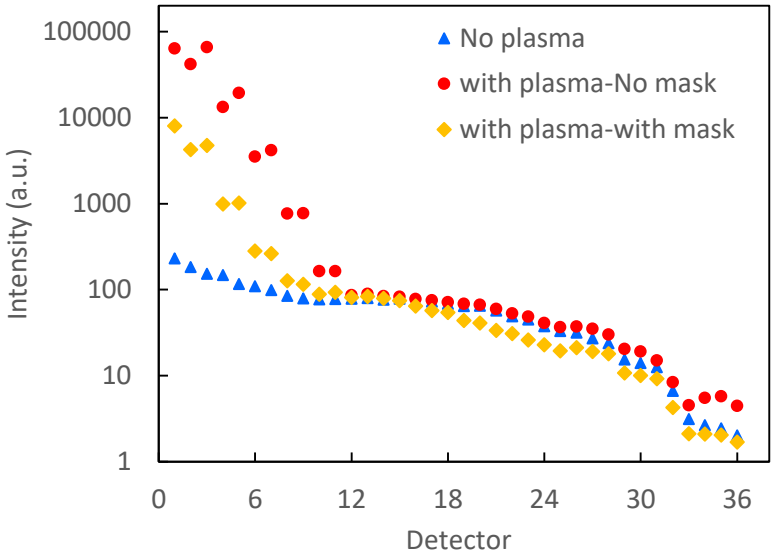

Figure 4.13. Experimentally measured background light on detectors: no plasma (blue triangles); plasma without shields (red circles); plasma with shields (orange rhombuses)

The shields had an aperture to transfer of gas from the torch to the measurement volume. The effect of the aperture size of front shield was studied in terms of light scattering. The size of aperture controlled the flow rate of particle-contained hot gas passing through the test section. Of course, the aperture size had dual effects; on the scattering intensity of the particles and on the refraction of the laser beam in the measurement section. Figure 4.14 shows the scattering intensity of particles for the aperture sizes of 1.5, 3.0, and 6.0 mm, which were measured under optimum spray conditions. The scattering intensity was minimum around the detector 11 and it was maximum around detectors 27 and 28 which correspond to glass particles of 4 μm for all the cases. Generally, if the number density of the particles was uniform when the diameter aperture was doubled, the scattering intensity should have increased four times. Comparison of result of three apertures confirmed that the particles were not distributed uniformly in the spray. As an example, the peak of the intensity increased from around 25 to 50 (a.u.) when the aperture size changed from 1.5 mm to 3.0 mm. Particularly, it was observed that the scattered intensity did not elevate to more than 75 (a.u.) when the orifice size increased to 6.0 mm. Therefore, the number density of particles at the center of the plume was greater than the number density at the periphery. Consequently, by

increasing the diameter of the aperture, the average of number density of particles all over the measurement section reduced. Moreover, the diameter of the laser beam was finite to 10 mm and a larger aperture did not introduce any more particles in the measurement volume.

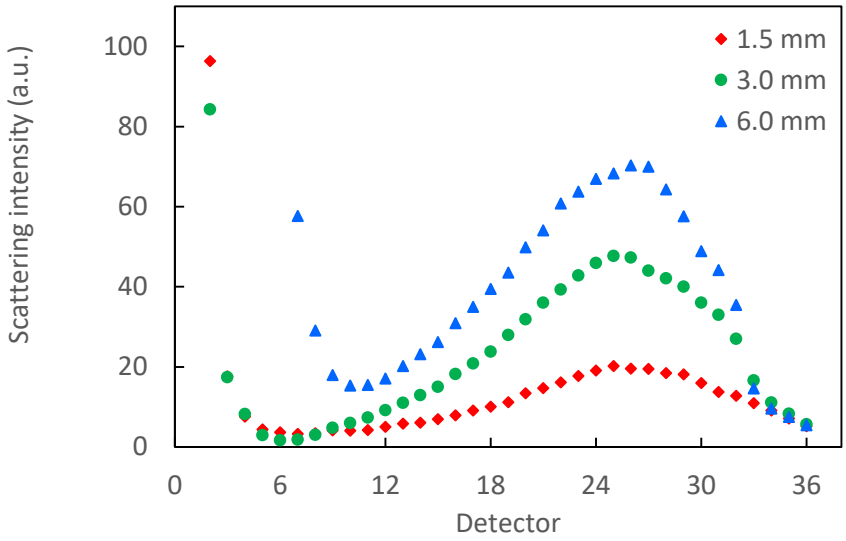

Figure 4.14. Effect of aperture size of the shield on received scattering intensity by the particles in the detectors

Besides the fact that the aperture size impacted the total scattering intensity of particles, it also modified the temperature and temperature gradient of the gas in the measurement volume. The temperature was raised as aperture size was increased. As a result, a high temperature and temperature gradient caused the laser beam to refract, which consequently generated superfluous intensity in the first detectors. Altogether, it was helpful to optimize the system by maximizing the scattering signal while minimizing refraction. For this ambivalent effect of the aperture size on the measurement, the optimum size was specified in terms of SNR which was defined as the ratio of raw signals from particles over the background. Figure 4.15 shows SNR for three aperture sizes at the detectors 27 and 28 where the peak of scattering intensity for glass particles was situated. SNR was the highest for the middle size aperture (3.0 mm) and it was around 3.25. Two statements were suggested for this observation: First, the 3.0 mm aperture limited amount of hot gas that changed of temperature in measurement volume and consequently the noise reduced; Second, the width of a cylinder of hot gas in the measurement volume was smaller and respectively the light refraction was less.

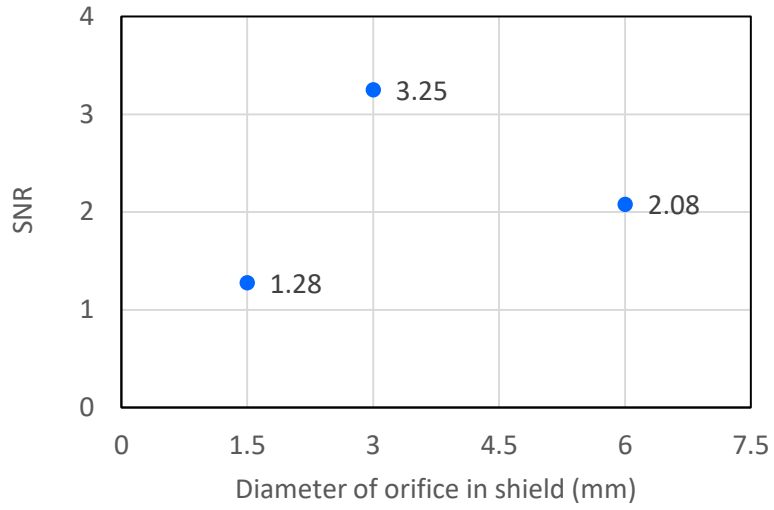

Figure 4.15. Signal-to-noise ratio (SNR) for three aperture sizes of the shield

4.4.3. Time-resolved Measurement

The stability of the scattering intensity by in-flight particles was accessed through a time-resolved measurement acquired at 10 kHz. Figure 4.16 presented the scattering intensity at detectors 1, 11, and 28. The signal fluctuated noticeably in the detector 1 and the signal fluctuation in the next detectors was reduced gradually. The signal in detector 11 shows almost no significant fluctuation. The scattering intensity from detector 11 to detector 28, which was the position of scattering peak, showed stable result. To find the origin of fluctuations, the Fourier transform (FT) of the signal was acquired. Analysis of FT result confirmed there wasn't any distinct frequency associated with the range of plasma fluctuations which expected to be between 2 – 6 kHz [33,166]. A possible source of low frequency fluctuations was the turbulence flow and gas instability at the measurement volume.

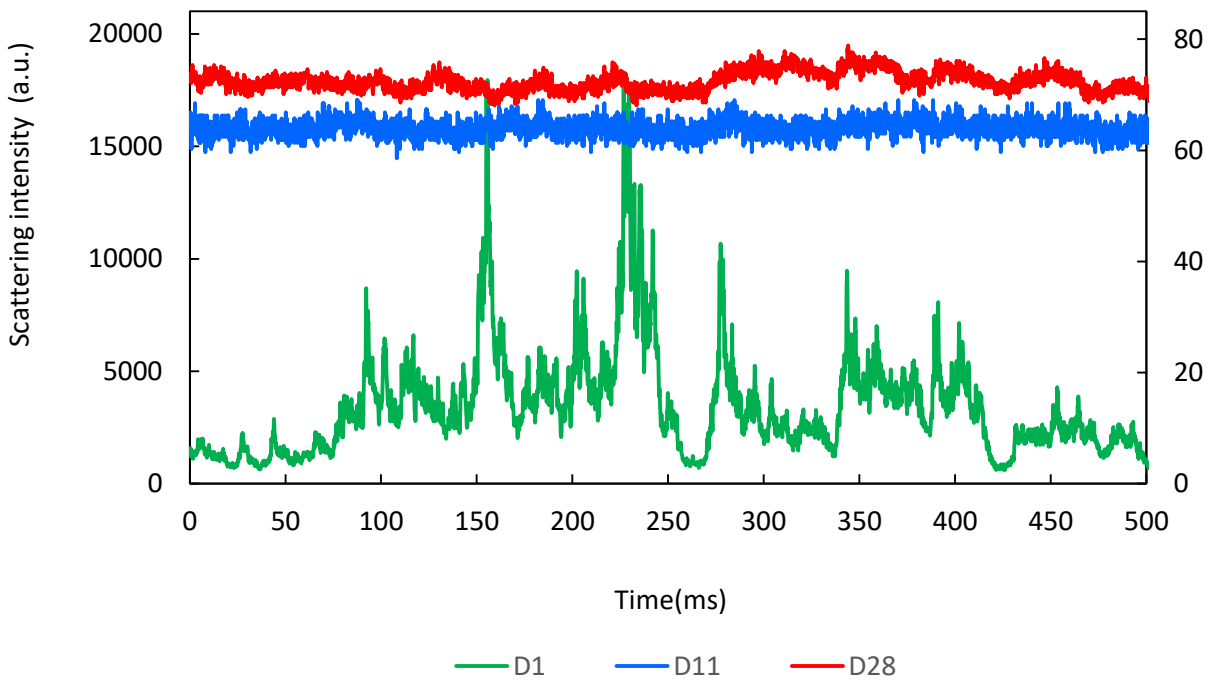

Figure 4.16. Scattering Intensity sampled at 10 kHz in detector number 1 (green line, scaled at left axis), detector number 11 (blue line), and detector number 28 (red line, both scaled at the right axis)

Figure 4.17 indicates the scattering signal of particles in the detectors under the two conditions of plasma spray and the wet dispersion unit. In comparison, both curves mostly showed the same trend; however, there were some discrepancies in the first and last detectors. In fact, the temperature gradient of gas mixture caused laser light to deviate, which was the source of the discrepancy in the first detectors. Besides, the medium of measurement was the air for the test of plasma spray and water for test of the wet dispersion unit. The index of refraction of air and water are 1.00 and 1.33 respectively. The calculation for a same particle size distribution in the two media illustrated that the scattering intensity in the water was more than the scattering intensity in the air in the angle where the last detectors were situated. Therefore, using the different media for the measurement was reason for the slight difference between the curves for the detectors from 30 – 36.

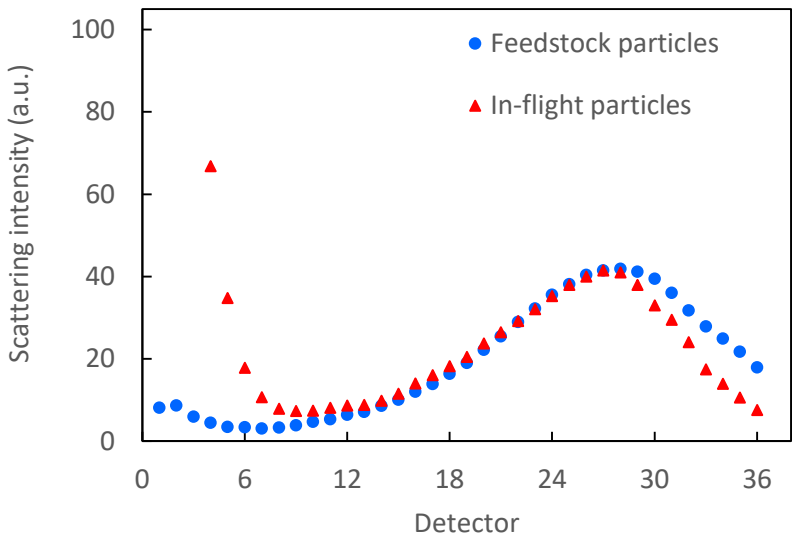

Figure 4.17. Scattering intensity of glass particles (feedstock powder in the wet dispersion unit compared to scattering intensity of the in-flight particles in plasma spray while the particles were not melted

The particle size distributions extracted from these scattering signals are shown in Figure 4.18. It is remarkable that D_{50} measured in the plasma spray and the wet dispersion unit were 4.7 and 4.6 µm, respectively. Accordingly, the difference of D_{50} under two conditions was 3.4%. The minimum particle size in two measurements was around 0.8 µm and the maximum particle size for in-light and feedstock particles were 17.1 and 14.7 µm respectively. Overall, the size distribution measured in the plasma condition and the wet dispersion unit were nearly identical. This result confirmed the LD system measured size of in-light particles correctly under the plasma condition. The accuracy and precision of measurement by the LD system are both better than 1% according to the manufacturer.

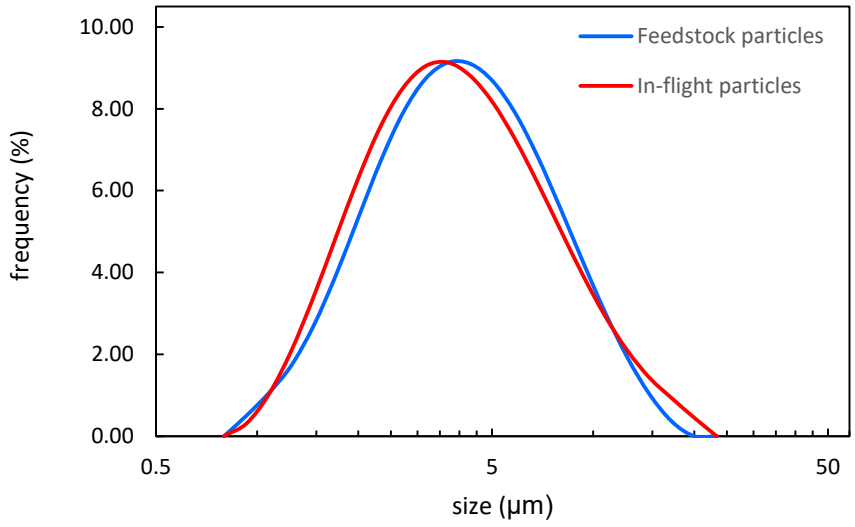

Figure 4.18. Particle size distribution of glass particles (feedstock powder in the wet dispersion unit compared to particle size distribution of the in-flight particles in plasma spray while the particles were not melted

The particles are assumed spherical in the LD system and all the calculations to find particle size distribution is based on this assumption. The feedstock powders for SPS processes are mostly nonspherical. However, they become molten in the plasma and form spherical shape while they move towards the substrate. Therefore in SPS, spherical particles present in the measurement volume. For the cases that the nonspherical particles would be in the measurement volume, the scattered light does not represent the particle thoroughly and the size distribution would be a rough estimation of the reality.

4.5.Conclusions

In this study, the light diffraction method was used to measure online the size of the in-flight particles in SPS process; *(i)*, the shields effectively controlled the number of particles and refraction in the measurement volume, *(ii)*, the size of apertures in the front shield was optimized in terms of SNR, *(iii)*, the plasma radiation from surrounding and scattered plasma by particles in the measurement volume was reduced to a negligible value compared to the scattered light from the laser of the diagnostic system, *(iv)*, the minimum number of particles needed to collect the required scattering signal was identified for the coating material, *(v)*, the monomodal scattering intensity verified that there is no droplet available in the measurement zone, and finally *(vi)*, a

comparison of size distribution in the plasma condition with the wet dispersion unit showed consistency between the size distribution of feedstock and in-flight particles.

It was concluded that the LD method has the potential to be applied for the online size measurement of the in-flight particles in the SPS process. However, to eliminate the effect of plasma from the measurement signal was quite challenging which still require more investigation. It is necessary to develop a protocol to validate the result of online measurement especially for smaller particles and the spray condition for the industrial coating powders.

Acknowledgement

The authors gratefully acknowledge Dr. Fadhel Ben Ettouil and Mr. Robert Oliver for their kind help in carrying out some experiments and test setup preparation. This project was funded by the Natural Sciences and Engineering Research Council of Canada (NSERC) and Canada Research Chair.

CHAPTER 5. CONCLUSIONS, CONTRIBUTIONS, AND RECOMMENDATIONS

5.1. Conclusions

This work is a contribution to the study of the suspension plasma spray (SPS) process in situ. The global characterization of the process involves phenomena from the exit of an injector to the formation of layers of splats on a substrate. In this research, characteristics of suspension spray from the effervescent atomizer and characteristics of in-flight particles in SPS were investigated. Different characterization methods including phase Doppler particle analyzer (PDPA), shadowgraph, light diffraction, and thermal emission were used to study droplets and in-flight particles in SPS. Result from Chapter 2 of this research about droplets of suspension spray in crossflow at room temperature characterized by PDPA, broadened the current understanding of the interaction between a spray and a flow. The result of Chapter 3 showed effective adaptation and improvement of available diagnostic system of atmospheric plasma spray (APS) which works based on thermal emission, provided an online monitoring system for measurement of temperature and velocity of in-flight particles in the developing process of SPS. Finally, the result of Chapter 4 showed that the light diffraction method has the potential to be used for size measurement of in-flight particles in SPS. The next paragraphs of this section provide the summary and conclusions in each chapter. The last paragraph of this section is devoted to the conclusions of the whole thesis.

In Chapter 2, the spray from an effervescent atomizer was studied in a quiescent and crossflow air configuration at room temperature. In the quiescent air, the effervescent atomizer produced the smaller suspension droplets than the water droplets. In crossflow air, size of droplets at downstream depends on the breakup of the liquid by the effervescent atomizer and breakup of droplets in the crossflow of the air. The cross-section of spray at downstream of the atomizer showed the fine droplets at the center were enveloped by relatively larger droplets independent of the particle concentration at least up to 10 wt.%. Velocity of droplets at downstream was governed by the velocity of the transverse flow. Large droplets with higher momentum in the direction of

the spray centerline either broke up into smaller droplets who reached the velocity of the transverse flow, or they overpenetrated and did not transfer downstream. The water and suspension droplets with relatively different size sprayed in the quiescent air had a negligible velocity difference at downstream. It is interesting to mention the particles in the fluid, up to concentration of 10 wt%, does not change the size of the droplets significantly in the crossflow. The result showed that the droplets at the center of spray in the cross-section had relatively the higher velocity and smaller size, which resulted in the lower volume flux. The maximum of volume flux of droplets was at the level of the atomizer exit which can be as a result surface breakup of the suspension close to the exit of the atomizer. This study showed that particles inside droplets of suspensions, contained up to 10 wt.% glass particles of an average 4 μm and the index of refraction of 1.5, changed light scattering around the droplets. However, this change did not compromise the result of size and velocity measurement by PDPA.

After evaporation of the liquid phase of the suspension droplets, the remaining were in-flight particles. In Chapter 3, the temperature in-flight particles was characterized by using two systems: a double-point measurement system (AccuraSpray G3C designed for the APS process) which provided an estimation of temperature and a single-point measurement system (AccuraSpray 4.0 better adapted for the SPS process) which showed a good agreement with the background information. The single-point measurement system with a readjusted bandpass filter predicted the continuously decreasing trend of temperature and velocity in terms of increasing the measurement distance from the torch. Moreover, the system showed that an increase in the power of the plasma elevated the temperature of the in-flight particles. Collected splats at relatively a wide range of the spray distance confirmed the evolution of temperature and velocity of in-flight particles in the representative distance measured by the new system. The measurement condition has an impact on temperature. An enhanced filtering of the spectrum improves the measurement particularly at a shorter standoff distance. Finally, the single-point measurement system targets the characterization of the in-flight particles in the SPS process successfully measured the temperature and velocity of in-flight particles.

In addition to temperature measurement, in Chapter 4, a feasibility study was conducted to measurement the size of in-flight particles by a light diffraction method in SPS process. The result showed LD method has the potential to characterize the light scattering signal from the in-flight

particles and consequently to measure the size; however, it was necessary to apply some strategies to control the scattering signal at the detector. The refraction of light in the measurement volume was minimized by using a shield between the measurement volume and the plasma. The aperture in the shield was optimized in terms of SNR. The minimum number of particles for effective measurement was identified. Applying a proper bandpass filter and considering proper detectors (angle of scattering), size of the in-flight particles was measured for the glass suspension. The result of in-flight measurement under the plasma condition showed a good agreement with result of the wet dispersion unit.

To conclude the thesis, characterization of droplets and particles in SPS includes a systematic approach to recognize challenges in the first step, and implementation of strategies to deal with the challenges in the second step. In general, limitations originated from the small size of target, characterizing by optical diagnostic systems in a turbulent flow and severe spray conditions under significant optical noises should be fully understood and addressed. A series of filtering, masking, and data handling strategies in addition to further technology developments should be applied to eliminate physically and optically these limitations. Finally, the result of characterization should be verified and validated. Characterization based on this procedure can be employed for the further development of SPS process and for the evolution of components in spraying.

5.2. Contributions

In this research, I selected two stages of the SPS process where there was investigated less and there was a gap of knowledge in the literature. Namely, characteristics of suspension droplets and characteristics of in-flight particles were investigated. In general, the main contributions of this research are to further develop the process and to further develop the diagnostic system in SPS. The study of spray produced by the effervescent atomizer in crossflow showed the potential of the atomizer for further development of the SPS process. Moreover, online monitoring of the in-flight particles in SPS could be achieved by using the light scattering and the thermal emission techniques. The main contributions of this research are summarized in the following:

- This research was a pioneer to characterize the capability of an effervescent atomizer to introduce suspension droplets in the crossflow which was systematically investigated in Chapter 2. This work studied the effect of the solid concentration (particle) on the

suspension spray and the droplets in the crossflow by the single counting method of PDPA.

- This study actually contributed in the development of a new version of a diagnostic system to measure both the temperature and velocity of in-flight particles in SPS as explained in Chapter 3. Moreover, the author validated the performance of the new system through experiments of temperature measurement in SPS process.
- This is the very first study to measure size of in-flight particles in SPS as described in Chapter 4. This research established the basis for the detailed analysis of the scattered signal to measure the size of in-flight particles in SPS by a light diffraction method for the first time. I contributed to the identification of the main sources of noise on the measurements and I suggested strategies and confirmed their effectiveness to reduce the influence of the noise sources to achieve more reliable particle size measurements in the SPS process.

5.3. Recommendation for Future Works

This research highlighted a series of questions regarding the online characterization of the SPS process. For a better understanding and further development of the SPS process, as well as improvement of diagnostic techniques, some suggestions for future research work are listed below:

- Interaction of suspension spray with a crossflow under a plasma condition needs to be investigated. Although atomizer and crossflow had influence on breakup and characteristics of droplets, effect of the heat transfer to the droplet should be studied. Furthermore, the capability of PDPA for online analysis of droplets in SPS requires to be examined.
- Measurement of temperature and velocity close to the substrate is suggested as a future work. Temperature and velocity of in-flight particles before impingement on the substrate need to be further explored. The effect of substrate temperature and shape on the temperature and velocity of in-flight particles needs to be investigated to have a more comprehensive understanding of the process.
- A sampling system (a sampler) is recommended to be developed for measuring the size of in-flight particles in SPS. It is suggested to employ an air or a water-cooled tube for sampling the particles. The sampling tube could direct the particles to the measurement

volume where noises of the SPS process for the light diffraction method are attenuated.

- Online measurement of particle size is proposed for a higher plasma power. Capability of light diffraction method should be evaluated for plasma condition for coating materials with high melting point such as YSZ and TiO_2. Moreover, size measurement of submicron in-flight particles is suggested to identify strengths and limitations of the method.

REFERENCE LIST

[1] J. Tucker, C. Robert, ASM Handbook, Volume 5A: Thermal Spray Technology, ASM International, 2013.

[2] P.L. Fauchais, J. Heberlein, M. Boulos, Thermal Spray Fundamentals: From Powder to Part, Springer Science & Business Media, 2014.

[3] R. Vassen, A. Stuke, D. Stöver, Recent developments in the field of thermal barrier coatings, J. Therm. Spray Technol. 18 (2009) 181-186.

[4] R. Jaworski, L. Pawlowski, C. Pierlot, F. Roudet, S. Kozerski, F. Petit, Recent developments in suspension plasma sprayed titanium oxide and hydroxyapatite coatings, J. Therm. Spray Technol. 19 (2010) 240-247.

[5] H. Tsukuda, A. Notomi, N. Histatome, Application of plasma spraying to tubular-type solid oxide fuel cells production, J. Therm. Spray Technol. 9 (2000) 364-368.

[6] M. Aghasibeig, C. Moreau, A. Dolatabadi, R. Wuthrich, Fabrication of nickel electrode coatings by combination of atmospheric and suspension plasma spray processes, Surface and Coatings Technology. 285 (2016) 68-76.

[7] N. Sharifi, M. Pugh, C. Moreau, A. Dolatabadi, Developing hydrophobic and superhydrophobic TiO 2 coatings by plasma spraying, Surface and Coatings Technology. 289 (2016) 29-36.

[8] F. Tarasi, M. Medraj, A. Dolatabadi, J. Oberste-Berghaus, C. Moreau, Effective parameters in axial injection suspension plasma spray process of alumina-zirconia ceramics, 17 (2008) 685-691.

[9] P. Fauchais, M. Vardelle, S. Goutier, A. Vardelle, Key Challenges and Opportunities in Suspension and Solution Plasma Spraying, Plasma Chem. Plasma Process. 35 (2015) 511-525.

[10] P. Fauchais, M. Vardelle, Sensors in Spray Processes, J. Therm. Spray Technol. 19 (2010) 668-694.

[11] P. Fauchais, M. Vardelle, S. Goutier, Latest researches advances of plasma spraying: From splat to coating formation, J. Therm. Spray Technol. 25 (2016) 1534-1553.

[12] L. Pawlowski, Suspension and solution thermal spray coatings, Surface and Coatings Technology. 203 (2009) 2807-2829.

[13] P. Fauchais, M. Vardelle, S. Goutier, A. Vardelle, Key challenges and opportunities in suspension and solution plasma spraying, Plasma Chem. Plasma Process. 35 (2015) 511-525.

[14] H. Kassner, R. Siegert, D. Hathiramani, R. Vassen, D. Stoever, Application of suspension plasma spraying (SPS) for manufacture of ceramic coatings, J. Therm. Spray Technol. 17 (2008) 115-123.

[15] P. Fauchais, M. Vardelle, A. Vardelle, S. Goutier, What Do We Know, What are the Current Limitations of Suspension Plasma Spraying? J. Therm. Spray Technol. (2015) 1-10.

[16] E. Meillot, D. Damiani, S. Vincent, C. Caruyer, J. Caltagirone, Analysis by modeling of plasma flow interactions with liquid injection, Surface and Coatings Technology. 220 (2013) 149-156.

[17] S.A. Esfarjani, A. Dolatabadi, A 3D simulation of two-phase flow in an effervescent atomizer for suspension plasma spray, Surface and Coatings Technology. 203 (2009) 2074-2080.

[18] J. Chin, A. Lefebvre, A design procedure for effervescent atomizers, Journal of Engineering for Gas Turbines and Power. 117 (1995) 266-271.

[19] A.H. Lefebvre, V.G. McDonell, Atomization and Sprays, CRC press, 2017.

[20] A. Saleh, G. Amini, A. Dolatabadi, Penetration of Aerated Suspension Spray in a Gaseous Crossflow, Atomization and Sprays. 28 (2018).

[21] M.Y. Leong, V.G. McDonell, G.S. Samuelsen, Effect of ambient pressure on an airblast spray injected into a crossflow, J. Propul. Power. 17 (2001) 1076-1084.

[22] J. Fazilleau, C. Delbos, V. Rat, J. Coudert, P. Fauchais, B. Pateyron, Phenomena involved in suspension plasma spraying part 1: Suspension injection and behavior, Plasma Chem. Plasma Process. 26 (2006) 371-391.

[23] C. Delbos, J. Fazilleau, V. Rat, J. Coudert, P. Fauchais, B. Pateyron, Phenomena involved in suspension plasma spraying part 2: Zirconia particle treatment and coating formation, Plasma Chem. Plasma Process. 26 (2006) 393-414.

[24] K. VanEvery, M.J. Krane, R.W. Trice, H. Wang, W. Porter, M. Besser, D. Sordelet, J. Ilavsky, J. Almer, Column formation in suspension plasma-sprayed coatings and resultant thermal properties, J. Therm. Spray Technol. 20 (2011) 817-828.

[25] G. Dwivedi, T. Wentz, S. Sampath, T. Nakamura, Assessing process and coating reliability through monitoring of process and design relevant coating properties, J. Therm. Spray Technol. 19 (2010) 695-712.

[26] J.O. Berghaus, J.G. Legoux, C. Moreau, F. Tarasi, T. Chraska, Mechanical and thermal transport properties of suspension thermal-sprayed alumina-zirconia composite coatings, J. Therm. Spray Technol. 17 (2008) 91-104.

[27] C. Kang, H. Ng, S. Yu, Comparative study of plasma spray flow fields and particle behavior near to flat inclined substrates, Plasma Chem. Plasma Process. 26 (2006) 149-175.

[28] J.O. Berghaus, S. Bouaricha, J.G. Legoux, C. Moreau, Injection conditions and in-flight particle states in suspension plasma spraying of alumina and zirconia nano-ceramics, (2005) 2-4.

[29] B. Aziz, P. Gougeon, C. Moreau, Temperature measurement challenges and limitations for in-flight particles in suspension plasma spraying, J. Therm. Spray Technol. 26 (2017) 695-707.

[30] J.C. Owens, Optical refractive index of air: dependence on pressure, temperature and composition, Appl. Opt. 6 (1967) 51-59.

[31] L. Pawlowski, Suspension and solution thermal spray coatings, Surface and Coatings Technology. 203 (2009) 2807-2829.

[32] P. Fauchais, M. Vardelle, S. Goutier, A. Vardelle, Specific measurements of in-flight droplet and particle behavior and coating microstructure in suspension and solution plasma spraying, J. Therm. Spray Technol. 24 (2015) 1498-1505.

[33] R. Etchart-Salas, V. Rat, J. Coudert, P. Fauchais, N. Caron, K. Wittman, S. Alexandre, Influence of plasma instabilities in ceramic suspension plasma spraying, J. Therm. Spray Technol. 16 (2007) 857-865.

[34] O. Marchand, P. Bertrand, J. Mougin, C. Comminges, M. Planche, G. Bertrand, Characterization of suspension plasma-sprayed solid oxide fuel cell electrodes, Surface and Coatings Technology. 205 (2010) 993-998.

[35] O. Marchand, L. Girardot, M. Planche, P. Bertrand, Y. Bailly, G. Bertrand, An insight into suspension plasma spray: injection of the suspension and its interaction with the plasma flow, J. Therm. Spray Technol. 20 (2011) 1310-1320.

[36] P.J. Santangelo, P.E. Sojka, A holographic investigation of the near-nozzle structure of an effervescent atomizer-produced spray, Atomization and sprays. 5 (1995).

[37] S. Sovani, P. Sojka, A. Lefebvre, Effervescent atomization, Progress in energy and combustion science. 27 (2001) 483-521.

[38] J. Whitlow, A.H. Lefebvre, Effervescent atomizer operation and spray characteristics, Atomization and Sprays. 3 (1993).

[39] M. Lund, P.E. Sojka, A.H. Lefebvre, P. Gosselin, Effervescent atomization at low mass flow rates. Part I: The influence of surface tension, Atomization and Sprays. 3 (1993).

[40] M.V. Panchagnula, P.E. Sojka, Spatial droplet velocity and size profiles in effervescent atomizer-produced sprays, Fuel. 78 (1999) 729-741.

[41] F. Zhao, Z. Ren, B. Xu, H. Zhang, C. Fu, Brief overview of effervescent atomizer application, 1300 (2019) 012043.

[42] M. Zaremba, J. Kozák, M. Malý, L. Weiß, P. Rudolf, J. Jedelský, M. Jícha, An experimental analysis of the spraying processes in improved design of effervescent atomizer, Int. J. Multiphase Flow. 103 (2018) 1-15.

[43] M. Liu, Y. Duan, T. Zhang, Evaluation of effervescent atomizer internal design on the spray unsteadiness using a phase/Doppler particle analyzer, Exp. Therm. Fluid Sci. 34 (2010) 657-665.

[44] C. Sun, Z. Ning, X. Qiao, M. Lv, Y. Li, J. Zhao, X. Wang, Study on effervescent spray morphology based on internal gas-liquid two-phase flow patterns, European Journal of Mechanics-B/Fluids. 74 (2019) 123-138.

[45] M.O. Wittner, H.P. Karbstein, V. Gaukel, Spray performance and steadiness of an effervescent atomizer and an air-core-liquid-ring atomizer for application in spray drying processes of highly concentrated feeds, Chemical Engineering and Processing-Process Intensification. 128 (2018) 96-102.

[46] H.P. Gadgil, A. Dolatabadi, B. Raghunandan, Mass distribution studies in effervescent sprays, Atomization and Sprays. 21 (2011).

[47] L. Qian, J. Lin, H. Xiong, T.L. Chan, Theoretical investigation of the influence of liquid physical properties on effervescent atomization performance, Journal of Fluids Engineering. 133 (2011) 101205.

[48] M. Ochowiak, L. Broniarz-Press, S. Rozanska, J. Rozanski, The effect of extensional viscosity on the effervescent atomization of polyacrylamide solutions, Journal of Industrial and Engineering Chemistry. 18 (2012) 2028-2035.

[49] X. Fan, G. Yu, J. Li, X. Zhang, C. Sung, Investigation of vaporized kerosene injection and combustion in a supersonic model combustor, J. Propul. Power. 22 (2006) 103-110.

[50] S.D. Sovani, P.E. Sojka, A.H. Lefebvre, Effervescent atomization, Progress in Energy and Combustion Science. 27 (2001) 483-521.

[51] A. Sinha, R.S. Prakash, A.M. Mohan, R. Ravikrishna, Airblast spray in crossflow–structure, trajectory and droplet sizing, Int. J. Multiphase Flow. 72 (2015) 97-111.

[52] A. Saleh, G. Amini, A. Dolatabadi, Penetration of Aerated Suspension Spray in a Gaseous Crossflow, Atomization and Sprays. 28 (2018).

[53] M. Vardelle, A. Vardelle, P. Fauchais, M. Boulos, Plasma—particle momentum and heat transfer: Modelling and measurements, AIChE J. 29 (1983) 236-243.

[54] J. Mishin, M. Vardelle, J. Lesinski, P. Fauchais, Two-colour pyrometer for the statistical measurement of the surface temperature of particles under thermal plasma conditions, Journal of Physics E: Scientific Instruments. 20 (1987) 620.

[55] J. Fincke, C. Jeffery, S. Englert, In-flight measurement of particle size and temperature, Journal of Physics E: Scientific Instruments. 21 (1988) 367.

[56] J.R. Fincke, W.D. Swank, R.L. Bewley, D.C. Haggard, M. Gevelber, D. Wroblewski, Diagnostics and control in the thermal spray process, Surface and Coatings Technology. 146 (2001) 537-543.

[57] S. Coulombe, M. Boulos, In-flight particle diagnostics in induction plasma processing, Plasma Chem. Plasma Process. 15 (1995) 653-675.

[58] O.P. Solonenko, Complex investigation of thermophysical processes in plasma-jet spraying, Pure and Applied Chemistry. 62 (1990) 1783-1800.

[59] J. Blain, F. Nadeau, L. Pouliot, C. Moreau, P. Gougeon, L. Leblanc, Integrated infrared sensor system for on line monitoring of thermally sprayed particles, Surface engineering. 13 (1997) 420-424.

[60] P. Gougeon, C. Moreau, V. Lacasse, M. Lamontagne, I. Powell, A. and Bewsher, A new Sensor for on-line Diagnostics of Particles under Thermal Spraying Conditions. Advanced Processing Techniques, C. Lall and A. J. Neupaver (Eds), International Conference on Powder Metallurgy and Particule Materials, Toronto, Canada, Metal Powder Industries Federation, APMI. 6 (1994) 199-210.

[61] C. Moreau, P. Gougeon, M. Lamontagne, V. Lacasse, G. Vaudreuil, P. Cielo, On-line control of the plasma spraying process by monitoring the temperature, velocity, and

trajectory of in-flight particles, in Thermal spray industrial applications, C. C. Berndt and S. Sampath (Eds.), Proc. National Thermal Spray Conference, 20-24 June 1994, Boston, Mass., ASM International. (1994) 431-437.

[62] C. Moreau, P. Gougeon, A. Burgess, D. Ross, Characterization of particle flows in an axial injection plasma torch, Advances in Thermal Spray Science and Technology, C. C. Berndt and S. Sampath (Eds.), Proc. National Thermal Spray Conference, Houston, Texas, ASM International. (1995) 141-147.

[63] P. Fauchais, G. Montavon, M. Vardelle, J. Cedelle, Developments in direct current plasma spraying, Surface and Coatings Technology. 201 (2006) 1908-1921.

[64] G. Mauer, R. Vaßen, D. Stöver, Plasma and particle temperature measurements in thermal spray: approaches and applications, J. Therm. Spray Technol. 20 (2011) 391-406.

[65] G. Mauer, R. Vaßen, S. Zimmermann, T. Biermordt, M. Heinrich, J. Marques, K. Landes, J. Schein, Investigation and comparison of in-flight particle velocity during the plasma-spray process as measured by laser Doppler anemometry and DPV-2000, J. Therm. Spray Technol. 22 (2013) 892-900.

[66] J.F. Bisson, M. Lamontagne, C. Moreau, L. Pouliot, J. Blain, F. Nadeau, Ensemble In-Flight Particle Diagnostics under Thermal Spray Conditions, (2001) 705-714.

[67] J. Vattulainen, E. Hämäläinen, R. Hernberg, P. Vuoristo, T. Mäntylä, Novel method for in-flight particle temperature and velocity measurements in plasma spraying using a single CCD camera, J. Therm. Spray Technol. 10 (2001) 94-104.

[68] J. Craig, R. Parker, Particle temperature and velocity measurements by two-wavelength streak imaging. (2003) 1107-1112.

[69] S.P. Mates, D. Basak, F.S. Biancaniello, S.D. Ridder, J. Geist, Calibration of a two-color imaging pyrometer and its use for particle measurements in controlled air plasma spray experiments, J. Therm. Spray Technol. 11 (2002) 195-205.

[70] D. Wroblewski, G. Reimann, M. Tuttle, D. Radgowski, M. Cannamela, S. Basu, M. Gevelber, Sensor issues and requirements for developing real-time control for plasma spray deposition, J. Therm. Spray Technol. 19 (2010) 723-735.

[71] G. Mauer, R. Vaßen, D. Stöver, Comparison and Applications of DPV-2000 and Accuraspray-g3 diagnostic Systems, J. Therm. Spray Technol. 16 (2007) 414-424.

[72] A. Killinger, R. Gadow, G. Mauer, A. Guignard, R. Vaßen, D. Stöver, Review of new developments in suspension and solution precursor thermal spray processes, J. Therm. Spray Technol. 20 (2011) 677.

[73] C. Kang, H. Ng, S. Yu, Comparative study of plasma spray flow fields and particle behavior near to flat inclined substrates, Plasma Chem. Plasma Process. 26 (2006) 149-175.

[74] C. Moreau, J. Bisson, R. Lima, B. Marple, Diagnostics for advanced materials processing by plasma spraying, Pure and applied chemistry. 77 (2005) 443-462.

[75] S. Zimmermann, E. Vogli, M. Kauffeldt, M. Abdulgader, B. Krebs, B. Rüther, K. Landes, J. Schein, W. Tillmann, Supervision and measuring of particle parameters during the wire-arc spraying process with the diagnostic systems Accuraspray-g3 and LDA (Laser-Doppler-Anemometry), J. Therm. Spray Technol. 19 (2010) 745-755.

[76] B. Cetegen, W. Yu, In-situ particle temperature, velocity, and size measurements in dc arc plasma thermal sprays, J. Therm. Spray Technol. 8 (1999) 57-67.

[77] S. Zimmermann, K. Landes, A particle image shape imaging (PSI) investigation of particles in a plasma jet, Materials Science and Engineering: A. 383 (2004) 153-157.

[78] K. Landes, Diagnostics in plasma spraying techniques, Surface and Coatings Technology. 201 (2006) 1948-1954.

[79] R. Rampon, O. Marchand, C. Filiatre, G. Bertrand, Influence of suspension characteristics on coatings microstructure obtained by suspension plasma spraying, Surface and Coatings Technology. 202 (2008) 4337-4342.

[80] A. McDonald, C. Moreau, S. Chandra, Use of thermal emission signals to characterize the impact of fully and partially molten plasma-sprayed zirconia particles on glass surfaces, Surface and Coatings Technology. 204 (2010) 2323-2330.

[81] Z. Zeng, S. Kuroda, H. Era, Comparison of oxidation behavior of Ni–20Cr alloy and Ni-base self-fluxing alloy during air plasma spraying, Surface and Coatings Technology. 204 (2009) 69-77.

[82] F. Tarasi, M. Medraj, A. Dolatabadi, J.O. Berghaus, C. Moreau, Amorphous and crystalline phase formation during suspension plasma spraying of the alumina–zirconia composite, Journal of the European Ceramic Society. 31 (2011) 2903-2913.

[83] E. Aubignat, M.P. Planche, A. Allimant, D. Billieres, L. Girardot, Y. Bailly, G. Montavon, Effect of suspension characteristics on in-flight particle properties and coating microstructures achieved by suspension plasma spray, Journal of Physics: Conference Series. 550 (2014) 012019 (10 pp.).

[84] E. Aubignat, M. Planche, D. Billieres, A. Allimant, L. Girardot, Y. Bailly, G. Montavon, Optimization of the injection with a twin-fluid atomizer for suspension plasma

spray process using three non-intrusive diagnostic tools, Journal of Visualization. 19 (2016) 21-36.

[85] C. Tu, Z. Yin, J. Lin, F. Bao, A Review of Experimental Techniques for Measuring Micro-to Nano-Particle-Laden Gas Flows, Applied Sciences. 7 (2017) 120.

[86] G. Gouesbet, A review on measurements of particle velocities and diameters by laser techniques, with emphasis on thermal plasmas, Plasma Chem. Plasma Process. 5 (1985) 91-117.

[87] N. Tayali, C. Bates, Particle sizing techniques in multiphase flows: a review, Flow Meas. Instrum. 1 (1990) 77-105.

[88] D.L. Black, M.Q. McQuay, M.P. Bonin, Laser-based techniques for particle-size measurement: a review of sizing methods and their industrial applications, Progress in energy and combustion science. 22 (1996) 267-306.

[89] P. Gougeon, C. Moreau, In-flight particle surface temperature measurement: influence of the plasma light scattered by the particles, J. Therm. Spray Technol. 2 (1993) 229-233.

[90] W.D. Bachalo, Method for measuring the size and velocity of spheres by dual-beam light-scatter interferometry, Appl. Opt. 19 (1980) 363-370.

[91] W. Bachalo, M. Houser, Phase/Doppler spray analyzer for simultaneous measurements of drop size and velocity distributions, Optical Engineering. 23 (1984) 235583.

[92] TSI, Phase Doppler Particle Analyzer, Laser Doppler Velocimeter (LDV), Operations Manual. (2005).

[93] H. Albrecht, N. Damaschke, M. Borys, C. Tropea, Laser Doppler and Phase Doppler Measurement Techniques, Springer Science & Business Media, 2013.

[94] J. McClymer, Precise determination of the refractive index of suspended particles: light transmission as a function of refractive index mismatch, American Journal of Physics. 84 (2016) 602-605.

[95] F.W. Sears, M.W. Zemansky, H.D. Young, University Physics, Addison-Wesley, 1987.

[96] A. Cengel, HEHT TRANSFER, (2007).

[97] G. Mauer, R. Vaßen, D. Stöver, Detection of melting temperatures and sources of errors using two-color pyrometry during in-flight measurements of atmospheric plasma-sprayed particles, Int. J. Thermophys. 29 (2008) 764-786.

[98] Y.S. Touloukian, D.P. DeWitt, Thermal radiative properties: Nonmetallic solids. (1972).

[99] J. Manara, R. Brandt, J. Kuhn, J. Fricke, T. Krell, U. Schulz, M. Peters, W.A. Kaysser, Emittance of Y~ 2O~ 3 stabilised ZrO~ 2 thermal barrier coatings prepared by electron-beam physical-vapour deposition, HIGH TEMPERATURES HIGH PRESSURES. 32 (2000) 361-368.

[100] P. Coates, D. Lowe, The Fundamentals of Radiation Thermometers, CRC Press, 2016.

[101] J. Swithenbank, J.M. Beer, D.S. Taylor, D. Abbot, G.C. McCreath, A laser diagnostic technique for the measurement of droplet and particle size distribution, AIAA 14th Aerospace Sciences Meeting, Washington, D.C. (1976) 69-76.

[102] C.F. Bohren, D.R. Huffman, Absorption and Scattering of Light by Small Particles, John Wiley & Sons, 2008.

[103] M. Bass, E.W. Van Stryland, D.R. Williams, W. Wolfe, Handbook of Optics Fundamentals, Techniques, and Design Volume I, Optical Society of America, ISBN: 0-07-047740-7. (1995).

[104] T. Igushi, H. Yoshida, Influence of the number of detectors by laser scattering method for estimation of particle size, Rev. Sci. Instrum. 83 (2012) 055103.

[105] L.P. Bayvel, J. Knight, G. Robertson, Alternative Model-Independent Inversion Programme for Malvern Particle Sizer, Particle & Particle Systems Characterization. 4 (1987) 49-53.

[106] C.F. Bohren, D.R. Huffman, Absorption and Scattering of Light by Small Particles, John Wiley & Sons, 2008.

[107] P.L. Fauchais, J.V. Heberlein, M.I. Boulos, Thermal Spray Fundamentals: From Powder to Part, Springer Science & Business Media, 2014.

[108] A. Vardelle, C. Moreau, J. Akedo, H. Ashrafizadeh, C.C. Berndt, J.O. Berghaus, M. Boulos, J. Brogan, A.C. Bourtsalas, A. Dolatabadi, The 2016 thermal spray roadmap, J. Therm. Spray Technol. 25 (2016) 1376-1440.

[109] N. Sharifi, M. Pugh, C. Moreau, A. Dolatabadi, Developing hydrophobic and superhydrophobic TiO2 coatings by plasma spraying, Surface and Coatings Technology. 289 (2016) 29-36.

[110] M. Aghasibeig, A. Dolatabadi, R. Wuthrich, C. Moreau, Three-dimensional electrode coatings for hydrogen production manufactured by combined atmospheric and suspension plasma spray, Surface and Coatings Technology. 291 (2016) 348-355.

[111] O. Aranke, M. Gupta, N. Markocsan, X. Li, B. Kjellman, Microstructural Evolution and Sintering of Suspension Plasma-Sprayed Columnar Thermal Barrier Coatings, J. Therm. Spray Technol. 28 (2019) 198-211.

[112] F. Toma, L. Berger, D. Jacquet, D. Wicky, I. Villaluenga, Y. de Miguel, J. Lindeløv, Comparative study on the photocatalytic behaviour of titanium oxide thermal sprayed coatings from powders and suspensions, Surface and Coatings Technology. 203 (2009) 2150-2156.

[113] T. Wriedt, U. Manasse, K. Bauckhage, Deconvolution of PDA size distributions from sprays of optically inhomogeneous liquids, 2052 (1993) 137-144.

[114] U. Manasse, T. Wriedt, K. Bauckhage, Reconstruction of Real Size Distributions Hidden in Phase-Doppler Anemometry results obtained form droplets of inhomogeneous liquids, Particle & particle systems characterization. 11 (1994) 84-90.

[115] O. Köser, T. Wriedt, Iterative inversion of phase-Doppler-anemometry size distributions from sprays of optically inhomogeneous liquids, Appl. Opt. 35 (1996) 2537-2543.

[116] F. Onofri, L. Bergougnoux, J. Firpo, J. Misguich-Ripault, Size, velocity, and concentration in suspension measurements of spherical droplets and cylindrical jets, Appl. Opt. 38 (1999) 4681-4690.

[117] D.W. Litchfield, D.G. Baird, The rheology of high aspect ratio nano-particle filled liquids, Rheology Reviews. 2006 (2006) 1.

[118] A. Reyes-Coronado, A. García-Valenzuela, C. Sánchez-Pérez, R. Barrera, Measurement of the effective refractive index of a turbid colloidal suspension using light refraction, New Journal of Physics. 7 (2005) 89.

[119] https://imagej.nih.gov/ij/docs/guide/146.html,.

[120] L.G. Dodge, D.J. Rhodes, R.D. Reitz, Drop-size measurement techniques for sprays: comparison of Malvern laser-diffraction and Aerometrics phase/Doppler, Appl. Opt. 26 (1987) 2144-2154.

[121] Phase Doppler Particle Analyzer (PDPA),Laser Doppler Velocimeter (LDV) Operations Manual, February 2006.

[122] J. Lin, L. Qian, H. Xiong, Relationship between deposition properties and operating parameters for droplet onto surface in the atomization impinging spray, Powder Technol. 191 (2009) 340-348.

[123] C. Ejim, M. Rahman, A. Amirfazli, B. Fleck, Effects of liquid viscosity and surface tension on atomization in two-phase, gas/liquid fluid coker nozzles, Fuel. 89 (2010) 1872-1882.

[124] G. Mauer, A. Guignard, R. Vaßen, D. Stöver, Process diagnostics in suspension plasma spraying, Surface and Coatings Technology. 205 (2010) 961-966.

[125] C. Moreau, J. Bisson, R. Lima, B. Marple, Diagnostics for advanced materials processing by plasma spraying, Pure and applied chemistry. 77 (2005) 443-462.

[126] S. Sampath, V. Srinivasan, A. Valarezo, A. Vaidya, T. Streibl, Sensing, control, and in situ measurement of coating properties: an integrated approach toward establishing process-property correlations, J. Therm. Spray Technol. 18 (2009) 243-255.

[127] S. Coulombe, M. Boulos, In-flight particle diagnostics in induction plasma processing, Plasma Chem. Plasma Process. 15 (1995) 653-675.

[128] J. Fincke, C. Jeffery, S. Englert, In-flight measurement of particle size and temperature, Journal of Physics E: Scientific Instruments. 21 (1988) 367.

[129] J.R. Fincke, W.D. Swank, R.L. Bewley, D.C. Haggard, M. Gevelber, D. Wroblewski, Diagnostics and control in the thermal spray process, Surface and Coatings Technology. 146 (2001) 537-543.

[130] J. Blain, F. Nadeau, L. Pouliot, C. Moreau, P. Gougeon, L. Leblanc, Integrated infrared sensor system for on line monitoring of thermally sprayed particles, Surface engineering. 13 (1997) 420-424.

[131] B. Aziz, P. Gougeon, C. Moreau, Temperature measurement challenges and limitations for in-flight particles in suspension plasma spraying, J. Therm. Spray Technol. 26 (2017) 695-707.

[132] R. Vaßen, H. Kaßner, G. Mauer, D. Stöver, Suspension plasma spraying: process characteristics and applications, J. Therm. Spray Technol. 19 (2010) 219-225.

[133] B. Aziz, P. Gougeon, C. Moreau, Temperature measurement challenges and limitations for in-flight particles in suspension plasma spraying, J. Therm. Spray Technol. 26 (2017) 695-707.

[134] https://www.oerlikon.com/ecomaXL/files/metco/oerlikon_DSMTS-0001.10_8YO_ZrO_HOSP.pdf&download=1,.

[135] J. Tucker, C. Robert, ASM Handbook, Volume 5A: Thermal Spray Technology, ASM International, 2013.

[136] P. Fauchais, G. Montavon, R. Lima, B. Marple, Engineering a new class of thermal spray nano-based microstructures from agglomerated nanostructured particles, suspensions and solutions: an invited review, J. Phys. D. 44 (2011) 093001.

[137] H. Kassner, R. Siegert, D. Hathiramani, R. Vassen, D. Stoever, Application of suspension plasma spraying (SPS) for manufacture of ceramic coatings, J. Therm. Spray Technol. 17 (2008) 115-123.

[138] A. Vardelle, C. Moreau, J. Akedo, H. Ashrafizadeh, C.C. Berndt, J.O. Berghaus, M. Boulos, J. Brogan, A.C. Bourtsalas, A. Dolatabadi, The 2016 Thermal Spray Roadmap, J. Therm. Spray Technol. (2016) 1-65.

[139] R. Jaworski, L. Pawlowski, C. Pierlot, F. Roudet, S. Kozerski, F. Petit, Recent developments in suspension plasma sprayed titanium oxide and hydroxyapatite coatings, J. Therm. Spray Technol. 19 (2010) 240-247.

[140] R. Vaßen, M.O. Jarligo, T. Steinke, D.E. Mack, D. Stöver, Overview on advanced thermal barrier coatings, Surface and Coatings Technology. 205 (2010) 938-942.

[141] W. Fan, Y. Bai, Review of suspension and solution precursor plasma sprayed thermal barrier coatings, Ceram. Int. 42 (2016) 14299-14312.

[142] A. Killinger, R. Gadow, G. Mauer, A. Guignard, R. Vaßen, D. Stöver, Review of new developments in suspension and solution precursor thermal spray processes, J. Therm. Spray Technol. 20 (2011) 677.

[143] P. Fauchais, M. Vardelle, S. Goutier, Latest Researches Advances of Plasma Spraying: From Splat to Coating Formation, J. Therm. Spray Technol. 25 (2016) 1534-1553.

[144] J.O. Berghaus, S. Bouaricha, J.G. Legoux, C. Moreau, Injection conditions and in-flight particle states in suspension plasma spraying of alumina and zirconia nano-ceramics, Thermal Spray 2005: Thermal Spray connects: Explore its surfacing potential! (DVS-ASM). (2005) 2-7.

[145] C.T. Crowe, Multiphase Flow Handbook, CRC press, 2005.

[146] K. Pourang, C. Moreau, A. Dolatabadi, Effect of substrate and its shape on in-flight particle characteristics in suspension plasma spraying, J. Therm. Spray Technol. 25 (2016) 44-54.

[147] P. Fauchais, M. Vardelle, Sensors in spray processes, J. Therm. Spray Technol. 19 (2010) 668-694.

[148] J.R. Fincke, W.D. Swank, R.L. Bewley, D.C. Haggard, M. Gevelber, D. Wroblewski, Diagnostics and control in the thermal spray process, Surface and Coatings Technology. 146 (2001) 537-543.

[149] P.L. Fauchais, J.V. Heberlein, M.I. Boulos, Thermal Spray Fundamentals: From Powder to Part, Springer Science & Business Media, 2014.

[150] C. Moreau, M. Lamontagne, Method and apparatus for monitoring the temperature and velocity of plasma sprayed particles, National Research Council of Canada. (1993).

[151] P. Gougeon, C. Moreau, V. Lacasse, M. Lamontagne, I. Powell, A. and Bewsher, A new Sensor for on-line Diagnostics of Particles under Thermal Spraying Conditions. Advanced Processing Techniques, C. Lall and A. J. Neupaver (Eds), International Conference on Powder Metallurgy and Particule Materials, Toronto, Canada, Metal Powder Industries Federation, APMI. 6 (1994) 199-210.

[152] P. Gougeon, C. Moreau, F. Richard, On-Line control of plasma sprayed particles in the Aerospace industry, in Advances in Thermal Spray Science and Technology, C. C. Berndt and S. Sampath (Eds.), Proc. National Thermal Spray Conference, Houston, Texas, ASM International. (1995) 149-155.

[153] C. Moreau, P. Gougeon, A. Burgess, D. Ross, Characterization of particle flows in an axial injection plasma torch, Advances in Thermal Spray Science and Technology, C. C. Berndt and S. Sampath (Eds.), Proc. National Thermal Spray Conference, Houston, Texas, ASM International. (1995) 141-147.

[154] C. Moreau, P. Gougeon, M. Lamontagne, Method and apparatus for monitoring the diameter of thermally sprayed particles, Method and apparatus for monitoring the diameter of thermally sprayed particles. (1997).

[155] C. Moreau, P. Gougeon, M. Lamontagne, V. Lacasse, G. Vaudreuil, P. Cielo, On-line control of the plasma spraying process by monitoring the temperature, velocity, and trajectory of in-flight particles, in Thermal spray industrial applications, C. C. Berndt and

S. Sampath (Eds.), Proc. National Thermal Spray Conference, 20-24 June 1994, Boston, Mass., ASM International. (1994) 431-437.

[156] A. Killinger, P. Müller, R. Gadow, What Do We Know, What are the Current Limitations of Suspension HVOF Spraying? J. Therm. Spray Technol. (2015) 1-13.

[157] http://www.philiplaven.com/mieplot.htm,.

[158] J.C. Owens, Optical refractive index of air: dependence on pressure, temperature and composition, Appl. Opt. 6 (1967) 51-59.

[159] L. Zhang, J. Petit, J. Taine, Measurements of temperature profiles in gases by laser beam deflection, Revue de Physique Appliquee. 24 (1989) 401-410.

[160] C. Innocenti, A. Consortini, Refractive index gradient of the atmosphere at near ground levels, Journal of Modern Optics. 52 (2005) 671-689.

[161] C. Dumouchel, P. Yongyingsakthavorn, J. Cousin, Light multiple scattering correction of laser-diffraction spray drop-size distribution measurements, Int. J. Multiphase Flow. 35 (2009) 277-287.

[162] P. Gougeon, C. Moreau, In-flight particle surface temperature measurement: influence of the plasma light scattered by the particles, J. Therm. Spray Technol. 2 (1993) 229-233.

[163] I.S. Merrill, Introduction to radar systems, Mc Grow-Hill. (2001) 607-609.

[164] J. Swithenbank, J.M. Beer, D.S. Taylor, D. Abbot, G.C. McCreath, A laser diagnostic technique for the measurement of droplet and particle size distribution, AIAA 14th Aerospace Sciences Meeting, Washington, D.C. (1976) 69-76.

[165] O. Marchand, L. Girardot, M. Planche, P. Bertrand, Y. Bailly, G. Bertrand, An insight into suspension plasma spray: injection of the suspension and its interaction with the plasma flow, J. Therm. Spray Technol. 20 (2011) 1310-1320.

[166] J. Bisson, B. Gauthier, C. Moreau, Effect of plasma fluctuations on in-flight particle parameters, J. Therm. Spray Technol. 12 (2003) 38-43.